Agulhas Current variability determined from space: a multi-sensor approach

Marjolaine Rouault

Thesis Presented for the Degree of

DOCTOR OF PHILOSOPHY

November 2011

Department of Oceanography

UNIVERSITY OF CAPE TOWN

South Africa

To my children, Tanguy, Félix and Raphaël, the three primary colours in my life

Abstract

Satellite remote sensing datasets including more than 6 years of high frequency Sea Surface Temperature (SST) imagery as well as surface current observations derived from 18 years of merged-altimetry and over 2 years of Advanced Synthetic Aperture Radar (ASAR) observations are combined to study the variability of the Agulhas Current. The newly available range-directed surface currents velocities from ASAR, which rely on the careful analysis of the measured Doppler shift, show strong promise for monitoring the meso to sub-mesoscale features of the surface circulation. While the accuracy of ASAR surface current velocities suffers from occasional bias due to our current inability to systematically account for the wind-induced contribution to the Doppler shift signal, the ASAR surface current velocities are able to consistently highlight regions of strong current and shear. The synaptic nature and relatively high resolution of ASAR acquisitions make the ASAR derived current velocities a good complement to altimetry for the study of sub-mesoscale processes and western boundary current dynamics. Time-averaged range-directed surface currents derived from ASAR provide an improved map of the mean Agulhas Current flow, clearly showing the location of the Agulhas Current core over the 1000 m isobath and identifying the region at the shelf edge of the north-eastern Agulhas Bank as one of the most variable within the Agulhas Current. To determine the variability of the Agulhas Current, an algorithm to track the position of the current is developed and applied to the longer merged-altimetry and SST records. Limitations associated with altimetry near the coast favour the use of the SST dataset to track the position of the Agulhas Current in its northern region. In the southern Agulhas, where the current lies further from the coast, altimetry is suited to monitoring the position of the Agulhas Current. The front detection analysis conducted on the SST dataset in the northern Agulhas reveals the complex nature of Natal Pulses. The downstream passage of the Natal Pulses is associated with the generation of secondary offshore meanders at the inshore edge of the current. Perturbations formed during the passage of Natal Pulses evolve rapidly to either dissipate, re-merge with the initial Natal Pulse or in some rare occasion, detach from the Agulhas Current. Non-linear interactions between Natal Pulses and the topography are proposed as a mechanism through which energy could

be transferred towards the smaller scales and which could explain the downstream decrease in the number of large offshore meanders observed between Port Edward (31°S) and Port Elizabeth (34°S). Analyses conducted on the merged-altimetry and SST datasets both show that on average, only 1.6 Natal Pulses per year reach Port Elizabeth. Once they enter the southern Agulhas region, Natal Pulses reside for extensive periods of times (between 1 and 3 months) along the eastern Agulhas Bank causing significant cyclonic anomalies in the circulation along the continental shelf. While the propagations of large offshore meanders dominate the variability of the southern Agulhas Current's position, it is the wind-driven annual cycle which drives most of the current speed variability within the core of the southern Agulhas Current.

Acknowledgements

I would first like to thank my supervisor, Prof. Frank Shillington for making a path through the bureaucratic jungle to allow me to register for my PhD degree. I am also thankful for the encouragement and advice Prof. Shillington has given me throughout the thesis.

I would like to acknowledge the CSIR Ecosystem Earth Observation for its financial support and especially Dr. Stewart Bernard for giving me the space to do my PhD research.

Many thanks to the french crew at the CLS radar division in Brest, first for introducing me to the ASAR radial current product and then for their patience in helping me get a grasp of SAR imaging. Thanks to Dr. Alexis Mouche for his support and guidance during the write up of the 1st paper. To Dr. Fab, "merci beaucoup" for taking me out to kite and for the interesting scientific discussions in between. Thanks to Dr. B. Chapron of CERSAT for his very useful suggestions during the redaction of the 1st paper. From the CERSAT, I also want to thank Jean-Francois Piollé and Jean Tournadre for their support.

Many thanks also to Dr. Pierrick Penven for his enthusiasm and support during the making of the 2nd paper. His opinion on Chapter 6 was also much appreciated.

I am very grateful to Prof. Johnny Johannessen who has been a source of constant support and encouragement and a breath of fresh air on each of his visits to South Africa.

Last but not least, I would not be here if it was not for my dear husband, Dr. Mathieu Rouault, whose passion for science led me back to research and whose faith in my ability never wavered.

Contents

<div style="text-align: right;">

1

</div>

Introduction

1.1 Context and motivation

The Agulhas Current forms the western boundary of the wind-driven south Indian gyre. It flows along the continental shelf boundary of south-east Africa, from about 27°S to 40°S, where it reverses in a tight retroflection loop to become the eastward Agulhas Return Current. With a mean transport estimated to about 70 Sverdrup (1 Sverdrup = $10^6 m^3 s^{-1}$) and current speeds often in excess of 2 ms^{-1}, the Agulhas Current constitutes the strongest western boundary current of the Southern hemisphere (Lutjeharms [2006]; Bryden et al. [2005]). The Agulhas Current forms the main water pathway between the Indian and Atlantic oceans and is a major component of the global thermohaline circulation (Gordon [1985]; Beal et al. [2011]). The importance of the heat and salt leakage from the Agulhas Current to the Atlantic ocean has been widely acknowledged (Beal et al. [2011]). It has been shown that the Agulhas leakage dynamics influence the variability of the Atlantic overturning circulation (Weijer et al. [2001]; Biastoch et al. [2008b]) and that modulations in the Agulhas leakage might have altered the severity of past glacial periods (Bard and Rickaby [2009]). Both observations and model outputs suggest that the Agulhas Current leakage to the Atlantic has increased since the 1980' s with possibly far reaching consequences on the global climate (Rouault et al. [2009]; Biastoch et al. [2008a]). The Agulhas Current also influences the global climate through heat flux loss to the atmo-

sphere. Over the Agulhas Current core, about 5 times as much water vapour is transferred to the atmosphere in comparisons to neighbouring waters (Rouault et al. [2000]), with a strong impact on the regional weather and climate. The southern extension of the Agulhas Current where the current retroflects and which is referred to as the Retroflection, constitutes one of the most significant region of heat flux loss globally. A number of studies have linked variability in the greater Agulhas Current region with rainfall over large areas of South Africa (Walker [1990]; Jury et al. [1993]; Mason [1995]). On a regional scale, the Agulhas Current directly influences the oceanography of the continental shelves through a range of meso and sub-meso scale processes such as the shedding of rings, eddies or filaments, as well as the meandering or intrusion of the current onto the shelf (Lutjeharms [2006]). Economic activities along the continental shelf of south-east Africa which include fishing, oil and mineral exploration as well as intense shipping traffic, with the transport of crude oil from the Middle East to Europe are directly impacted by modulations in the path and strength of the Agulhas Current.

Despite its importance at both the regional and global scales, the Agulhas Current remains poorly sampled. The inter-annual and long-term variability of the Agulhas Current are unknown and there exists an ongoing debate on whether the Agulhas Current displays a seasonal cycle (Lutjeharms [2006]). Satellite remote sensing provides the only means of observing the Agulhas Current over the time-scale required to resolve its seasonal and inter-annual variability. While remote sensing data have been used in the past to characterise the Agulhas Current, many of these efforts have lacked the long term temporal component of the variability, only providing a synoptic picture of the state of the ecosystem at a given time (Walker [1986]; Lutjeharms et al. [2000]). Re-processed versions of older remote sensing datasets have become available, allowing us to study past events with greater accuracy over time-scales spanning 10 to 20 years. New remote sensing methods as well as more frequent and high resolution satellite observations are re-shaping the way we view the Agulhas Current and could allow us to improve our understanding of its variability. The highly variable and complex circulation associated with the Agulhas Current also provides an ideal natural laboratory for testing and developing new remote sensing products.

1.2 Objectives and approach

The Agulhas Current system is a challenging environment for remote sensing observations as it is affected by a wide range of processes occurring from the event to the inter-annual scale and from the coast to the global ocean. Over the Indian Ocean, large scale processes such as changes in the wind circulation, westward propagating Rossby waves or offshore eddies originating from the Mozambique or Madagascar regions constitute potential drivers of variability for the Agulhas Current. Variability intrinsic to the Agulhas Current also occurs on a wide range of scales from small filaments, shear-edge eddies or meanders to the shedding of large Agulhas Rings at the Retroflection (Lutjeharms [2006]). Cloud formation over the Agulhas Current severely restricts observations from visible and infra-red sensors from which it is possible to derive ocean parameters such a Sea Surface Temperature (SST) or chlorophyll concentrations. Radars which can "see" through clouds, might be seen as a good alternative to optical and infra-red sensors to observe the Agulhas Current. However, the proximity of the current to the coast over large regions of the Agulhas Current is detrimental to many radar based observations due to factors such as land contamination or atmospheric errors (Vignudelli et al. [2011]). One of the fundamental research goals of this thesis therefore is to answer the following question:

- **Is satellite remote sensing a suitable tool to study the dynamics and variability of the Agulhas Current ?**

  To answer this question we will evaluate both off-the-shelf and new remote sensing products, with the anticipation of demonstrating the feasibility of studying the Agulhas current's dynamics from space. Particular emphasis will be placed on a new and promising method for the measurements of current velocities using data collected from the Advanced Synthetic Aperture Radar (ASAR) instrument located onboard the ENVISAT satellite of the European Space Agency (ESA).

While assessing the limitations and capabilities of satellite-based observations over the Agulhas Current region is a pre-requisite to our study, our main objective lies in furthering our understanding of the physical processes driving the variability of the Agulhas Current upstream of the Retroflection. The objectives of this research can be expressed through the following key questions:

- **Is the Natal Pulse the dominant mode of variability in the Agulhas Current ?**

  Previous studies on the Agulhas Current have consistently pointed to the Natal Pulse as the dominant mode of variability upstream of the Retroflection region (Lutjeharms [2006]). These Natal Pulses have been described as large solitary meanders in the Agulhas Current, associated with a cold-water core and a cyclonic circulation (Lutjeharms and Roberts [1988];Bryden et al. [2005]). Statistical and time-series analysis of suitable remotely sensed data will be used to test the hypothesis that Natal Pulses dominate the variability of the Agulhas Current.

- **Is there a seasonal cycle in the Agulhas Current ?**

  While regional numerical models show seasonality in the transport of the Agulhas Current, in-situ or remote sensing datasets have not yet provided evidence of a seasonal cycle (Lutjeharms [2006]). The combined use of high frequency observations and long time-series spanning 10 to 20 years should help us to better resolve the annual cycle of the Agulhas Current.

- **What are the key drivers of the Agulhas Current variability ?**

  Once the frequency characteristics of the variability in the Agulhas Current are revealed, it will become necessary to determine the physical processes which drive the observed variability.

- **Are there similar time-scales in the northern and southern regions of the Agulhas Current ?**

One of the main advantages of satellite remote sensing compared to other forms of in-situ data acquisition is its ability to provide comprehensive spatial and temporal coverage over large regions of the ocean. The synoptic nature of remote sensing observations should help us identify regional differences within the Agulhas Current.

- **How does variability in the Agulhas Current impact on the coastal and shelf regions?**

High resolution and high frequency satellite datasets will be used to provide new insight on the current and shelf interaction processes. By combining sea surface temperature with ocean current information gathered from satellite observations, the aim will be to characterise and quantify the impact of features such as Natal Pulses on the neighbouring ecosystems.

Previous studies have related variability in the northern Agulhas Current to anomalous events in the southern Agulhas Current. In particular Natal Pulses have been linked to the formation of Agulhas Rings and on some occasion to early retroflections (Lutjeharms [2006]). A final question postulated therefore is:

- **How do upstream fluctuations in the Agulhas Current impact on the leakage of warm and salty Agulhas water into the Atlantic?**

1.3 Outline

An overview of the oceanography in the Agulhas Current region is provided in Chapter 2. The dynamics of the Agulhas Current are described. Characteristics of the source regions and the surrounding wind fields are briefly presented to provide background on the potential drivers of variability for the Agulhas Current. An introduction to the datasets used in this thesis is provided in Chapter 3. The principles of data acquisition from satellite based sensors together with some of the main assumptions made when deriving ocean parameters such as SST and surface current speeds are discussed. In Chapter 4, an assessment of the newly available ASAR surface current velocities is done for the Agulhas Current region. The ability of both the ASAR

and altimetry derived surface current measurements to represent the dynamics of the Agulhas Current are discussed. Based on the findings of Chapters 3 and 4, the datasets best suited to study the variability in the Agulhas Current are then selected to study the variability of the northern (Chapter 5) and southern (Chapter 6) Agulhas Current at the intra-seasonal and seasonal time-scales. Results presented in this thesis are discussed within individual chapters. The summary and conclusions of this research are drawn in Chapter 7.

2

The Agulhas Current

The book of Lutjeharms [2006] provides a thorough and extensive review of the Agulhas Current system which includes most of the contemporary research. This chapter recalls some of the fundamental characteristics of the Agulhas Current's dynamics relevant to this thesis.

The Agulhas Current forms the western boundary current of the South Indian subtropical gyre. The Agulhas Current originates near the South-African / Mozambican border, at about 27°S and flows poleward to 40°S, transporting large volumes of sub-tropical water towards the southern ocean. At its southern extension, the Agulhas Current overshoots the African continent and reverses in a tight retroflection loop to flow back eastward into the Indian Ocean as the Agulhas Return Current.

2.1 Mean dynamics

Like other western boundary currents, the Agulhas Current is an intense and narrow flow characterised by strong velocity gradients and a central warm core, with isopycnal lines sloping steeply towards the coast (Goschen and Schumann [1990]; Casal et al. [2009]; Bryden et al. [2005]). The Agulhas Current can be divided into three regions: the northern Agulhas Current located between 26°S and 34°S where the current flows in close proximity to the coast,

the southern Agulhas Current (east of the Agulhas Bank) where the Agulhas Current detaches from a wider continental slope, and the Agulhas Retroflection, between 36°S and 40°S, where the current undergoes a sudden change of direction (Lutjeharms [2006]). Thermal and sea level surface signatures associated with the Agulhas Current enable the mapping of the Agulhas Current's path from space, using observations of Sea Surface Height (SSH) and SST from altimeters and radiometers (Figure 2.1).

It is in the northern Agulhas Current that the strongest flows are observed with mean maximum velocities of about 1.5 ms^{-1} (van der Vaart and de Ruijter [2001]) and peak monthly velocity of around 2.6 ms^{-1} (Lutjeharms [2006]). Current measurements collected using an array of moorings over a 9 month period show that at 32°S (near Port Edward) the Agulhas Current is on average 200 km wide and 2200 m deep[1] . At 32°S, the Agulhas Current core lies on average within 31 km from the coast and the width of the current core (estimated by Bryden et al. [2005] using the 0.5 ms^{-1} isotachs) is about 90 km. The average total poleward transport in the Agulhas Current has been estimated to 69.7 Sv, making the Agulhas Current the one of the strongest western boundary current in the world (Bryden et al. [2005]). Acoustic Doppler Current Profiler (ADCP) measurements have revealed a V-shaped pattern across the Agulhas Current (Beal and Bryden [1999]; Bryden et al. [2005]). Current velocities increase nearly linearly from the coast to the location of the current maxima, followed by a more progressive decrease in current speeds offshore. The vertical distribution of the current shows that the position of the current maxima moves offshore with increasing depth and that underneath the Agulhas Current lies an undercurrent flowing in a direction opposite to that of the Agulhas Current. In their measurements, Bryden et al. [2005] have found the vertical transition from the Agulhas Current to the undercurrent flow to be sudden, with no gradual rotation in the current vectors and stated that it provided an indication of the strong topographic steering.

Analyses based on ship-drift data (Gründlingh [1983]) indicate that from the northern Natal Bight (28°S) to Port Elizabeth (34°S), the Agulhas Current grows downstream in both size

---

[1]In their analysis, Bryden et al. [2005] used the 0 ms^{-1} isotach to define the vertical extent of the Agulhas Current
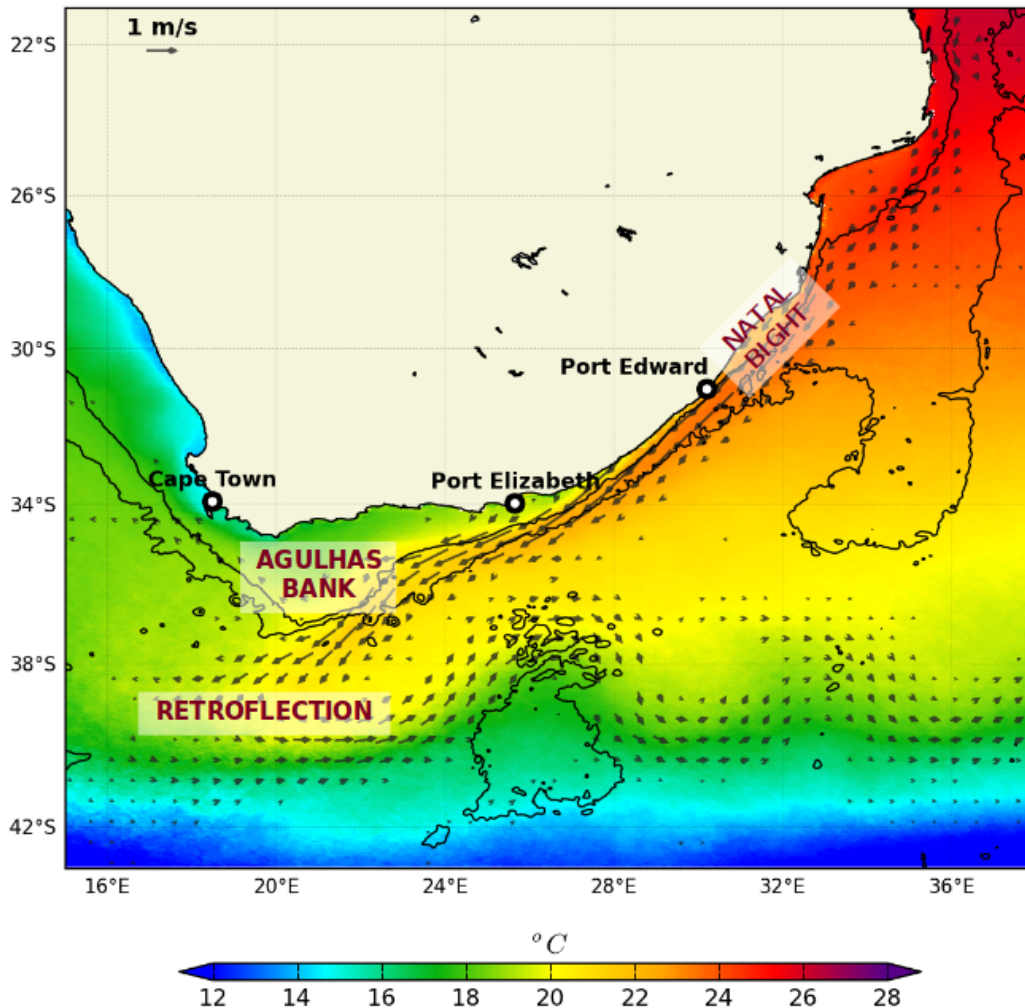
Figure 2.1: *Annual climatological mean of SST (in °C) over the greater Agulhas Current region. Overlaid are mean geostrophic current vectors derived from altimetry. Black contour lines indicate the position of the 1000 m and 3000 m isobaths. The Agulhas Current is a narrow and intense flow which closely follows the 1000 m depth contour along the African coastline, transporting large volumes of warm water from the tropics towards the southern ocean. At about 17°E, 40°S, the Agulhas Current reverses in a tight retroflection loop to become the eastward flowing Agulhas Return Current. The SST climatology was derived using the NOAA Pathfinder data collected from 1982 to 2009. The geostrophic currents were derived using the CNES-CLS09 MDT of Rio and Larnicol [2011]. Geostrophic currents with mean speeds below 0.1 ms^{-1} have been excluded from the plot.*

and strength. This downstream intensification of the Agulhas Current was confirmed in analyses conducted using Lowered Acoustic Doppler Current Profiler (LADCP) profiles acquired at different locations across the Agulhas Current (Donohue et al. [2000]). In a detailed analysis on the downstream evolution of the Agulhas Current, Casal et al. [2009] found that the downstream increase transport in the Agulhas Current occurred due to the deepening of the Agulhas Current and that it could be related to the increase in Sverdrup transport downstream. Some hydrographic data seems to indicate that the downstream increase in the Agulhas current transport is not maintained in the southern Agulhas, (Gordon et al. [1987]).

The hydrographic properties of the Agulhas Current reveal a current split along its dynamical core into an inshore and an offshore region. Inshore of the Agulhas Current core, water masses originating from the Indian ocean and composed primarily of Red Sea Water (RSW) and Subtropical Surface Water (STSW) are encountered. By contrast, the water masses which make up the offshore boundary of the Agulhas current originate predominantly from the Atlantic ocean, the Southern Ocean and the south-east Indian Ocean (Beal et al. [2006]). Along its 1000 km journey south from the northern Natal Bight to the Agulhas Bank, the Agulhas Current retains this hydrographic structure despite the highly energetic and strong sheared flow (Donohue et al. [2000]; Beal et al. [2006]). In their analysis of the potential vorticity structure of the Agulhas Current, Beal et al. [2006] suggested that topographic steering together with the strong potential vorticity gradients across the Agulhas Current were the two main inhibitors of horizontal mixing in the Agulhas Current. Combined ADCP and LADCP transects undertaken during the Agulhas Undercurrent Experiment (AUCE) campaign in 2003 (Bryden et al. [2005]) clearly highlight the vertical structure across the Agulhas Current and its downstream evolution from 32°S to 36°S (Figure 2.2).

2.2   Remote forcing of the Agulhas Current

The Agulhas Current forms the western boundary of the sub-tropical Indian Ocean and constitutes the main pathway for the oceanic transfer of heat from the tropics to the pole. Through
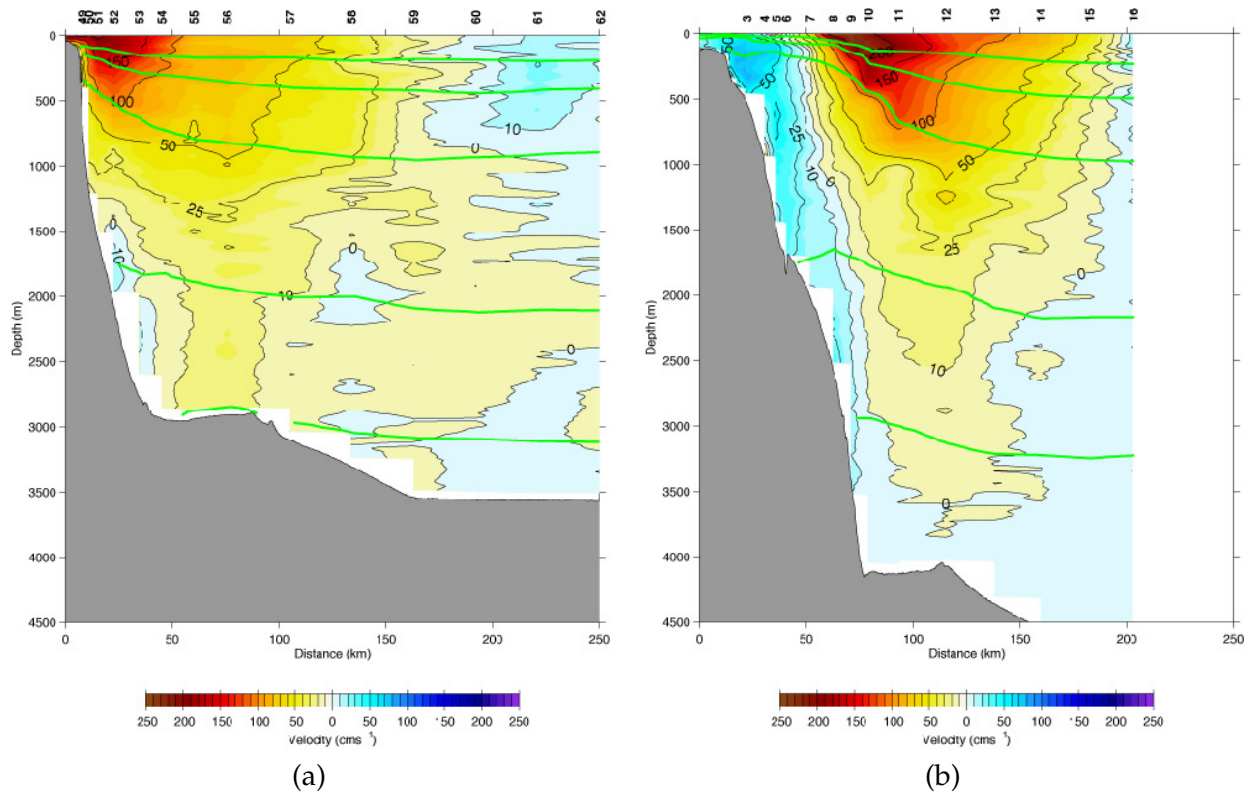
Figure 2.2: *Combined LADCP and ADCP measurements undertaken during the AUCE campaign in 2003 at 32°S (a) and 36°S (b). Colour contours show the vertical distribution of the along-shore velocity across the Agulhas Current. Green contours represent neutral surfaces separating layers of, from top to bottom, Tropical Surface Water (TSW), SubTropical Surface Water (STSW), thermocline waters (including SubAntarctic Mode Water), Red Sea (RSW) and AntArctic Intermediate Water (AAIW), and Upper/Lower North Atlantic Deep Water (NADW). Positive values in shades of red and yellow are indicative of the south-westward flow associated with the Agulhas Current. Shades of blue indicate the presence of a under-current flowing north-eastward under the Agulhas Current. The location of the Agulhas Current maxima moves offshore with increasing depth with the level of no-motion exhibiting a V-shape pattern. These images were downloaded from* http: //www.rsmas.miami.edu/personal/lbeal/current.html.

its sources regions, the Agulhas Current is connected to the variability of the Indian Ocean. Changes in atmospheric forcing and resulting variations in the strength and position of the subtropical gyre as well as fluctuations in the Indonesian throughflow are all factors which may influence the inter-ocean transports south of Africa. This section provides a review of the major drivers of variability within the South Indian Ocean and the sources regions of the Agulhas Current.

2.2.1 Wind forcing

The dominant feature of the atmospheric circulation in the South Indian Ocean is the South Indian Anticyclone. The South Indian Anticyclone is centred at about 30°S and drives an anticyclonic motion bounded to the north by the South-Equatorial Current (SEC), to the South by the sub-tropical convergence and closed to the west by the southward flowing Agulhas Current (de Ruijter et al. [2005]). Their estimate of the mean poleward Agulhas Current transport driven by the mean wind-stress curl amounts to 50 Sv at 32°S, a value well below the 70 Sv reported by Bryden et al. [2005]. The difference between the measured Agulhas Current transport and that estimated using the Sverdrup relation have been attributed to contributions from the regional and the ocean's overturning circulations (Lutjeharms [2006]). One component of the overturning circulation important to the Agulhas is the Indonesian throughflow, with a contribution estimated to be about 10 Sv (de Ruijter et al. [2005]).

The South Indian Anticyclone varies in position and strength throughout the year. During the austral winter (May to July), it is located further north and associated with a weaker anticyclonic gyre. In the austral summer months (December to February), the South Indian Anticyclone is located further south and drives a strengthened anticyclonic circulation (Ffield et al. [1997]; Matano et al. [2002]). Plots of wind-stress and wind-stress curl derived for January and July from the QuikSCAT wind climatology of Risien and Chelton [2008], clearly highlight seasonal variations in the wind-driven circulation of the South-Indian ocean gyre (Figure 2.3). Seasonal forcing associated with the Indian ocean monsoon generate Kelvin waves which propagate along the equatorial waveguide and southwards towards the Indonesian coast. Upon

reaching the eastern boundary, these Kelvin waves are partially reflected as westward propagating Rossby waves (Perigaud and Delecluse [1992]; Yang et al. [1998]). The preferred route for Rossby waves propagation show as regions of high SSH variability in the Indian ocean along the 12°S and 25°S zonal bands (de Ruijter et al. [2005]). In their analysis, Xie et al. [2002] found that Rossby waves could account for up to 50% of the total SST variance in the western tropical South Indian Ocean. The frequency of Rossby waves within latitude band 20°S - 30°S was shown to vary at both inter-annual and sub-annual time-scales. Evidence of Rossby waves occurring at sub-annual frequencies of 2 per year (Morrow and Birol [1998]) and 4 times per year (Schouten et al. [2002]; Palastanga et al. [2007]) were found. Other studies on the inter-annual variability of the south Indian Ocean have shown that SSH anomalies related to the Indian Ocean dipole (IOD) or to the El Niño Southern Oscillation (ENSO) constitute major forcing mechanisms for Rossby waves (Xie et al. [2002]; Baquero-Bernal and Latif [2005]).

Changes in the Indonesian throughflow as well as wind driven variability over the South Indian Ocean are transmitted to the source regions of the Agulhas Current through the SEC (Gordon et al. [1997]; Ridderinkhof et al. [2010]). Upon reaching the eastern shore of Madagascar at 15°E, the SEC branches into a northern and southern flow, feeding two main sources for the Agulhas Current: the Mozambique and the East Madagascar currents. Figure 2.4 provides a schematic of the circulation in the South Indian ocean. Major currents and sources for the Agulhas Current are drawn over regions of high variability. The branching out of the SEC at the eastern shore of Madagascar appears clearly in colour contours of Eddy Kinetic Energy (EKE) derived from absolute geostrophic currents.

2.2.2 Forcing from the source regions

The three recognised sources of the Agulhas Current are the southern branch of the East Madagascar Current, flow through the Mozambique Channel and recirculation in the South West Indian Ocean subgyre part of the Agulhas Current, west of 70°E (Lutjeharms [2006]).

The South East Madagascar Current (SEMC) originates from the southward flowing branch of the SEC. The SEMC current is about 120 km wide with typical peak current speeds of 1 ms^{-1}
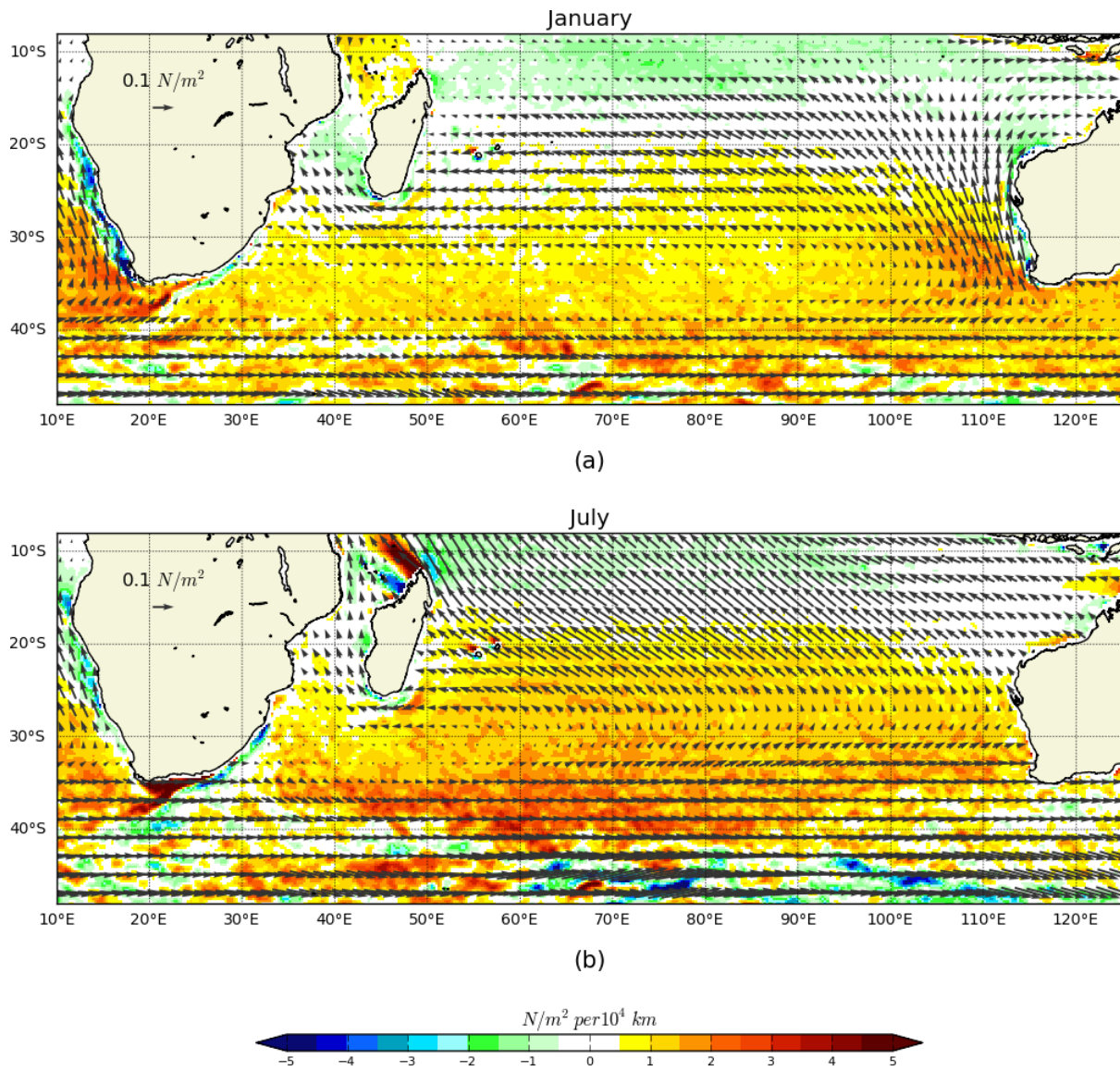
Figure 2.3: *Mean wind-stress and wind-stress curl derived for January (a) and July (b) from the quikSCAT climatology of* Risien and Chelton *[2008]. Colour contours of the wind-stress curl are overlaid with wind-stress vectors.*
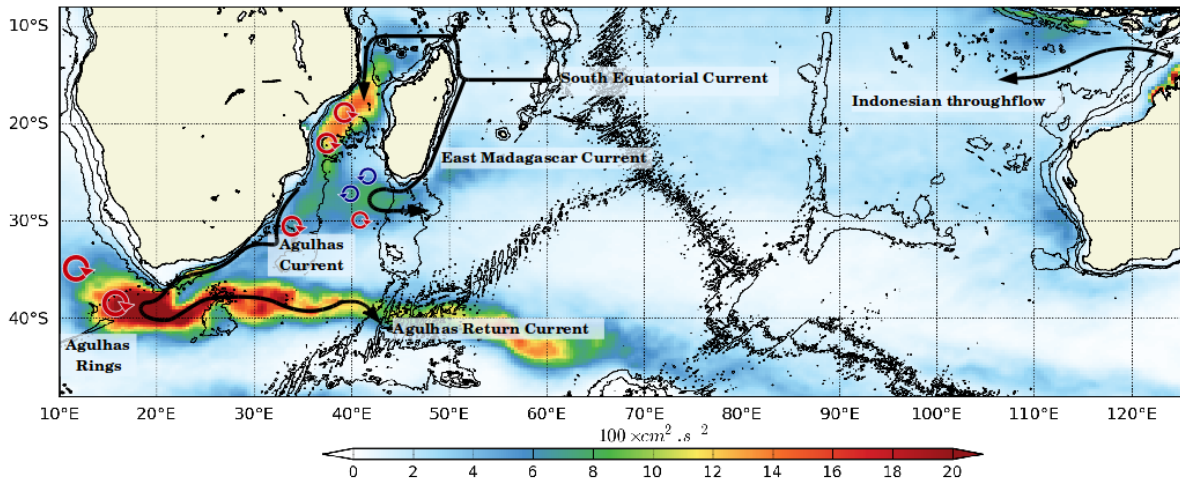
Figure 2.4: *Schematic of the circulation in the South Indian Ocean. Colour contours of mean EKE derived from absolute geostrophic currents are overlaid with outlines of the main currents. The absolute geostrophic current were calculated by combining AVISO maps of SLA with the CNES-CLS09 MDT of Rio and Larnicol [2011].*

(Swallow et al. [1988]; Nauw et al. [2008]). The mean poleward transport of the SEMC estimated from observations range from 20 Sv (Schott et al. [1988]; Donohue and Toole [2003]) to 37 Sv (Nauw et al. [2008]), while transport of the SEMC derived from numerical models vary between 30 Sv (Matano et al. [2002]; Quartly et al. [2006]) and 35 Sv (Hermes et al. [2007]). Using output from a high resolution model, Siedler et al. [2009] found that close to 50% of SEMC contributes to the Agulhas Current. The contribution from the SEMC to the Agulhas Current occurs in the form of cyclonic and anti-cyclonic eddies which tend to drift south-westward towards the northern Agulhas Current (Biastoch et al. [1999]; Quartly and Srokosz [2002]; de Ruijter et al. [2004]). Analyses of altimeter data indicate that on average 4 anticyclonic eddies per year occur south of Madagascar (Schouten et al. [2003]), with the eddy frequency increasing during negative phases of the Indian Ocean Dipole and El Niño cycles (de Ruijter et al. [2004]). Despite the suggested link between the SEC and the SEMC variability (Schouten et al. [2003]; de Ruijter et al. [2004]), observations at 23°S across the SEMC have not revealed any seasonality in the current (Swallow et al. [1988]).

In the Mozambique channel, the flow is dominated by the passage of large anti-cyclonic

eddies propagating southwards towards the Agulhas Current (de Ruijter et al. [2002]). These large anti-cyclonic eddies occur 5 to 6 times per year (van der Werf et al. [2010]), they have spatial scales of 300 to 350 km and move downstream at speeds of 3 to 6 km/day. The contribution of the Mozambique channel flow to the Agulhas Current transport has been estimated from observations, to be about 17 Sv by Ridderinkhof et al. [2010] and 18 Sv by Donohue and Toole [2003]. Current measurements collected from moorings over more than 4 years were able to identify seasonal as well as inter-annual fluctuations in the southward transport through the Mozambique channel (Ridderinkhof et al. [2010]). Seasonal fluctuations in the southward transport of the Mozambique current had a mean amplitude of 4 Sv, reaching a maximum in austral winter. The seasonality of the Mozambique flow was found to lag changes in the wind field over the western Indian Ocean by about 1 month. In their analysis, Ridderinkhof et al. [2010] suggested that at the inter-annual time-scales, the poleward transport through the Mozambique channel was modulated by the strength of the SEC with a time-lag of about 1 year. Ridderinkhof et al. [2010] estimated the magnitude of these inter-annual variations to be about 9 Sv.

Previous studies based on the analysis of hydrographic data (Gordon et al. [1987]; Stramma and Lutjeharms [1997]) suggested that the most important source for the Agulhas Current was through recirculation in a South West Indian Ocean subgyre. Gordon estimated that south of 32°S, the Agulhas Current transport was enhanced by a further 30 Sv from the recirculation subgyre, while Donohue and Toole [2003] estimated that this recirculation contributed 29 Sv to the Agulhas Current transport. Boebel et al. [2003] observed the shedding of cold eddies from the northern boundary of the Agulhas Return Current and into the recirculation regime between the Agulhas Current proper and the Agulhas Return Current. However, Lutjeharms [2006] noted that the pathways and transport estimated by Gordon et al. [1987] and Stramma and Lutjeharms [1997] for the South West Indian subgyre were subject to considerable uncertainties arising from the wide station spacing of their hydrographic sections. In a recent study on the downstream evolution of the Agulhas Current, Casal et al. [2009] found no evidence of an inertial re-circulation into the Agulhas Current.

Due to a lack of observations, two out of the proposed three sources for the Agulhas Current remain largely unknown. The variability and flow characteristics of the SEMC and the recirculation through the subgyre of the South West Indian ocean are uncertain and so are their impact on the Agulhas Current.

2.3 Variability of the Agulhas Current

The northern Agulhas Current, the southern Agulhas Current and the Agulhas Retroflection are each associated with different oceanographic processes and variability. In the northern Agulhas Current the current core flows very close to the shore (Bryden et al. [2005]) with remarkably little variability (Gründlingh [1983]). The oceanography of the southern Agulhas Current region is reminiscent of that associated with other western boundary currents and is characterised by a wide range of meso- and sub-mesoscale processes such as rings, eddies, filaments or plumes (Lutjeharms [2006]). The Agulhas Retroflection region, where the Agulhas Current undergoes a sudden change of direction to become the Agulhas Return Current, has long been described as the region of highest variability in the southern hemisphere (Cheney et al. [1983]). The complexity of the circulation in the Agulhas Retroflection region has been widely documented (Lutjeharms [2006]) and is mainly dominated by the intermittent shedding of large Agulhas Rings and their associated secondary circulation.

The seasonality of the Agulhas Current remains a matter of debate. Numerical ocean model results show a seasonal variation in the Agulhas Current, with a minimum poleward transport in austral winter (August) and a maximum in austral summer (February) (Biastoch et al. [1999]; Matano et al. [2002]; Hermes et al. [2007]; Chang [2009]). The seasonality of the Agulhas Current seems to be confirmed to some extent by satellite observations of a strengthening of the Agulhas Retroflection variability during the summer months (Weeks et al. [1998]; Matano et al. [1998]). Matano et al. [2002] and Hermes et al. [2007] argued that seasonal fluctuations in the Agulhas Current transport could be attributed to modulations in the Mozambique channel flow. Seasonal changes in the Mozambique flow were in turn related to variations in the

strength of the SEC induced by wind forcing in the South Indian ocean, in agreement with the findings of (Ridderinkhof et al. [2010]). Matano et al. [2008] could not corroborate the connection they previously established between the Mozambique flow and the Agulhas Current at seasonal time-scales. In-situ observations and analyses of ship-drift data in the Agulhas Current were not able to reveal evidence of a seasonal cycle in the Agulhas Current (Pearce and Grundlingh [1982]; Gründlingh [1983]; Bryden et al. [2005]).

What the observations have shown is that from the northern Natal Bight (28°S) to Port Elizabeth (34°S), the Agulhas Current displays remarkably little variability. In the northern Agulhas, the current is encountered in close proximity to the shore for about 80% of the time (Gründlingh [1983]; Bryden et al. [2005]). The stability of the northern Agulhas has been attributed to the topographic steering of the current by the very steep continental slope (Lutjeharms and van Ballegooyen [1984]; de Ruijter et al. [1999]). In their study on the stability of the Agulhas Current, de Ruijter et al. [1999] argue that instabilities in the northern Agulhas can only develop at the Natal Bight, an embayment of the northern Agulhas where the steepness of the continental slope relaxes. These instabilities, first observed by Harris et al. [1978] have been termed Natal Pulses after their region of origin (Lutjeharms and Roberts [1988]). Previous studies (Bryden et al. [2005]; Lutjeharms [2006]) have pointed to the Natal Pulse as the dominant mode of variability upstream of the Agulhas Retroflection.

Natal Pulses have been described as large solitary meanders in the Agulhas Current associated with a cold-water core and a cyclonic circulation inshore of the current (Lutjeharms and Roberts [1988]; Bryden et al. [2005]). The formation, growth and propagating speed of Natal Pulses have been inferred from in-situ measurements (Beal and Bryden [1999]; Bryden et al. [2005]), satellite remote sensing imagery such as SST (Lutjeharms and Roberts [1988]; Lutjeharms et al. [2003b]) or altimetry (de Ruijter et al. [1999]; van Leeuwen et al. [2000]), as well as from numerical modelling experiments (Biastoch et al. [2008b]; Tsugawa and Hasumi [2010]). More recent studies on Natal Pulses have shown that these offshore meanders originate in the Natal Bight as a result of a barotropic instability and grow steadily in size as they propagate downstream with phase velocities of 10 to 20 km/day (van der Vaart and de Ruijter [2001];

Lutjeharms [2006]). Natal Pulses occur at irregular time intervals of 50 to 240 days (de Rui-jter et al. [1999]), with a mean frequency of 4 to 6 per year (Bryden et al. [2005]; Lutjeharms [2006]). Lagrangian float observations have revealed that Natal Pulses can extend to the full depth of the Agulhas Current (Lutjeharms et al. [2001]). Natal Pulses strongly influence coastal and shelf regions where they drive localized upwelling (Bryden et al. [2005]) and participate in the export of pollutants or fish-larvae from the northern to the southern Agulhas regions. Natal Pulses are also thought to play an important part in the downstream variability of the Agulhas Current and the subsequent leakage of warm and salty Agulhas Current water into the Atlantic ocean. In particular, they have been linked to the formation of Agulhas Rings (van Leeuwen et al. [2000]) and on some occasion to early retroflections (Lutjeharms and van Ballegooyen [1988]).

In the southern Agulhas, south of 35^oS, the Agulhas Current is no longer stabilised by the steep continental shelf and begins to exhibit numerous meanders, plumes and eddies (Lutje-harms [2006]). Along the Agulhas Bank, meanders and shear edge eddies are often seen at the inshore border of the Agulhas Current. These meanders and shear edge eddies grow down-stream as they move southward along the Agulhas Bank with typical propagation speeds of 19 km/day. Warm water plumes of Agulhas water are often seen trailing behind the crest of these southward propagating meanders (Lutjeharms [2006]).

3

Remote sensing data and measurements methods

The dynamics and variability of the Agulhas Current in this thesis are studied using SST observations retrieved from Infra-Red (IR) sensors as well as surface currents derived from altimeters and Synthetic Aperture Radar (SAR) measurements. Here, we provide a brief overview of the theory behind SST observations from IR sensors and surface current measurements from altimeters and SARs.

3.1 Infrared SST observations

Heat radiated by the ocean's surface at a particular wavelength can be related to its apparent temperature (known as the brightness temperature) through the Planck's blackbody equation. At the ocean's surface the brightness temperature is obtained by multiplying the Planck's emitted radiation to the emissivity of the sea surface. The emissivity of the sea surface in the thermal IR (3-15 μm) is normally assumed to vary between 0.98 and 0.99 and can be estimated using models or regression techniques based on in-situ measurements (Robinson [2004]). The water leaving radiance is attenuated by atmospheric gases (primarily CO2, CH4 and NO_2), aerosols and water vapour before it reaches the top of the atmosphere, with water vapour accounting for most of the needed atmospheric correction (Barton and Checet [1989]; Kilpatrick et al. [2001]). IR observations of SST are therefore restricted to wavelengths within the 3.5 to

4.1 μm and/or the 10 to 12.5 μm bands, where atmospheric attenuation is reduced and emittance is high (Robinson [2004]). Most atmospheric correction algorithms use the differences in attenuation at two selected bands to gain information on the atmospheric composition for each sampled pixel. According to Barton [1995], all IR SST algorithms follow the same basic form of:

$$SST = aT_i + b(T_i - T_j) + c \tag{3.1}$$

where T_i and T_j are brightness temperature measurements in channels i and j and a, b and c are constants. The coefficients a, b and c in equation 3.1 are recovered using radiative transfer models to predict the brightness temperature for a wide variety of atmospheric states. Empirical models based on matching databases of in-situ observations are then used to relate the measured radiances to values of SST. Thermal IR sensors have been deployed onboard satellite since the late 1960s and can now measure SST with an accuracy of 0.1 °C - 0.2 °C (Donlon [2010]). But these observations can only be made in cloud-free conditions. Cloud contaminations can induce significant data loss in SST imagery as they obscure the ocean surface, absorb surface-leaving radiation, and re-emit this energy at lower temperatures. Most datasets of IR derived SST routinely available have been subjected to automatic cloud screening procedures to remove contaminated data. Cloud detection algorithms usually involve masking pixels in the SST image which are significantly cooler than either neighbouring pixels and/or the climatological value (Robinson [2004]). In regions of strong thermal gradients, automatic cloud screening procedures often result in the loss of good geophysical data.

IR observations of SST in the Agulhas Current region suffer from cloud contamination due to the high level of evaporation above the current core (Rouault et al. [2000]). Off Port Elizabeth, the Agulhas Current drives a semi-permanent upwelling circulation and strong thermal gradients are often encountered between the shelf waters and the inshore front of the Agulhas Current (Rouault et al. [1995]; Lutjeharms [2006]). Automated cloud screening procedures result in a low number of observations in the Pathfinder SST dataset in the coastal and shelf

regions of Port Elizabeth [1]. The effect of cloud contamination on the sampling of the Agulhas Current from IR SST observations is well illustrated in Figure 3.1. In this thesis we will investigate the use of high frequency SST data acquisitions from the geo-stationary Meteosat Second Generation satellite (MSG-2). The main payload on the MSG-2 satellite is the Spinning Enhanced Visible and InfraRed Imager (SEVIRI). SEVIRI images the Earth at a 15 minutes sampling interval using 12 spectral channels (4 visible/near-IR and 8 IR channels) with spatial resolutions of 1 km and 3 km. SEVIRI provides 20 times more information than previous Meteosat satellites with unique capabilities for imaging the ocean's surface. Figure 3.2 provides an example of the SST imaging capacity from the Pathfinder and SEVIRI datasets. High frequency acquisitions from the SEVIRI sensor provide better coverage over the Agulhas Current region.

3.2 Altimetry

3.2.1 Measurement principles

Radar altimeters are active instruments which emit a microwave signal and record the returned echo (or waveform) from the ocean's surface. The most commonly used frequency for altimeters is the Ku-band (13.6 GHz). The power, shape and phase of the returned radar echoes are analysed to retrieve Sea Surface Height (SSH), Significant Wave height (SWH) and wind speed at the ocean's surface. The echo waveform over the ocean has a shape which can be described analytically using the Brown model (Brown [1977]). The analysis of the waveform is done by comparing the measured waveform to the fitted analytical model. A schematic representation of an altimeter waveform over the ocean is provided in Figure 3.3. As the radar signal impinges on the ocean's surface, the amplitude of the echo suddenly increases. In calm seas, the amplitude of the reflected signal increases sharply from the moment the leading edge of the radar hits the ocean's surface. In rough seas, the radar signal is reflected across a multitude

---

[1]The Pathfinder dataset is derived from daily IR observations from the NOAA/NASA Advanced Very High Resolution Radiometer (AVHRR) at a 1 km spatial resolution
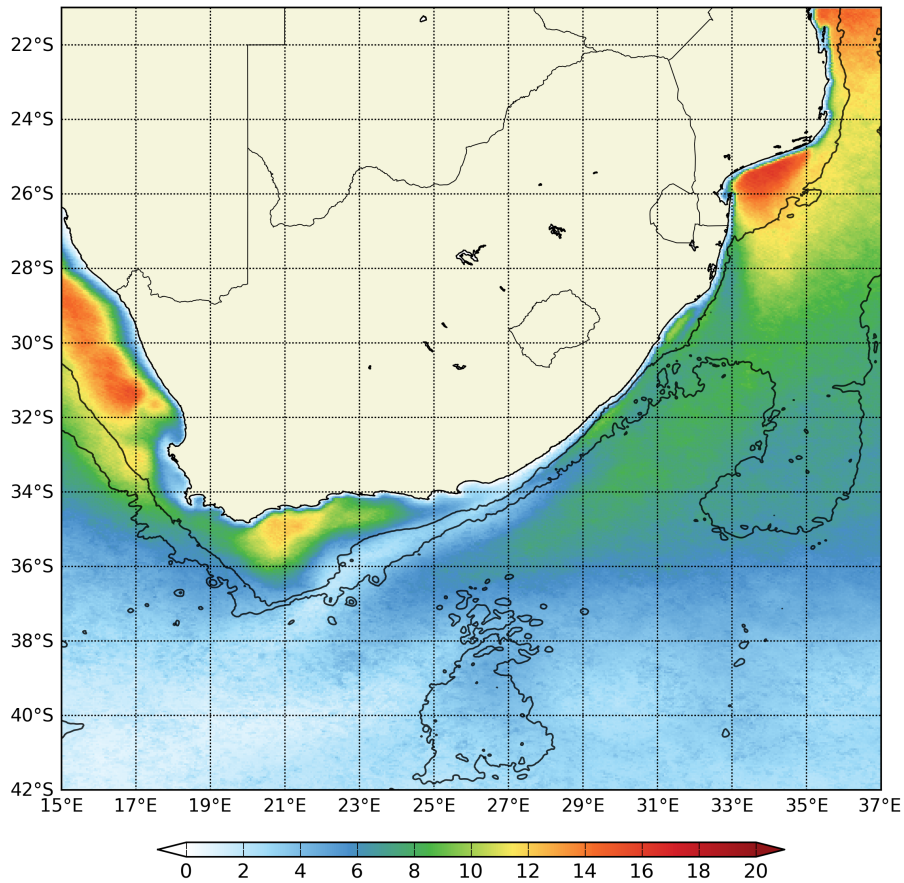
Figure 3.1: *Average number of monthly SST observations calculated over the 1985 to 2009 period from the NOAA Pathfinder de-clouded dataset (version 5). The Agulhas Current, the Agulhas Retroflection and the Agulhas Return Current are very poorly sampled by IR sensors due to high evaporation rates and resulting cloud formation over these regions (Rouault et al. [2000]). Cloud screening procedures result in very few observations being available in the coastal and shelf waters off Port Elizabeth, where temperature gradients between coastal and offshore waters are large. Black contour lines indicate the position of the 1000 m and 3000 m isobaths.*

Figure 3.2: *Daily composite of de-clouded SST on the 15th of January 2009 for (a) Pathfinder (version 5) and (b) SEVIRI. The high frequency acquisitions of SST from the SEVIRI sensor allow a better imaging of the Agulhas Current. Black contour lines indicate the position of the 1000 m and 3000 m isobaths.*

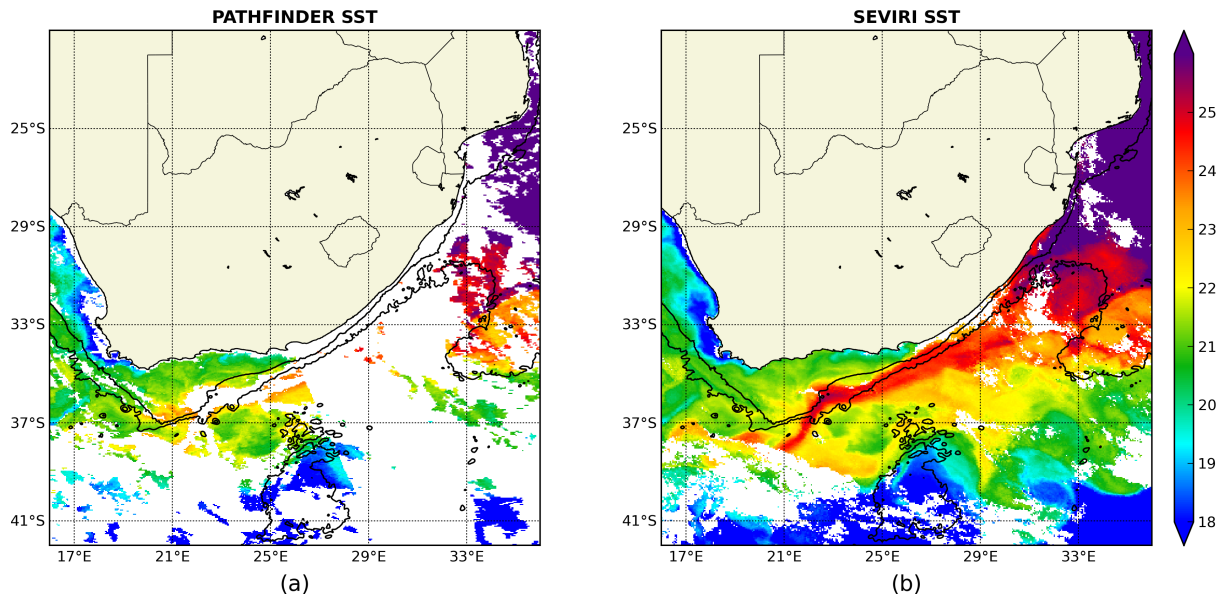of ocean waves crests, causing the amplitude of the returned echo to increase more gradually, with the slope of the leading edge being inversely proportional to wave height. The backscatter coefficient (noted as σ_0) measures the strength of the returned radar echo and is related to the wind-induced roughness of the sea-surface. Empirical methods can then be used to estimate wind speeds from σ_0. The slope of the trailing edge is linked to any deviation from nadir of the radar pointing (antenna mispointing). The time delay between the emitted and received echo provide an estimate of the distance between the satellite and the ocean's surface though the relation:

$$t = \frac{2R}{c} \tag{3.2}$$

where t is the time delay between the emitted and received signal, R is the satellite's range (or distance above ocean) and c is the speed of the emitted electromagnetic wave (Robinson [2004]).
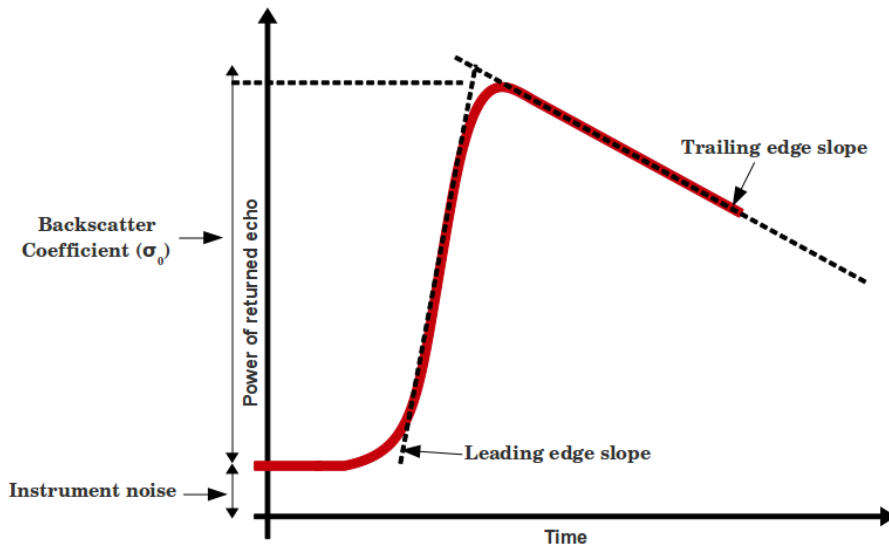
Figure 3.3: *Schematic representation of an altimeter waveform over the ocean.*

3.2.2   From SSH to ocean currents

To track variations in time of the ocean's SSH, altimeter observations are referenced to a rough approximation of the Earth's surface, called the reference ellipsoid. The height of the altimeter with respect to the reference ellipsoid is called the altitude. The SSH measured by the altimeter at a given time is then expressed as:

$$SSH = Altitude - Range. \tag{3.3}$$

A range of factors influence the SSH. A schematic of the relationship between the different contributors to the SSH measured by altimeters is provided in Figure 3.4. The geoid represents the influence of the Earth gravity field on the SSH. Tides (both earth and ocean), sea state and winds are additional factors which contribute to the SSH. Two particularly important measurements for oceanographers using altimetry data are the mean dynamic topography (MDT) and the Sea Level Anomaly (SLA). The MDT, which is the difference between the mean sea level and the geoid, represents the influence of long-term averaged currents on the sea surface height, while the SLA accounts for the currents variability after the effects of tides, atmospheric

pressure and sea state have been removed. The Absolute Dynamic Topography (ADT) can then be re-created by adding the MDT to the SLA routinely measured by altimeters.
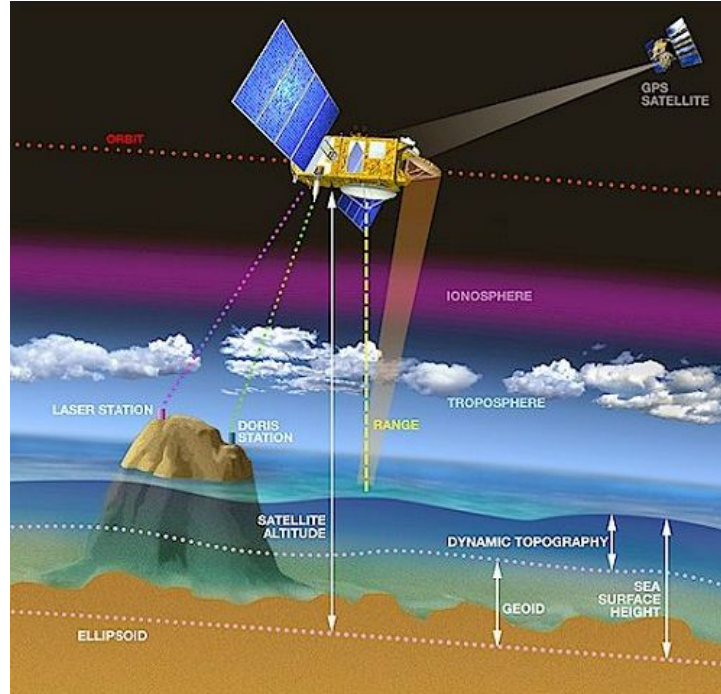
Figure 3.4: *Parameters required for the derivation of an absolute dynamic topography from Altimeters (image downloaded from* `http: // earth. eo. esa. int` *)*

The ADT is related to the near-surface oceanic velocity field through the geostrophic approximation:

$$
\begin{aligned}
u_g &= -\frac{g}{f}\frac{\partial ADT}{\partial y} \\
v_g &= \frac{g}{f}\frac{\partial ADT}{\partial x}
\end{aligned}
\tag{3.4}
$$

where u_g and v_g are the zonal and meridional geostrophic velocities, g is the gravity acceleration, and f is the Coriolis parameter.

The emergence of global MDT datasets (Niiler et al. [2003]; Rio and Hernandez [2004]; Vianna et al. [2007]) have provided oceanographers with a meaningful frame of reference for their SSH measurements. Over the last few years, MDT datasets have been combined with

measurements of the SLA to estimate the ADT and its associated current fields. Comparisons between several MDTs were made to select the MDT best suited to represent the mean dynamical structure of the Agulhas Current (described in Section 2.1 of Chapter 2). Figure 3.5 shows absolute geostrophic current speeds derived from the MDTs of Rio and Hernandez [2004], Rio and Larnicol [2011] and Vianna and Menezes [2010]. The MDT which represents best the mean Agulhas Current dynamics is the recently derived CNES-CLS09 MDT of Rio and Larnicol [2011]. The CNES-CLS09 MDT was computed using a method similar to that described in Rio and Hernandez [2004]. The Mean Sea Surface (MSS) used for the derivation of the CNES-CLS09 MDT is calculated from a 7 year (1993-1999) mean of altimeter SSH measurements and a first-guess MDT is defined as the difference between the MSS and the geoid output from the GRACE gravity model. The initially low spatial resolution of the first-guess MDT ($\simeq 300$ km) is improved through the assimilation of in situ observations and climatological data. The CNES-CLS09 MDT derived by Rio and Larnicol [2011] is provided on a $1/4^o$ resolution grid. The assimilation of extended datasets of drifting buoy velocities (1993-2008) and dynamic heights (1993-2007) into the CNES-CLS09 MDT significantly improves the portrayal of western boundary currents from altimetry (Rio and Larnicol [2011]).

3.2.3 Sources of errors and uncertainties

Measuring the ocean's sea surface height with an accuracy of 1 to 2 cm from heights of 800 to 1400 km and a platform moving at an average speed of about 7 km/s requires an exact knowledge of the satellite's position relative to the Earth at any given time. Modern instruments rely on onboard navigation systems (such as DORIS, PRARE instruments and/or GPS receivers) to determine the properties of satellites' orbits. Satellite Laser Ranging (SLR) measurements from a network of ground stations are also used to track the positions of satellites in space. These tracking systems are able to correct for instrumental errors such as inclination, atmospheric drag or gravity forces acting on the satellite (Robinson [2004]).

Observations of SSH from space are subject to a range of geophysical errors. These errors can be estimated or predicted using additional onboard instruments (such as microwave ra-
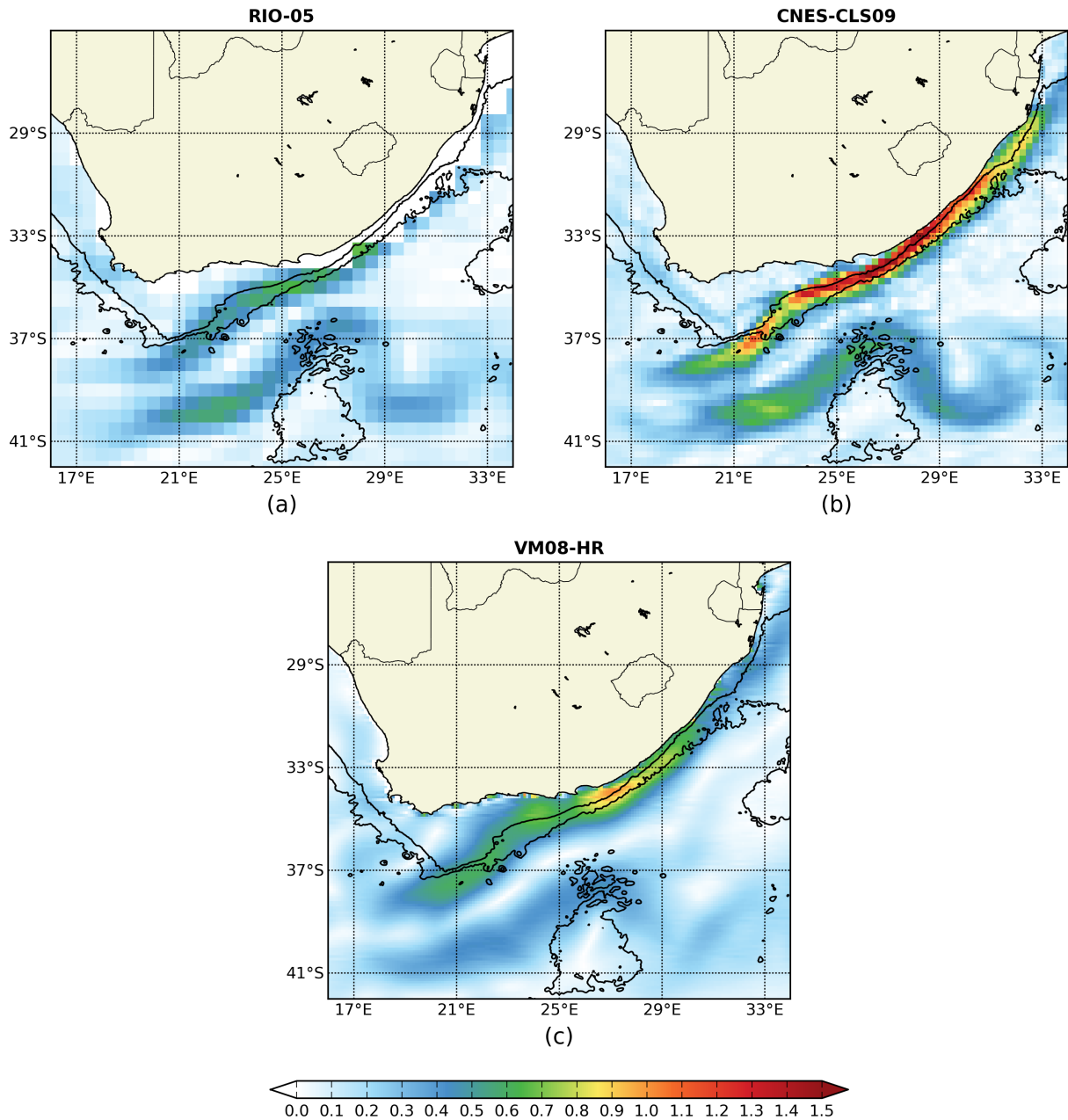
Figure 3.5: *Mean geostrophic current speeds derived from the (a) Rio-05 (Rio and Hernandez [2004]), (b) CNES-CLS09 (Rio and Larnicol [2011]) and (c) VM08-HR (Vianna and Menezes [2010]) MDTs. The CNES-CLS09 MDT of Rio and Larnicol [2011] benefits from the assimilation of extended in-situ dataset and is best able to represent the time-averaged circulation of the Agulhas Current.*

diometers or radars operating at different frequencies) as well as analytical and geophysical models. In the atmosphere, the propagation of electromagnetic waves is delayed primarily at the level of the ionosphere and the troposphere. The ionospheric correction accounts for the delays in the propagation of the altimeter's pulse caused by a frequency dispersion of the electromagnetic waves. At the troposphere two types of corrections are required. The dry topospheric correction accounts for the delays in electromagnetic wave propagation due to all gases, while the wet tropospheric correction accounts for the effect of water vapour. The dry topospheric effect is proportional to sea level pressure and can be corrected using atmospheric model pressure forecasts. Most modern altimeters use an onboard microwave radiometers to provide simultaneous measurements of the water content and improve the wet tropospheric correction (Chelton et al. [2001]).

At the ocean's surface, waves, tides or winds affect the sea surface slope. Sea surface height biases are corrected using empirical methods. Tidal variations are corrected by using tidal models. Global tidal models have benefited from the assimilation of SSH observations from previous altimeters (in particular TOPEX/ POSEIDON) and can now resolve tidal variations in the open ocean with an accuracy of 1 to 2 cm (Le Provost [2000]). In coastal and shelf regions however, tidal predictions are difficult to achieve due to non-linear interactions between tidal waves, bathymetry or local winds. Changes in sea pressure over the ocean due to atmospheric pressure loading are corrected by using forecast from global atmospheric models such as ECMWF. To study ocean circulation from altimetry, it is necessary to refer SSH measurements to the geoid rather than the reference ellipsoid. Current measurements of the Earth gravity field are able to resolve the geoid over length scales of the order of 100 km (C. et al. [2005]), while global gravity models resolve the geoid with resolution of a few hundred kilometers (Rio and Hernandez [2004]). Assuming the geoid is stationary, the time varying part of the ocean circulation can be reproduced by subtracting the mean SSH and working with height anomalies. However this procedure also removes the MDT which has a strong signature in western boundary current regions such as the Agulhas Current.

Since the mid-1990s, there have been a minimum of two altimeters in space. There are

currently 4 altimeters in orbit (Jason 1, Jason 2, Envisat and CryoSat-2). Measurements along the altimeter's tracks are averaged over 1 second of flight, implying that the spatial resolution along the altimeter track is about 7 km. Altimeters have cross track spacing varying between 30 and 300 km and repeat cycles ranging from 10 to 35 days (Vignudelli et al. [2008a]; Vignudelli et al. [2011]).

3.3 Synthetic Aperture Radars

3.3.1 Principles of observations

Real Aperture Radars (RAR) and SAR are side-looking radars which illuminate the ocean's surface in a direction perpendicular to the flight line, within an area defined as the radar's footprint (Figure 3.6). Along the satellite's path (in the azimuth direction), echoes returned from the radar pulses are recorded, processed and converted to digital data to produce a two-dimensional image of the ocean's surface. The resolution in the azimuth (X_a) and range (X_r) directions for a RAR are given by:

$$X_a = \frac{h\lambda}{Lcos\theta} \qquad and \qquad X_r = \frac{c\tau}{2sin\theta} \tag{3.5}$$

where h is the distance between the satellite and the ocean's surface, λ is the radar's wavelength, L is the length of the antenna, θ is the radar incidence angle, τ is the pulse duration and c is the pulse speed (Danilo [2009]).

SARs were designed to improve on the resolution of RARs. According to Equation 3.5, the range resolution can be improved by shortening the pulse duration τ. This is achieved through a technique called "pulse chirping", which consists in generating a long pulse with a linear frequency modulation. Pulse chirping provides the advantage of simulating a short pulse while maintaining the adequate level of the transmitted energy for low signal-to-noise ratio. In the azimuth direction, the resolution is increased by using the synthetic aperture principle to simulate a very long radar antenna. The synthetic aperture principle relies on the
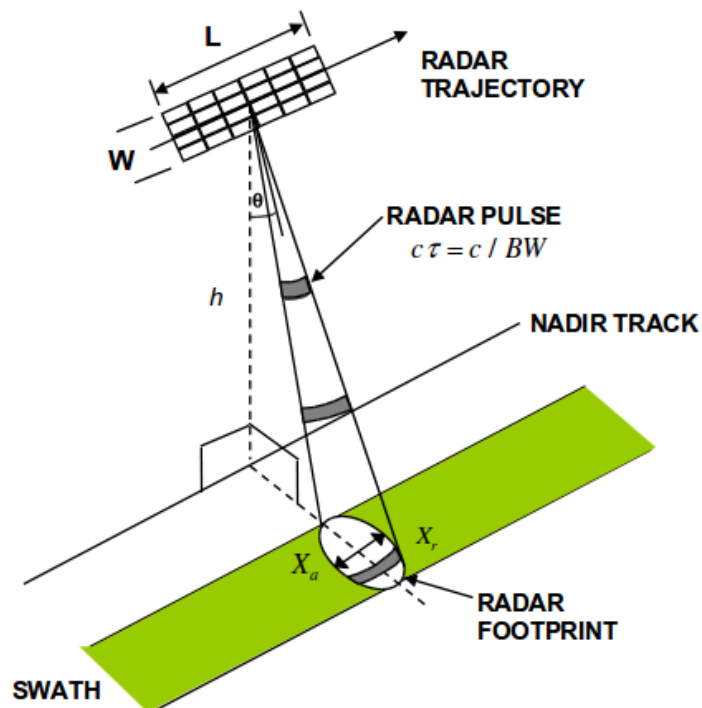
Figure 3.6: *Imaging geometry of a side looking radar (image downloaded from* `http://earth.eo.esa.int`*)*

careful analysis of the phase of the returned radar echoes. Using information on the Doppler shift of the return signals, SAR are able to correctly phase the return signals with respect to each other. SAR are thus able to "listen" to the return signals for longer periods of time, with the effect of all echoes having been received simultaneously by an antenna of length equal to the path length over which the radar signals were collected. For the ASAR instrument onboard Envisat, the length of the synthetic antenna is approximately 20 km. Through the synthetic aperture principle, the azimuth resolution for SAR systems becomes largely independent of target range and improves with a smaller antenna (Robinson [2004]; Samuel et al. [2004]).

Over the ocean, radar echoes are backscattered primarily through Bragg scattering, with the short Bragg-scale waves having similar wavelength to that of the emitted radar pulse (5 to 6 cm for the ASAR C-band radar). The spatial distributions of the short Bragg waves imaged by SARs, also referred to as the sea surface roughness, is affected by a wide variety of oceanographic and atmospheric signals. Variable wind speed, changes in stratification in the

atmospheric boundary layer, swell waves, internal waves, currents and films on the ocean's surface are all factors which influence the distribution of the Bragg waves into patterns which can be recognised in the SAR images (Holt [2004]). SARs provide high resolution imagery of the ocean's surface, independent of light and cloud conditions. SARs are the only instruments in space that can simultaneously provide direct measurements of surface current, wave and wind fields, and their products are used operationally to detect ships and oil spills; to track propagation of swell fields across ocean basins; and to monitor ice motions. The main challenge to the analysis of SAR images for oceanography lies in adequately separating the different oceanographic signatures observed in the images of the sea surface roughness.

3.3.2 Extracting current velocity from ASAR

The principle of surface current measurements from ASAR is similar to that of land-based radar measurement systems and involves the extraction of a line of sight velocity from information contained in the frequency spectrum of the returned radar echoes. The line of sight velocity can then be projected onto a horizontal plane to provide a range-directed surface current velocity. With precise information on the satellite's orbit and the antennae's attitude, it becomes possible to very accurately remove the effect of the motion of the satellite relative to the Earth from the Doppler spectrum. Over the ocean, the resulting Doppler anomaly thus contains information solely related to the motion of the sea surface roughness elements, which reflects the combined action of the wind, waves and current motions. Previous experiments using interferometry have demonstrated the ability of SARs to measure surface currents from airborne platforms (Goldstein and Zebker [1987]; Shemer et al. [1993]; Romeiser et al. [2005]). In 2004, Chapron et al. [2004] proposed a new methodology to derive surface current information from a single SAR antennae. Using the methodology of Chapron et al. [2004] and the Doppler centroid estimates provided by ESA in the metadataset of ASAR Wide Swath Medium (WSM) resolution images (Madsen [1989]; Chang and Curlander [1992]; `http://envisat.esa.int/ handbooks/asar/CNTR2-6.htm#eph.asar.prodalg.levb.alg.descr.dopfreq`), the radar division of Collecte Localisation Satellites (CLS) now processes all ASAR WSM images acquired

over the Agulhas Current region on a systematic basis (Collard et al. [2008]; Johannessen et al. [2008]). For each ASAR WSM acquisition, the Doppler centroid anomaly is extracted from the total Doppler centroid using a geometrical model. The Doppler centroid anomaly is then further processed to compensate along-track large cross section variations (induced by instrumental or signal processing errors) using land surface references. State of the art radar imaging models are required in order to precisely account for the relative influence of the wind, waves and currents on the mean motion of the sea surface roughness elements and its associated Doppler anomaly. Recent studies using both numerical (Johannessen et al. [2008]) and empirical models (Collard et al. [2008]) have shown promising results with range-directed surface current velocities determined with an rms error equivalent to about 0.2 ms^{-1}. The ASAR surface current velocities presented in this thesis are derived using the CDOP neural model network of Collard et al. [2008]. For each ASAR scene, ECMWF re-analysis winds are used in combination with the CDOP model to predict all wave motion contributions dependent on the wind speed and direction, with the exception of wave-current interactions. Previous studies (Mouche et al. [2008]; Johannessen et al. [2005]) have shown that short period waves contribute the most to the Doppler anomaly signal. Since these short waves quickly reach an equilibrium with the winds, most of their contribution to the Doppler anomaly is therefore removed when correcting for the influence of winds on the mean motion of sea surface roughness elements. The derivation of surface current velocities from the Doppler centroid anomaly can then be summarised as a 3-step process: 1) calculating the Doppler centroid anomaly by removing the relative motion of the satellite to the Earth, 2) removing the wind-induced contributions from the total Doppler centroid anomaly and, 3) converting the Doppler centroid anomalies to range-directed surface velocities. The ASAR derived velocities provide a measure of the absolute surface current velocity across the track of the satellite, with positive values indicating a flow moving away from the radar. In this thesis, the velocities derived from the ASAR dataset are referred to as the ASAR range velocities. Over the Agulhas Current region, one descending (morning) and one ascending (evening) ASAR WSM image has been obtained every 3.5 days since July 2007. Near real time range-directed surface current velocities derived from ASAR

34

are freely available for download on the soprano website (`http://soprano.cls.fr`). A total of 472 ascending and 315 descending ASAR WSM images collected between the 2nd of August 2007 and the 10th of September 2009 were used. Figure 3.7 shows the number of observations collected from ASAR in the Agulhas Current on the satellite's ascending and descending paths and over the 2-years period of analysis. The sampling of ASAR range velocities over the Agulhas Current region is not homogeneous, with most of the satellite's image acquisitions occurring between East London and Cape Agulhas (20°E to 28 °E).
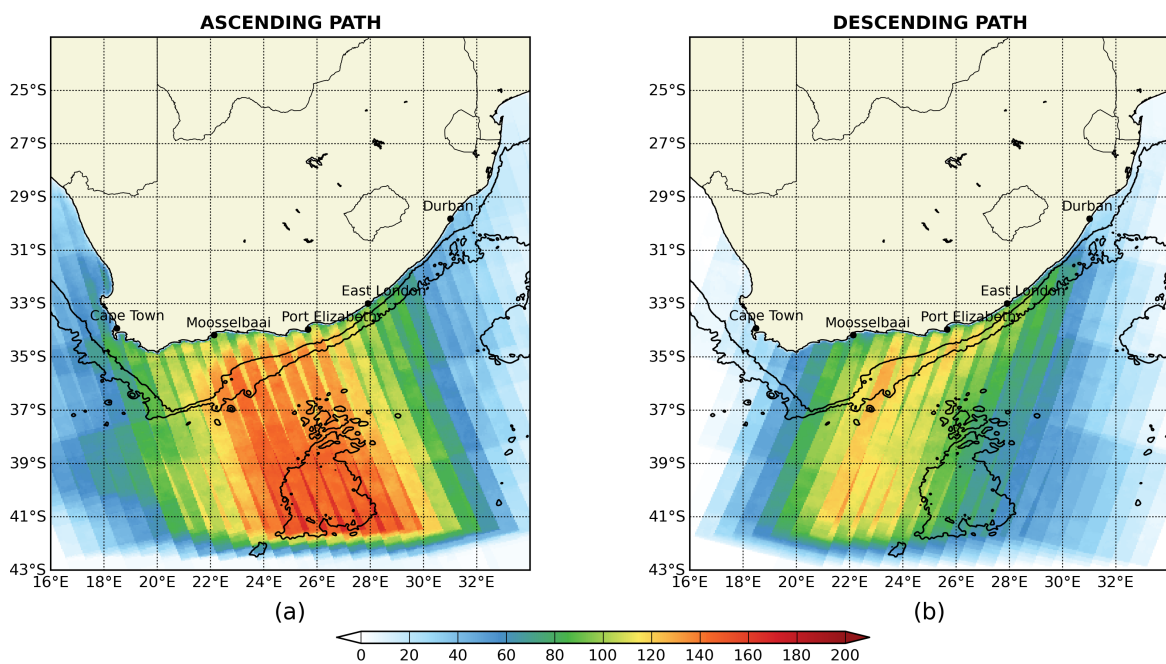
Figure 3.7: *Number of ASAR WSM images collected over the Agulhas Current region between the 2nd of August 2007 and the 10th of September 2009. (a) and (b) show the number of observations obtained during the ENVISAT satellite's ascending and descending paths, respectively.*

4

Mapping Agulhas Current velocities from space

4.1 Introduction

The range-directed surface current velocities derived from ASAR provide a completely new type of information to the scientific community and offer a unique opportunity to further our understanding of the Agulhas Current system, particularly in regions where other remote sensing techniques might be challenged by factors such as land contamination, cloud coverage, isothermal flows or strong ageostrophic flows. This chapter assesses the ability of the ASAR velocities to capture the synoptic surface flow and illustrates how ASAR derived surface current velocities can complement other remote sensing techniques to better portray the highly complex and variable dynamics of the Agulhas Current circulation. In Section 4.3 the potential and limitations of ASAR range velocities are illustrated through comparisons with Lagrangian drifter observations and a model sensitivity study. The ability of both the ASAR velocities and the altimetry to represent the time-averaged circulation of the Agulhas Current system is ad-

dressed in Section 4.3.3. At the end of Section 4.3, two case studies are presented to illustrate the potential use of ASAR derived velocities for oceanographic research. The conclusions of this chapter are drawn in Section 4.4.

4.2   Data and Methods

The region of study encompasses the greater Agulhas Current system, including the Agulhas Current proper, the Agulhas Retroflection and the Agulhas Return Current and is defined as lying within 16^oE - 34^oE and 23^oS - 43^oS (see Figure 3.7). Surface current velocities used in this study are derived from ASAR measurements as well as merged altimetry and Lagrangian drifters datasets. SST data are used to help validate some of the observations seen in the altimetry and ASAR imagery. The SST data is collected from the SEVIRI instrument onboard the MSG-2 satellite and is processed by the French ERS Processing and Archiving Facility (CER-SAT).

An example of ASAR Doppler centroid anomalies and resulting range velocities acquired during one of Envisat's ascending path is given in Figure 4.1. Figure 4.1a shows a Doppler centroid anomaly map generated over the southern Agulhas region for the 8th of May 2008. The colour plot in Figure 4.1b shows ASAR range velocities derived from the Doppler centroid anomaly map of Figure 4.1a, after wind-induced contributions have been removed. The negative surface current velocities (in the green to blue colour range) indicate a flow towards the south-west, while positive velocities (in the yellow to red colour range) indicate a north-easterly surface flow. Shades of green and blue along the Agulhas Bank clearly show the presence of the southward flowing Agulhas Current. The Agulhas Return Current is captured in shades of yellow, further south in the image.

Near real time maps of sea surface height anomalies (NRT-MSLA) are combined with the newly available CNES-CLS09 MDT of Rio and Larnicol [2011] to produce maps of absolute geostrophic current velocity. The NRT-MSLA product consists in a merged dataset of the latest high-quality data produced from the OSTM/Jason-2, Jason-1 and Envisat altime-

ters. It is provided on a rectilinear grid with a spatial resolution of $1/3^o$. Both the CNES-CLS09 MDT and the NRT-MSLA products used in this study are available for download on the Archiving, Validation and Interpretation of Satellite Oceanographic data (AVISO) website (http://www.aviso.oceanobs.com).

Surface Lagrangian drifter data processed in real time mode by the Coriolis data assembly centre (http://www.coriolis.eu.org/cdc/tsg_and_buoy_data.htm) are used to validate the ASAR range velocities. The Lagrangian drifters are surface floats equipped with a holey-sock drogue centred at 15 m. The data collected from such drifters are routinely processed and quality controlled by dedicated data assembly centres. Details of the quality control procedure for the real time drifter buoys can be found in the Argo data manual. For our study, we downloaded all surface Lagrangian drifter data collected from the 31st of July 2007 to the 23rd of April 2009. The criterion for the collocation of the drifter and the ASAR datasets was to retain all drifter data collected within 12 hours of the ASAR image acquisition and then to identify the drifters closest to the ASAR data points within a 5 km radius. After imposing our selection criteria for the ASAR collocations, a total of 53 drifters and 4215 collocations in the region of study were obtained. From these drifter data, only those of best quality and therefore associated with a flag value of 1 were retained. The drifter velocity observations were then projected to obtain a range-directed surface velocity directly comparable to that measured by ASAR.

Figure 4.1b illustrates how AVISO, drifter and ASAR observations of the surface circulation can be compared.

There are significant differences between SAR and altimetry-based observations of surface current velocities. SAR observations provide a direct measurement of the surface current velocity in the radar range direction, while altimetry provides an indirect (geostrophy-based) measurement of the surface flow. In regions of invariant flow, the accuracy of the absolute surface geostrophic currents is therefore strongly dependent on the precision of the selected MDT. SAR and altimetry measurements also differ significantly in their temporal and spatial coverage. While altimetry benefits from a better global coverage, geostrophic currents derived from altimetry can only be obtained along the altimeter's track with repeat cycles varying between
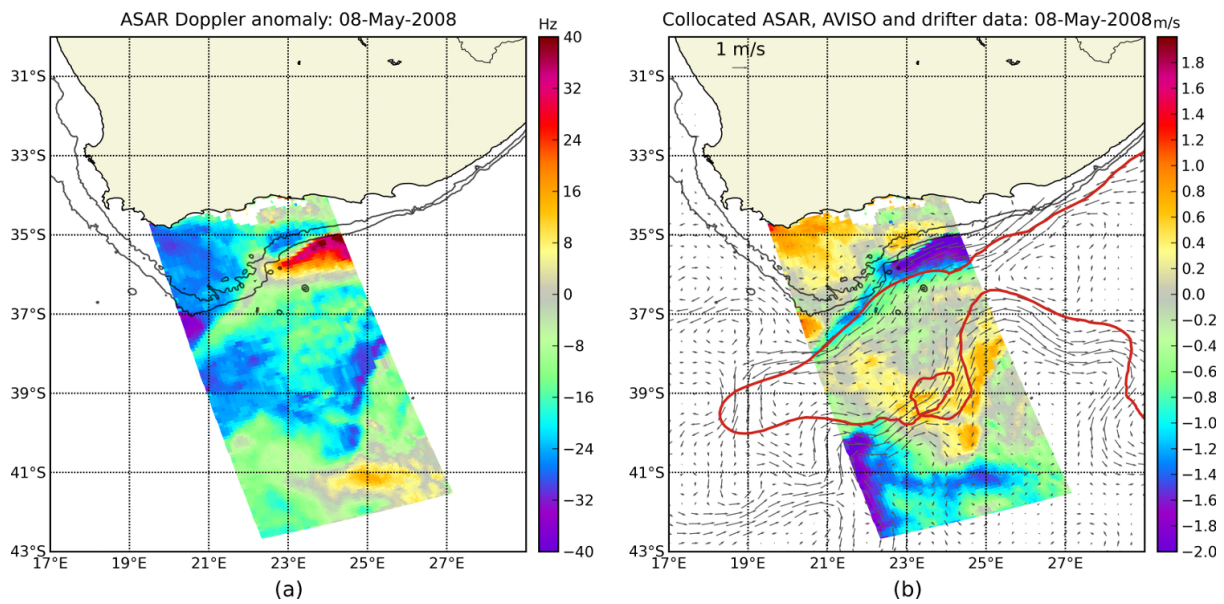
Figure 4.1: *(a) Map of ASAR Doppler centroid anomaly (in Hz) corrected for large along track cross-section variations and biases over land for the 8th of May 2008. (b) Resulting ASAR range-directed surface current velocity in ms^{-1}. Overlaid are vectors of geostrophic velocities derived by combining the CNES-CLS09 MDT to the AVISO NRT-MSLA product of that day. The trajectory of Lagrangian surface drifter no. 14926 between the 9th of June 2008 and the 21st of July 2008 is plotted as a red line. The stippled lines in panels (a) and (b) indicate the positions of the 200 m and 100 m isobaths.*

10 and 35 days. As a consequence, both temporal as well as spatial interpolation are required to produce global maps of geostrophic currents. Although the synoptic representation of the surface circulation as shown in the AVISO dataset is compromised by the spatial and temporal interpolation required to merge data from multiple altimeters, the NRT-MSLA product is the only dataset available which allows direct comparison between the maps of the circulation captured with the altimeters and ASAR, over the length of the ASAR dataset.

4.3 Results and discussion

4.3.1 Comparisons between ASAR and Lagrangian drifters velocities

Direct comparisons between ASAR and drifters velocities provided an effective means of assessing the ability of ASAR range velocities to portray the flow dynamics. From 4215 collocations obtained mainly in the Agulhas Return Current region, the mean bias and rms error between the ASAR and the drifters range velocities was equal to 0.13 m.s^{-1} and 0.56 m.s^{-1}, respectively. It was found that the overall performance of the ASAR surface current velocities was negatively impacted by a few outliers. To illustrate the ability of the ASAR range velocities to represent the observed flow as well as highlight the main sources of discrepancies, we selected to focus our analysis on two drifters (no. 14926 and no. 33681). Comparisons with drifter no. 33681 showed that ASAR was able to capture regions of intense flow, with both ASAR and drifters showing surface range velocities in excess of 1.7 m.s^{-1}. The ability of ASAR to capture strong currents was also apparent in comparisons made with drifter no. 14926 (Figure 4.2b). With drifter no. 14926 however, the initial bias and rms error associated with the ASAR velocities were large due to a few outliers. A careful manual examination of the ASAR images used in the drifter no. 14926 analysis showed that some of the ASAR velocities outliers could be attributed to large rain cells being present at 3 of the collocated data points. Those points are plotted as diamonds in Figure 4.2b. For C-Band radars such as the ASAR, rain drops impinging on the sea surface can cause a local increase or decrease in the amplitude of the Bragg waves measured by the radar (Alpers and Melsheimer [2004]). Such

modifications of the Bragg wave spectrum can result in compromised Doppler centroid estimates. In addition, the localized impact of rain cells on the local wind field (Atlas [1994]) is not captured in current global atmospheric models. In the presence of rain cells, the predicted Doppler shifts associated with the ECMWF winds will therefore be inaccurate and will further contribute to errors in the surface current velocities derived from ASAR. Additional outliers in the ASAR range velocity, plotted as stars in Figure 4.2b, appear to all be associated with low radar incidence angles. In the CDOP neural network model mentioned in Section 3.3.2, Collard et al. [2008] show that at low incidence angles, the returned radar echoes are stronger and dominated by larger and faster roughness elements. As a consequence, the contribution of vertical motions to the measured velocity increases at low radar incidence angles, making the extraction of a surface horizontal velocity from the Doppler centroid anomaly more challenging. The strong relationship between wind strength and short-period waves also implies that the relative impact of the wind on the Doppler anomaly increases with decreasing incidence angle. Due to the inverse relationship between the required wind correction on the Doppler anomaly and the radar incidence angle, inaccuracies in the predicted wind fields will induce larger errors in the ASAR range velocity at low radar incidence angles. Outliers associated with low radar incidence angles have a manifest impact on the ASAR range velocity dataset, as shown in Figure 4.2c. Over the whole study region, deviations from the mean ASAR range velocity are for most data points confined to within 1 m.s^{-1}, with few data points showing deviation from the mean in excess of 2 m.s^{-1}. For incidence angles below 30° however, the ASAR range velocity bias strongly increases, with deviations from the mean sometimes in excess of 4 m.s^{-1}. Although the range velocities derived from ASAR are on occasion able to represent the measured flow with incredible accuracy, the overall performance of the ASAR range velocity product is negatively impacted by a few outliers. These outliers are predominantly encountered at low radar incidence angles and can be attributed mostly to inaccuracies in the predicted wind fields.

(a)

(b)

(c)
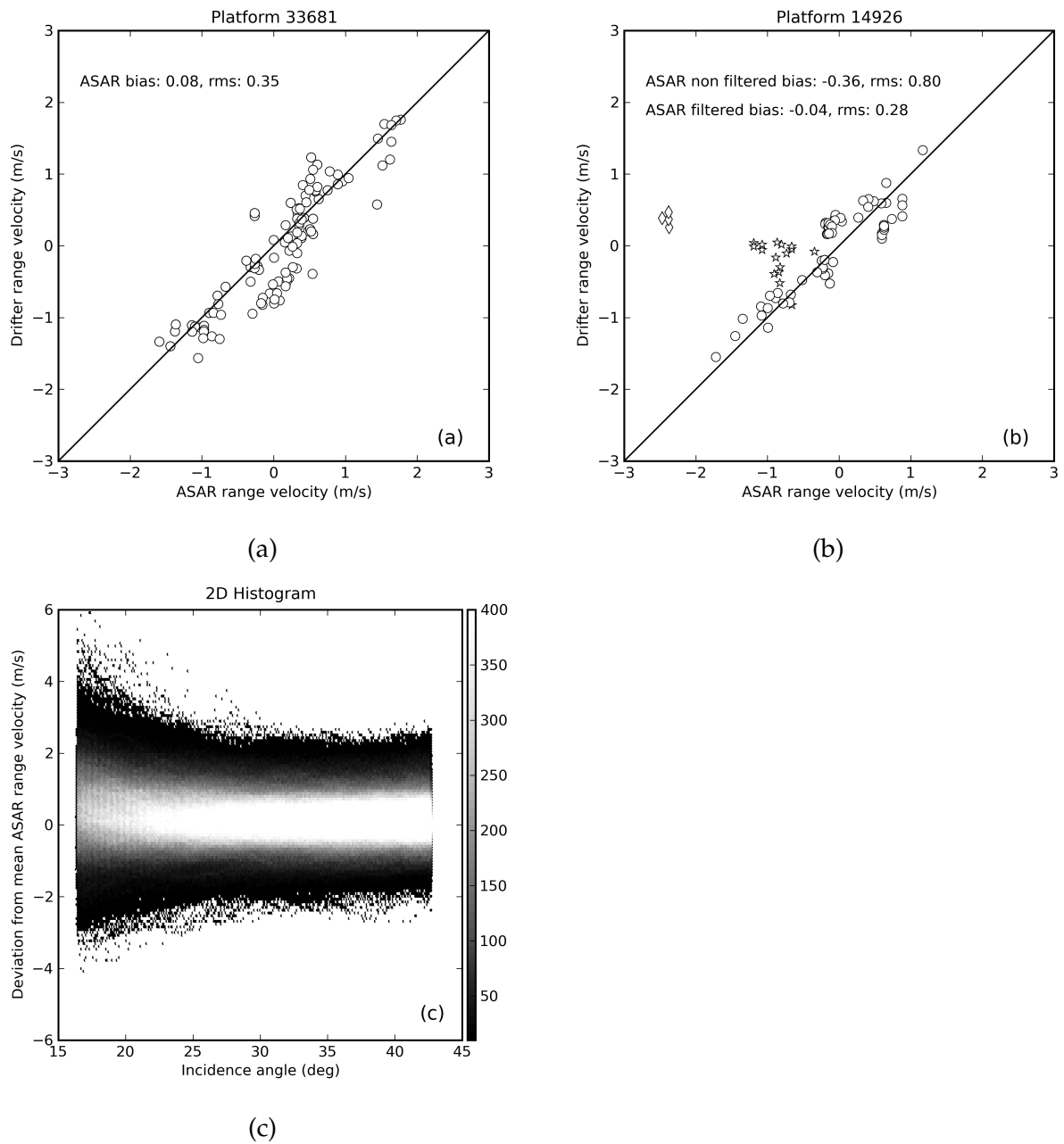
Figure 4.2: *Comparisons between the range-directed component of the ASAR and drifter surface current velocities (in m.s^{-1}) for drifter no. 33681 (a) and drifter no. 14926 (b). In panel (b), diamonds indicate ASAR data points flagged due to large rain cells being present, while the stars are ASAR outliers resulting from inaccurate wind field predictions at low radar incidence angles (less than 30°). Flagged data points have not been included in the calculation of the mean and bias. The two-dimensional histogram in panel (c) shows the relationship between the radar incidence angle and the deviation from the mean computed over the study domain. A larger number of outliers are observed at lower radar incidence angles.*

4.3.2 Sensitivity of ASAR range velocities to inaccurate wind predictions

The relationship between poorly predicted wind fields and errors in the ASAR range veloci-
ties can be better understood through a simple numerical experiment with the CDOP model
developed by Collard et al. [2008]. In our experiment, we first predict the ASAR range velocity
with the CDOP model, using a reference wind of 7 m.s^{-1} blowing in an upwind configuration
(towards the radar antenna). The CDOP model is then used once again to see how devia-
tions in speed and direction from the reference wind affect the predicted range velocity of the
surface current. Errors associated with inaccuracies in the input wind speed are plotted in Fig-
ure 4.3a, while errors associated with inaccuracies in the input wind directions are plotted in
Figure 4.3b. For a constant wind speed, upwind events are associated with stronger Doppler
anomaly signals than downwind events (Collard et al. [2008]). The upwind scenario used in
this model experiment therefore provides an upper-bound estimate of the ASAR range veloc-
ity error for a reference wind speed of 7 $m.s^{-1}$. Comparisons between wind fields measured
from scatterometers and those predicted from global atmospheric models such as ECMWF
have shown typical wind speed differences of about 2 m.s^{-1} and rms errors of about 20° in
the wind direction (Stoffelen and Anderson [1997]; Portabella et al. [2002]). According to Fig-
ure 4.3, each of these wind-induced error would translate into a maximum error in the ASAR
range velocity of about 0.2 m.s^{-1}. What the model clearly highlights is the relationship be-
tween the ASAR surface current velocity error and the radar incidence angle. The outputs
from the CDOP model corroborates the analysis outlined in Figure 4.2c, which showed a sud-
den increase in the ASAR range velocity error below radar incidence angles of 30°. This model
experiment also reveals the sensitivity of the ASAR surface current velocity error to inaccura-
cies in the wind direction, with a potential for small errors in the wind direction to significantly
reduce the accuracy of the estimated surface current velocity in the radar range direction. The
results of the CDOP model experiment emphasise the need for accurate wind predictions or
observations to precisely estimate the velocity of ocean surface currents from SAR observa-
tions.

(a)   (b)
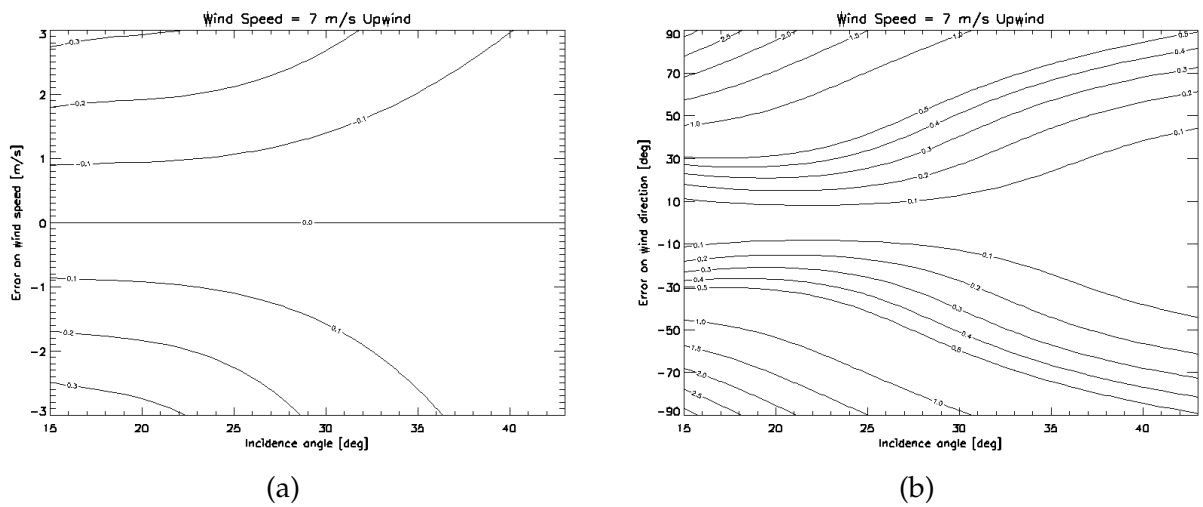
Figure 4.3: *CDOP simulations illustrating the relationship between inaccurate wind field predictions and resulting error in the predicted ASAR surface current velocity, using reference winds blowing in an upwind configuration (toward the radar antenna) at $7m.s^{-1}$. Panel (a) shows contour lines (in $m.s^{-1}$) of the simulated error in range-directed surface current velocity as a function of the incidence angle (x-axis, in °) and wind speed errors (y-axis, in $m.s^{-1}$). Panel (b) shows contour lines (in $m.s^{-1}$) of the simulated error in range-directed surface current velocity as a function of the incidence angle (x-axis in °) and wind direction errors (y-axis, in °). Both panels show an increase in the ASAR surface current velocity error at low radar incidence angles. The ASAR surface current velocity errors are particularly sensitive to inaccuracies in the wind directions.*

An alternative to using ECMWF wind re-analyses when processing ASAR range veloci-
ties would be to use wind vectors directly derived from the ASAR observations. But while
the feasibility of recovering wind speed and directions from SAR observations has long been
demonstrated (Stoffelen and Anderson [1997]; Monaldo and Beal [2004]), the systematic recov-
ery of wind vectors from SAR imagery still presents significant challenges. The main difficulty
lies in the retrieval of wind directions, which are needed to derive wind speed estimates. Sev-
eral methods have been proposed to recover wind directions from SAR observations. These
include using atmospheric forecast models, collocated scatterometers information or linear fea-
tures in the SAR image (Vachon and Dobson [1996]; Horstmann et al. [2004]). Current research
efforts focusing on the retrieval of autonomous wind directions from SAR by combining sea
surface roughness to Doppler information could significantly improve the accuracy of future
SAR surface current velocity products. Based on Figure 4.2c and the results of Section 4.3.2,
one should be particularly vigilant on the accuracy of input wind fields when considering
ASAR surface current velocities associated with radar incidence angles below 30°. For radar
incidence angles greater than 30°, the performance of the ASAR range velocity is expected to
be satisfactory. In the following section, maps of the mean range velocity computed from the
AVISO and ASAR datasets are used to compare the ability of the remote sensing datasets to
capture the mean circulation. ASAR range velocities at radar incidence angles below 30° are
not included in the calculation of the time-averaged maps in an attempt to filter out outliers
observed at low incidence angles.

4.3.3   Representing the mean circulation in the Agulhas Current system with ASAR and altimetry based measurements

Current velocities averaged over all ASAR ascending paths observations collected between
August 2007 and September 2009 (Figure 4.4a) were used to illustrate the potential of ASAR
range velocity measurements to portray the mean dynamics of the Agulhas Current. In an as-
cending path situation, the range velocities extracted from ASAR images are measured along
an axis about 75° from North and are roughly aligned with the main direction of propagation
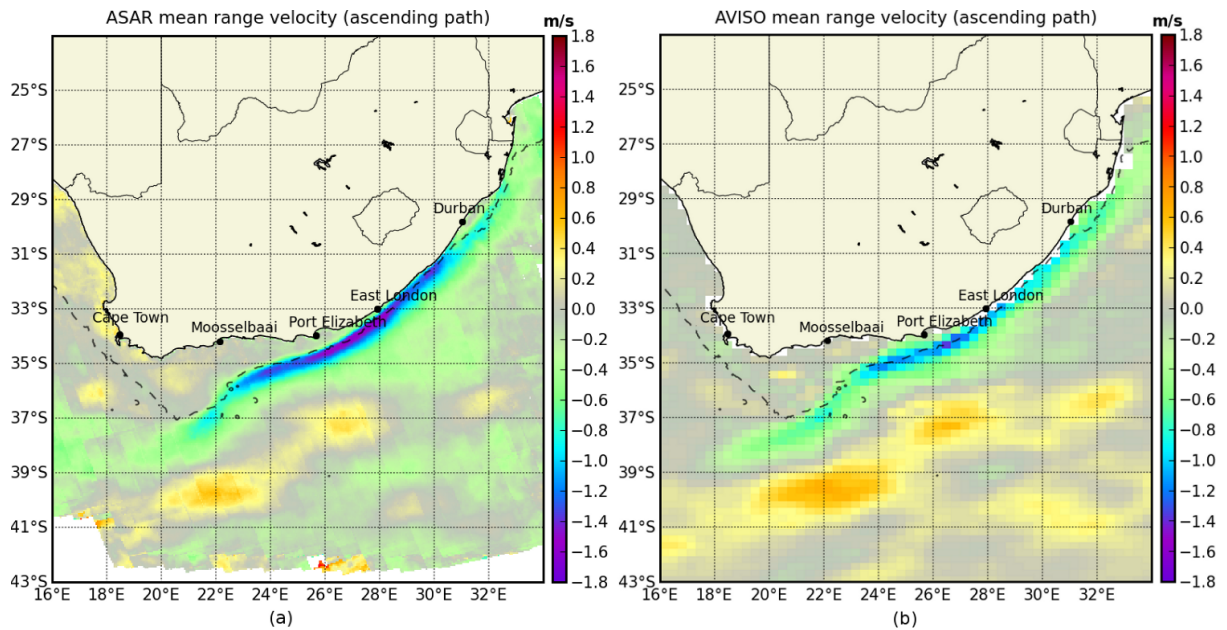
Figure 4.4: *Mean range-directed surface current velocity (in m.s^{-1}) in an ascending path configuration for ASAR (a) and AVISO (b). Positive values indicate a flow towards the north-east, about 75º from North. The ASAR mean was computed from 463 ASAR images collected over the Agulhas Current region, from the 2nd of August 2007 to the 10th of September 2009. Only data points with more than 10 observations and radar incidence angles greater than 30º were included in the calculation of the ASAR mean. AVISO current vectors were rotated in the ASAR directed range velocity. The stippled black line in panels (a) and (b) indicates the position of the 1000 m isobath.*

of the Agulhas Current. The velocities measured in the ascending path mode should therefore closely approximate the absolute speed of the Agulhas surface current. Maps of averaged range-directed surface current velocities computed for an ascending path configuration using both the ASAR and AVISO datasets (Figure 4.4), show that the mean position of the Agulhas Current, the position of its southern extension and the location of the Agulhas Return Current as represented by the AVISO datasets, agree well with those derived from ASAR. The ASAR range velocities in the core of the Agulhas Current exceed those derived from the AVISO datasets. Near Port Elizabeth and in the core of the Agulhas Current, the range velocity derived from ASAR is 1.5 m.s^{-1}, while that obtained by combining the CNES-CLS09 MDT with the AVISO NRT-MSLA is 1.1 m.s^{-1}. Peak range velocities in the Agulhas Return Current are similar for both the ASAR and AVISO datasets.

The properties of the Agulhas Current as portrayed by ASAR are consistent with those

derived from hydrographic surveys and remotely sensed SST maps (Bryden et al. [2005]; Lutjeharms [2006]). In the northern Agulhas region, the mean position of the Agulhas Current core as seen in the ASAR dataset closely follows the 1000 m isobath, in agreement with that derived from a large number of hydrographic sections (Gründlingh [1983]). The mean range velocities derived from ASAR corroborate the findings of Pearce and Grundlingh [1982], who estimated that mean annual current velocities in the northern Agulhas Current system varied between 1.4 m.s^{-1} and 1.6 m.s^{-1}, based on ship drift data. A parallel study (Chapron et al., in progress) which collocates remotely sensed SST with ASAR range velocities, also shows a strong coherency between the position of the maxima in SST and ASAR range velocity in the Agulhas Current, the Retroflection and the Agulhas Return Current regions, further confirming that the ASAR range velocities accurately position regions of intense flow. In the northern Agulhas region, the proximity of the current to the shore and its relatively invariant path make it very difficult for altimeters to accurately capture the mean flow dynamics from sea level anomaly measurements. Byrne and McClean [2008] have shown that in the Agulhas Current system, the steric height dominates the sea level anomaly signal both at the low (less than 20 days) and high frequencies, due to the invariant nature of the current's path (Gründlingh [1983]). As a consequence, in the Agulhas Current proper, an accurate estimate of the absolute geostrophic flow can only be achieved with a precise knowledge of the MDT. The use of the CNES-CLS09 MDT compared to the previously available Rio05 MDT of Rio et al. [2005] significantly improves the portrayal of the Agulhas Current dynamics from altimetry, increasing the peak Agulhas geostrophic current velocities in the Agulhas Current proper from about 0.5 m.s^{-1} to over 1 m.s^{-1} and enabling a better definition of the velocity gradient across the Agulhas Current (see figure 3.5 of chapter 3). The CNES-CLS09 MDT of Rio and Larnicol [2011] is a hybrid MDT, which makes use of extended datasets of drifting buoy velocities (1993-2008) and dynamic heights (1993-2007). In the Agulhas Current, where the MDT dominates the sea surface height signal, the time-averaged circulation obtained by combining the CNES-CLS09 MDT together with maps of sea level anomalies over the period 2007-2009 represents in reality a longer-term average due to the 15 years of in situ data assimilated in the CNES-CLS09

MDT. The time-averaged map of ASAR range velocities accurately captures both the intensity as well as the position of the Agulhas Current. The finer spatial resolution of the ASAR dataset improves the definition of the Agulhas Current's structure, compared to that derived from altimetry. The ASAR range velocities provide a new, independent observation method, which could be used in the future to better monitor year to year changes in the Agulhas Current.

4.3.4 Using ASAR velocities to reveal features of the Agulhas Current circulation

4.3.4.1 Capturing the sub-mesoscale circulation with ASAR

Some of the main advantages of SARs over other satellite remote sensing techniques is that they are able to image the ocean surface at a high spatial resolution, do not suffer from land contamination and can operate independently of cloud conditions. These characteristics make the SAR a promising sensor to study meso- and sub-mesoscale processes (1 to 100 km) and interactions between western boundary currents and the coastal shelf regions. In this section, we illustrate the ability of ASAR-based measurements to capture the smaller features of the circulation, with a case study of shear edge instabilities detected on the 27th of February 2008. The surface circulation revealed by ASAR on that date is compared to that depicted in AVISO and SST maps. In the second part of this section,it is shown that ASAR can consistently image the sub-mesoscale circulation and improve the understanding of the mean variability of the Agulhas Current system. ASAR range velocities measured on the 27th of February 2008 are plotted as colour contours in Figure 4.5a. Positive (yellow to red) range velocities indicate a surface flow towards the east-southeast while negative values (green to blue) are associated with a west-northwest surface flow. Overlaid are geostrophic current vectors obtained by combining the AVISO CNES-CLS09 MDT with the NRT-MSLA product for that day. Figure 4.5b shows the thermal signature of the surface waters derived from SEVIRI SST data collated over the 26th and 27th of February 2008. Two transect lines through the AVISO, SST and ASAR imagery have been extracted along the 20^oE and 23^oE longitudes. The positions of the transects are plotted as red lines in Figure 4.5a. Transect data appear in Figure 4.5c and Figure 4.5d. The

200 m and 1000 m isobaths are plotted as black lines on both Figure 4.5a and Figure 4.5b.

The SST imagery provided an intuitive representation of the surface circulation around the 27th of February 2008. Surface waters with SST signatures of more than 23^oC are plotted in shades of red in Figure 4.5b, and highlight the core of the Agulhas Current, the Agulhas Retroflection (around 16.5^oE and 41^oS) as well as the Agulhas Return Current. The southward flowing Agulhas Current, which roughly followed the 1000 m depth contour, the Retroflection region as well as the circulation associated with the Agulhas Return Current were captured by both the ASAR and AVISO velocity datasets in Figure 4.5a. There is a very good agreement between the patterns of surface circulation displayed in the SST and ASAR imagery. The maps of SST and ASAR range velocities both showed a widening of the Agulhas Current core around 23^oE, followed by a sharp bend southward at 21^oE and a subsequent narrowing of the current between 21^oE and 19^oE (Figure 4.5a and Figure 4.5b). Large ASAR velocities were associated with strong gradients in SST, and regions of local SST maxima in the Agulhas Current coincided with the position of the Agulhas Current core in the ASAR imagery (Figure 4.5c and Figure 4.5d). The surface geostrophic circulation derived by combining the CNES-CLS09 MDT and the NRT-MSLA did not highlight the localised widening or narrowing of the Agulhas Current, which was observed at 23^oE and 21^oE. In the transect extracted at 23^oE (Figure 4.5d), the position the Agulhas Current as seen in the AVISO datasets also appeared too far inshore. The AVISO and ASAR datasets showed strong discrepancies for regions located inshore of the Agulhas Current. The ASAR range velocities highlighted two regions of cyclonic flow inshore the Agulhas Current and centered around 23^oE, 35.5^oS and 20^oE, 37^oS. In the merged altimetry, no flow was detected inshore the Agulhas Current at 20^oE , while at 23^oE the ASAR and altimetry derived surface velocities were in opposite directions. Altimeters can precisely measure anomalies in the sea surface height at a spatial resolution of about 7 km along the satellite's track and are therefore very capable of detecting small shear-edge eddies such as those observed in Figure 4.5. However, the temporal and spatial smoothing required to map geostrophic currents from multiple altimeters implies that small-scale or transient features of the circulation will be misrepresented in merged altimetry products such as the AVISO NRT-
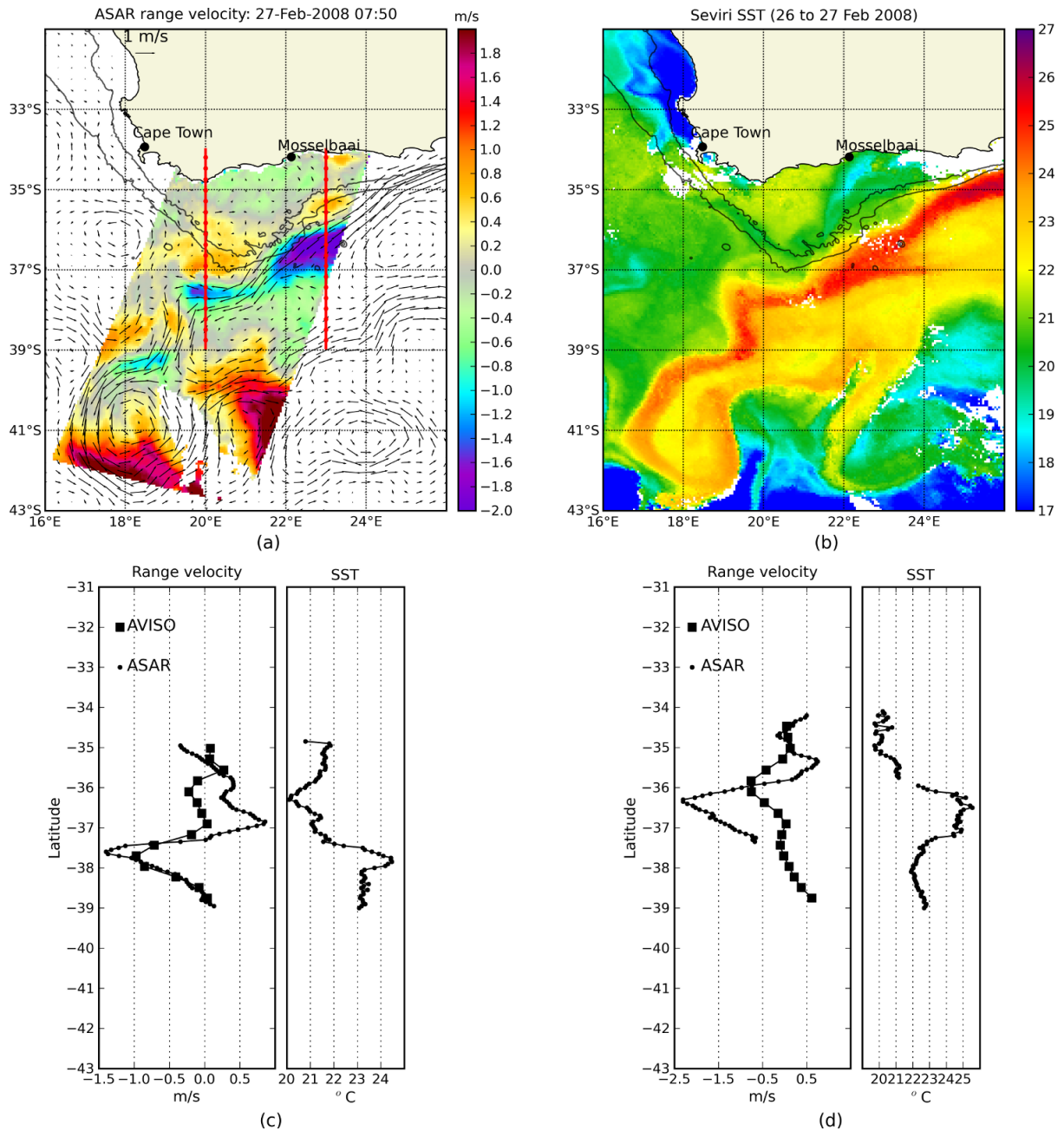
Figure 4.5: *Regions of sharp cyclonic shear and SST gradient located inshore of the Agulhas Current at 23ºE, 35.5ºS and 20ºE, 37ºS evidenced by ASAR and SST datasets on the 26th and 27th of February 2008. In panel (a), color contours of ASAR range-directed surface current velocities (in m.s^{-1}) are plotted with positive values (yellow and red) indicating an eastward flow. Overlaid are vectors of AVISO geostrophic currents on that same day. Panel (b) shows the SEVIRI mean SST (averaged over the 26th and 27th of February 2008). The lower two panels show transects of ASAR range velocity, AVISO range velocity and SST extracted at 20ºE (c) and 23ºE (d) and plotted as red lines in panel (a). Solid black lines in panels (a) and (b) indicate the position of the 200 m and 1000 m isobaths.*

MSLA. At 23°E, the ASAR range-directed velocities showed the presence of a surface counter current extending 60 km inshore of the Agulhas Current and with a width of about 160 km. This eastward flowing surface current is plotted in shades of yellow to orange in Figure 4.5a. Although no well-defined warm water plume could be seen at the southward edge of the cyclonic meander, waters in the across shelf return flow had a distinct SST signature, with SST 1°C warmer than those encountered on the Agulhas Bank and about 3°C cooler that those encountered in the Agulhas Current proper (Figure 4.5d). The maximum velocities measured by ASAR in the counter current reached 0.7 m.s^{-1}. The current velocities derived from ASAR around 23°E are thought to have been largely over-estimated, since the data points between 24°E and 22°E were coincident with low radar incidence angles, and therefore subject to larger errors. The ASAR range velocity at 23°E and in the core of the Agulhas Current peaked to 2.3 m.s^{-1}, a very high value in comparison to the 1 m.s^{-1} previously observed (Lutjeharms [2006]) and modelled (Penven et al. [2001]) in the southern Agulhas Current. The relatively large width of the current at 23°E and the fact that the ASAR range velocities were not aligned with the Agulhas Current flow would also imply that the ASAR range velocities around 23°E should have been well below the 2.3 m.s^{-1} value. Despite the presumably erroneous values derived from the ASAR Doppler anomaly at these low incidence angles, the ASAR range velocity map provided valuable information on the position of the Agulhas Current, its width and the existence of a surface counter flow along the continental shelf edge. It is worth noting that neither the SST nor the merged altimetry imagery provided evidence on the existence of the surface counter flow inshore of the Agulhas Current at 23°E. ASAR velocities at 20°E were coincident with high radar incidence angles ($>$30°) and roughly aligned with the main direction of propagation of the Agulhas Current. Therefore, the ASAR velocities around 20°E should be more representative. Between the 23°E and 20°E longitudes, the distance between the Agulhas Current core and its inshore front (the region of maximum SST and current velocity gradient inshore of the Agulhas Current core) decreased from 60 km to 30 km. The maximum ASAR range velocities at 20°E were 1.4 m.s^{-1} in the Agulhas Current and 0.9 m.s^{-1} in the surface counter flow of the eddy. The meander centered at 20°E had a well defined SST expression,

with a delineated plume of warm Agulhas water originating from the southern edge of the meander seen to loop back in a north-easterly direction towards the current. Based on the SST map in Figure 4.5b, the circumscribed cyclonic border eddy measured approximately 80 km by 220 km along the North/South and East/West directions, respectively. This large border eddy was associated with relatively colder water (Figure 4.5c). Previous studies (Harris et al. [1978]; Lutjeharms et al. [1989]) have shown that shear-edge eddies on the landward side of the Agulhas Current start developing due to an increase in the meandering of the Agulhas Current past Port Elizabeth. The downstream growth in size and strength of the meanders eventually leads to the development of an instability at the leading edge of the meander. This instability takes the form of a warm water plume, which may disperse over the Agulhas Bank or turn towards the current to form a cyclonic eddy (Lutjeharms [2006]). In situ as well as numerical experiments (Lutjeharms et al. [2003b]; Penven et al. [2001]) have suggested that border eddies such as that observed by ASAR at 20°E, eventually separate from the Agulhas Current to move westward into the South Atlantic Ocean. The detachment of these cyclonic eddies from the Agulhas Current has been attributed to the combined effect of the downstream advected cyclonic shear and the poleward termination of the Agulhas Bank, which eventually leads to the eddy separating through a flow detachment process (Penven et al. [2001]). Border eddies such as those captured in the ASAR imagery of the 27th of February 2008 are common features of western boundary currents (Koshlyakov [1986]) and their impact on the productivity of coastal shelf waters has been clearly demonstrated (Lee et al. [1981]). In the southern Agulhas Current, the ubiquitous presence of meanders and shear edge perturbations at the inshore edge of the current induces localized upwelling and contributes to the intensification of the thermocline on the Agulhas Bank through the input of warm Agulhas water in the upper layers (Largier et al. [1992]). Shear edge eddies along the Agulhas Bank also contribute to the transport of Cape Anchovy larvae from the spawning ground of the eastern Agulhas Bank to the nursery grounds of South's Africa west coast upwelling system (Probyn et al. [1995]). A proper quantification and understanding of the border shear edge eddies observed in the southern Agulhas Current is necessary to quantify the coastal shelf exchange as well as the

inter-ocean transport between the Indian and the Atlantic Oceans. Large scale observations of sea surface height variability over the Indian Ocean have always portrayed the Agulhas Retroflection and the Agulhas Return Current as the regions of maximum variability (Cheney et al. [1983]). These regions of high variability are also apparent in the AVISO standard deviation map of surface range velocities (Figure 4.6b). Using over 2 years of data collected over the Agulhas Current region with ASAR, we produced a map of the standard deviation for ASAR range velocities derived over all descending tracks. The descending track configuration lends itself well to capturing fluctuations in current speed at the northern edge of the Agulhas Current as it measures the intensity of the flow along a Northwest/Southeast axis (115° from North). The ASAR map of the standard deviation in range-directed surface current velocities (Figure 4.6a) shows two lines of high variability along the Agulhas Bank between 23^oE and 26.5^oE and from the tip of the Agulhas Bank to the Retroflection (from 18^oE to 21.3^oE). The ASAR dataset shows that the variability along the Agulhas continental shelf between Port Elizabeth and Mossel Bay is just as high as that encountered in the Retroflection region. In the standard deviation map produced from the AVISO datasets, increased variability along the Agulhas Bank is also observed but because the scales of variability along the Agulhas Bank are smaller, they are not always seen and are therefore under-estimated. The high resolution of the ASAR dataset also enables to differentiate between the intensity in variability along the shoreward and the seaward edges of the southern Agulhas Current, with most of the sub-mesoscale activity occurring along the shoreward edge of the Agulhas Current. Standard deviation maps derived for ascending path ASAR configurations (not shown) confirm that the magnitude of the variability in the retroflection region and along the Agulhas Bank are comparable.

4.3.4.2 Imaging the Natal Pulse with ASAR

In an attempt to identify perturbations in the Agulhas Current over the sampling period, a time series of ASAR and AVISO range-directed surface current velocities was extracted at 25.8^oE, 34.7^oS, at a location which corresponds to the mean position of the Agulhas Current core, offshore Port Elizabeth (Figure 4.7). This timeseries was derived using all ASAR ascending path
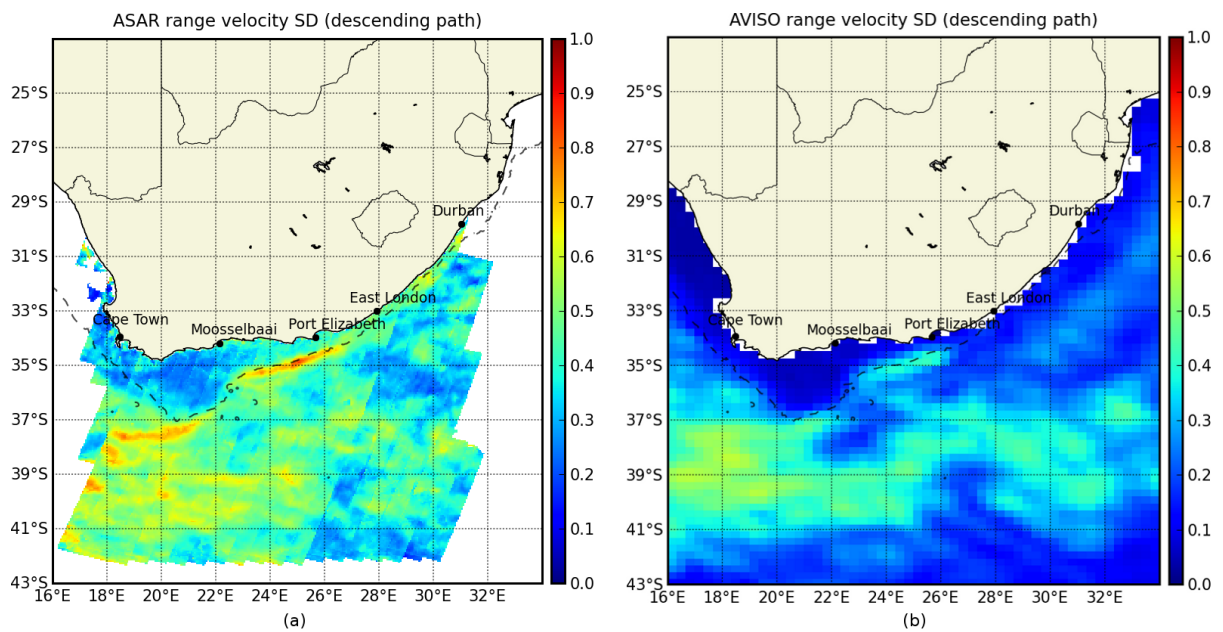
Figure 4.6: *Standard deviation for ASAR (a) and AVISO (b) east/south-east range-directed surface current velocities in a descending path configuration. The ASAR standard deviations were computed from 358 ASAR images collected over the Agulhas Current region, from the 2nd August 2007 to the 10th September 2009. Only data points with more than 10 observations and a radar incidence angle greater than 30° were included in the calculation of the ASAR mean. AVISO current vectors were rotated in the ASAR directed range velocity to simulate a descending path situation. The stippled black line in panels (a) and (b) indicates the position of the 1000 m isobath.*

Figure 4.7: *Fluctuations from the mean ASAR and AVISO range-directed surface current velocities (in m.s^{-1}) at the position of the mean local maxima in the Agulhas Current core, offshore Port Elizabeth (25.8ºE, 34.7ºS). A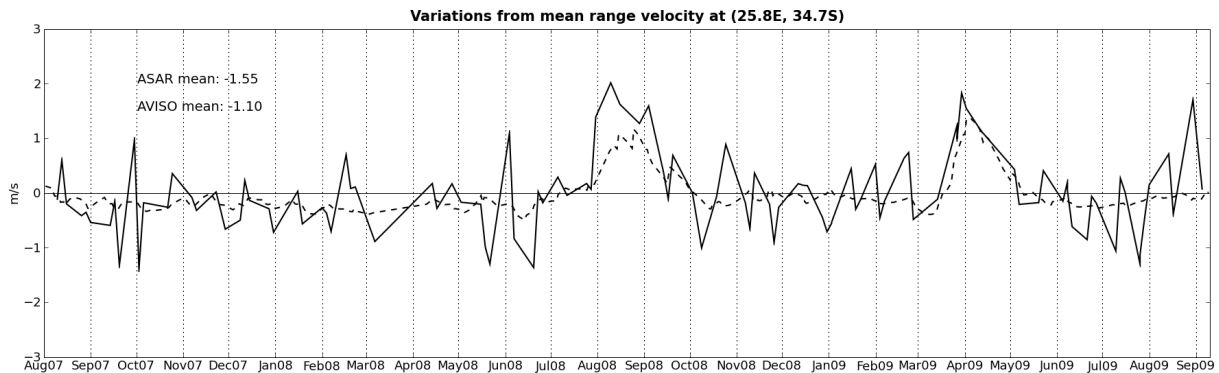SAR range velocities are derived for all ascending path observations collected between August 2007 and September 2009 and are plotted in a solid black line. The range-directed surface current velocities projected for ascending path configurations and calculated by combining the CNES-CLS09 MDT to the AVISO NRT-MSLA daily product are plotted in a dashed line. The largest anomalies in the ASAR and AVISO range velocities were observed in August 2008 and April 2009 and were associated with the passage of Natal Pulses.*

observations, when the surface velocity measured by ASAR is closely aligned with the main direction of propagation of the Agulhas Current. Variations from the mean ASAR range velocities are plotted with a solid black line. The time series of ASAR range velocities at 25.8ºE, 34.7ºS showed rapid and large fluctuations over periods of a few days and throughout the measurement period. Whether these high frequency fluctuations were real or due to "noise" can not be tested due to the absence of in situ measurements in the region. The range velocities derived from the AVISO datasets did not display high frequency modulations. This is due to the temporal as well as spatial smoothing required to produce merged maps of geostrophic currents from sea surface height measurements. Despite these differences, the ASAR and merged altimetry datasets were coherent in their identification of the largest perturbations in the Agulhas Current. Between August 2007 and September 2009 (Figure 4.7), two very large anomalies in the Agulhas Current were detected using the time series of AVISO and ASAR range velocities. These perturbations, which occurred around August 2008 and April 2009 and persisted for a period of about 1 month offshore Port Elizabeth were in each case, associated with the passage of a Natal Pulse.

Natal Pulses have been described as large solitary meanders which move downstream in

the Agulhas Current and find their origin in the Natal Bight (Lutjeharms [2006]). These large perturbations in the Agulhas Current are known to occur at irregular intervals ranging from 50 to 240 days (de Ruijter et al. [1999]) and are thought to dominate the annual variability of the Agulhas Current (Bryden et al. [2005]). Natal Pulses have an influence on both the local and downstream circulation of the Agulhas Current. Figure 4.8a shows the surface temperature distribution offshore Port Elizabeth during the passage of the first Natal Pulse detected in the time series. Colour contours of the ASAR range velocities overlaid with absolute geostrophic currents derived from the merged altimetry around the same period are shown in Figure 4.8b. The Natal pulse observed around the 12th and 13th of August 2008 had a diameter of 150 km. It was associated with a cyclonic circulation with a north-eastward flow of about 0.5 m.s^{-1} along the continental shelf and a south-westerly flow of approximately 0.5 m.s^{-1} in the displaced branch of the Agulhas Current. In the SST imagery (Figure 4.8a), the relatively cooler waters in the centre of the eddy were separated from the coastal inshore waters by a warm water plume originating from the Agulhas Current, while the Agulhas Current constituted the offshore boundary of the eddy. The ASAR range velocity map showed that the surface counter flow along the Agulhas Current's inshore edge extended all the way to the coast. Upstream from the trapped border eddy and close to the shore, ASAR range velocities indicated remnants of a south-westerly flow. In situ observations (Bryden et al. [2005]) have shown that Natal Pulses generate upwelling in the range of 50 m to 100 m near the continental slope. The unique capacity of the Doppler Shift method to provide information on the structure of the currents at the coast could be used in the future to better assess the local impact of Natal Pulses on the coastal ecosystem. Natal Pulses are also thought to play a role in the shedding of Agulhas Rings that move into and across the South Atlantic region (van Leeuwen et al. [2000]). It has been surmised that Natal Pulses may at times affect the downstream circulation of the Agulhas Current is such a way as to induce an early retroflection of the Agulhas Current (Lutjeharms and van Ballegooyen [1988]). The Natal Pulse observed on the 12th of August 2008 was the largest anomaly detected in the ASAR dataset offshore Port Elizabeth between August 2007 and September 2009 and is thought to have contributed to the early retroflection of
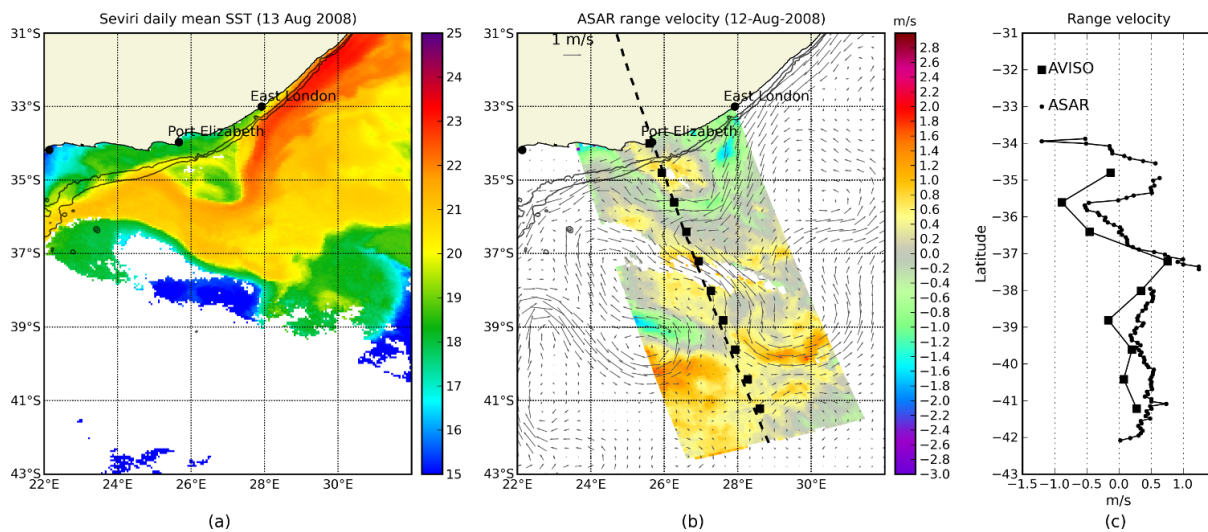
Figure 4.8: *Maps of SST and ASAR range-directed surface current velocity (in m.s^{-1}) during the passage of the Natal pulse are shown in panels (a) and (b). In (b), color contour of ASAR range-directed velocity are overlaid with absolute geostrophic current vectors derived by combining the AVISO MSLA (NRT) product with the CNES-CLS09 MDT. Surface temperature from the Meteosat second generation sensor (panel a) show the presence of a cold water core of 150 km diameter at the inshore edge of the Agulhas Current. Panel (b) shows range velocities derived from ASAR on the 12th of August 2008. Positive values indicate a flow towards the northeast. Negative values are associated with a south-westerly flow. A transect taken across the ASAR image in panel (c) illustrates the ability of ASAR and AVISO to capture the presence of a cyclonic flow, with ASAR providing additional information on the near-shore circulation. Solid black lines in panels (a) and (b) indicate the position of the 200 m and 1000 m isobaths.*

the Agulhas Current around September and October 2008.

4.4 Conclusion

ASAR observations of range-directed surface current velocities derived through the innovative use of the Doppler centroid shift provide a new means of imaging the complex upper ocean dynamics of the Agulhas Current region. The quasi-instantaneous nature of ASAR acquisitions in WSM images combined with the relatively high resolution of ASAR range velocity measurements allow synoptic maps of the Agulhas Current core to be produced for the first time. Comparisons between ASAR and drifter derived range velocities showed that inaccuracies in the magnitude of ASAR surface current velocities generally occur when erroneous wind fields are used for the removal of the wind-induced drift on the overall surface motion. The

impact of inaccurate wind fields on the quality of the derived surface current velocities is particularly pronounced at low radar incidence angles. As a first approach, it was proposed that only radar incidence angles greater than 30° should be used when computing time-averaged maps of ASAR range velocities. Based on our current understanding of the Agulhas Current system, the time-averaged map of ASAR range velocities seemed able to estimate the mean position and intensity of the Agulhas Current remarkably well. The ASAR range velocities provide a relatively direct and independent mode of observation for monitoring the intensity of the Agulhas Current which could be used to infer inter-annual fluctuations in the Agulhas Current transport. One of the main findings of this study was to reveal the importance of sub-mesoscale features in shaping the overall variability of the Agulhas Current system. The ability of ASAR to image fluctuations in the Agulhas Current's path, strength and width, highlight the regions of strong current shear and reveal the occurrence of small shear edge features and eddies, enabled us to show that the magnitude of the variability along the shelf of the Agulhas Bank is comparable to that observed in the Agulhas Retroflection. With an improved map of the Agulhas Current variability comes new considerations on the role sub-mesoscale processes play, not only at the local scales which regulate continental shelf exchange, but also on the larger scale dynamics associated with the Indo-Atlantic exchange. The unique ability of the ASAR range velocities to accurately position regions of strong flow and shear provides new opportunities for oceanographic research in the Agulhas Current and could lead to a better understanding of the Agulhas Current variability, the formation and development of instabilities in the current and the influence of the Agulhas Current on the shelf regions. Significant research effort to improve wind retrieval algorithms from SAR are underway, with the aim of producing wind speed and direction observations independent from the input of existing atmospheric models. The availability of accurate wind observations in the Agulhas Current region would greatly improve the accuracy of ASAR range velocities and could lead to the systematic assimilation of ASAR range velocities in numerical models or to the routine monitoring of Agulhas transport and variability.

5

Tracking the northern Agulhas Current's path

5.1 Introduction

The objective of this chapter is to gain further understanding on the variability of the Agulhas Current at the sub-seasonal time-scale. Previous studies on the Agulhas Current have pointed to the Natal Pulse as the dominant mode of variability north of the Retroflection (Lutjeharms [2006]). Natal Pulses are large meanders found at the inshore edge of the Agulhas Current which originate at the Natal Bight, near 28°S and propagate at the inshore edge of the Agulhas Current with downstream velocities of 10 to 20km/day (Lutjeharms [2006]). These large meanders in the Agulhas Current have been found to occur at irregular intervals (de Ruijter et al. [1999]) with a mean frequency of 4 to 6 per year (Bryden et al. [2005]). The formation, growth and propagating speed of Natal Pulses have been inferred from in-situ measurements (Beal and Bryden [1999]; Bryden et al. [2005]), satellite remote sensing imagery such as sea surface temperature (SST) (Lutjeharms and Roberts [1988]; Lutjeharms et al. [2003b]) or altimetry (de Ruijter et al. [1999]; van Leeuwen et al. [2000]), as well as from numerical mod-

elling experiments (Biastoch et al. [2008b]; Tsugawa and Hasumi [2010]). In Chapters 3 and 4, we highlighted some of the capabilities and limitations of altimetry and ASAR observations for imaging the circulation of the Agulhas Current. It was noted in Chapter 3 that the use of altimetry in the coastal regions poses serious challenges due to factors such as land contamination, atmospheric errors or inaccuracies in the estimation of the MDT, which result in the loss of data typically 50 km from the coast (Vignudelli et al. [2011]; Vignudelli et al. [2008b]; Madsen et al. [2007]). In the northern Agulhas Current, where Natal Pulses originate, observations from altimetry are compromised due to the close proximity of the Current to the shore. The spatial and temporal averaging required to map ocean currents from altimetry also implies that transient meso-scale features such as Natal Pulses might not be adequately resolved by altimetry (as noted in the Section 4.3.4.1 of Chapter 4). While ASAR range velocities might seem a good alternative to altimetry for tracking and following meso-scale perturbations from the northern to the southern Agulhas Current, ASAR range velocities still suffer from inaccurate wind corrections and the number of ASAR image acquisitions in the northern Agulhas is limited (see Figure 3.7). Case studies in Chapter 4 showed a good agreement between the pattern of circulation revealed in the ASAR and SEVIRI SST imagery. In this chapter, we have therefore decided to use the high frequency SST imagery collected from the SEVIRI to track perturbations in the northern Agulhas Current and follow their evolution as they progress downstream from the northern Natal Bight to Port Elizabeth. The focus of this chapter is not so much on the origin of perturbations in the northern Agulhas or the generation of Natal Pulses, but rather on the evolution of these perturbations downstream and on the variability of the northern Agulhas Current. Synoptic observations of the northern Agulhas Current at a high frequency show that a number of non-linear processes can occur at the Agulhas Current inshore front. The Seviri SST imagery provides some new insights on the variability of the northern Agulhas Current and on the nature of Natal Pulses. The data and methodology used in this study are presented in Section 5.2. In Section 5.3, we use both case studies as well as time-series of the position of the Agulhas Current's inshore front derived at 6 transects to characterise Natal Pulses and further our understanding of the northern Agulhas Current variability. The results

of the study are discussed in Section 5.4, followed by a summary in Section 5.5.

5.2 Data and Method

SST data collected from the SEVIRI instrument onboard the MSG-2 geostationary satellite are used to identify examples of instabilities in the northern Agulhas Current as well as derive time-series of the position of the Agulhas Current's inshore front across 6 transects. The region of study and the positions of the selected transects appears in Figure 5.1a. The transects, located between 29°S and 34°S, are referred to as the Natal Bight North, Natal Bight, Natal Bight South, Port Edward, East London and Port Elizabeth transects. The SST dataset used for our analysis consists of the Ocean and Sea Ice Satellite Application Facility (OSI-SAF) experimental hourly SST product (www.osi-saf.org), available on a 0.05° grid ($\simeq$ 5 km) and processed by the French ERS Processing and Archiving Facility (CERSAT). All analysis are undertaken using the de-clouded SST with no additional flag applied. More than 6 years of hourly SST data collected between the 1st of June 2004 and the 19th of October 2010 are used to derive time-series of the position of the Agulhas Current's inshore front. All case studies presented in the paper are based on daily composite maps derived from the hourly SST imagery. The time-series analysis is conducted using 3-day moving averages of SST, centred on the day of acquisition and with weights values of [1,3,1].

Like other western boundary currents, the Agulhas Current is an intense and narrow flow characterised by strong velocity gradients and a central warm core, with isopycnal lines sloping steeply towards the coast (Goschen and Schumann [1990]; Casal et al. [2009]; Bryden et al. [2005]). In the northern Agulhas, large SST gradients are encountered between the Agulhas Current and coastal and shelf waters (Lutjeharms [2006]). This is particularly true off the Natal Bight and Port Elizabeth regions, where the Agulhas Current drives a semi-permanent upwelling circulation (Rouault et al. [1995]; Lutjeharms [2006]). The distinct thermal signature of the Agulhas Current as well as the large SST gradients at its inshore boundary should make SST a suitable tracer for tracking the path of the Agulhas Current's inshore front. The
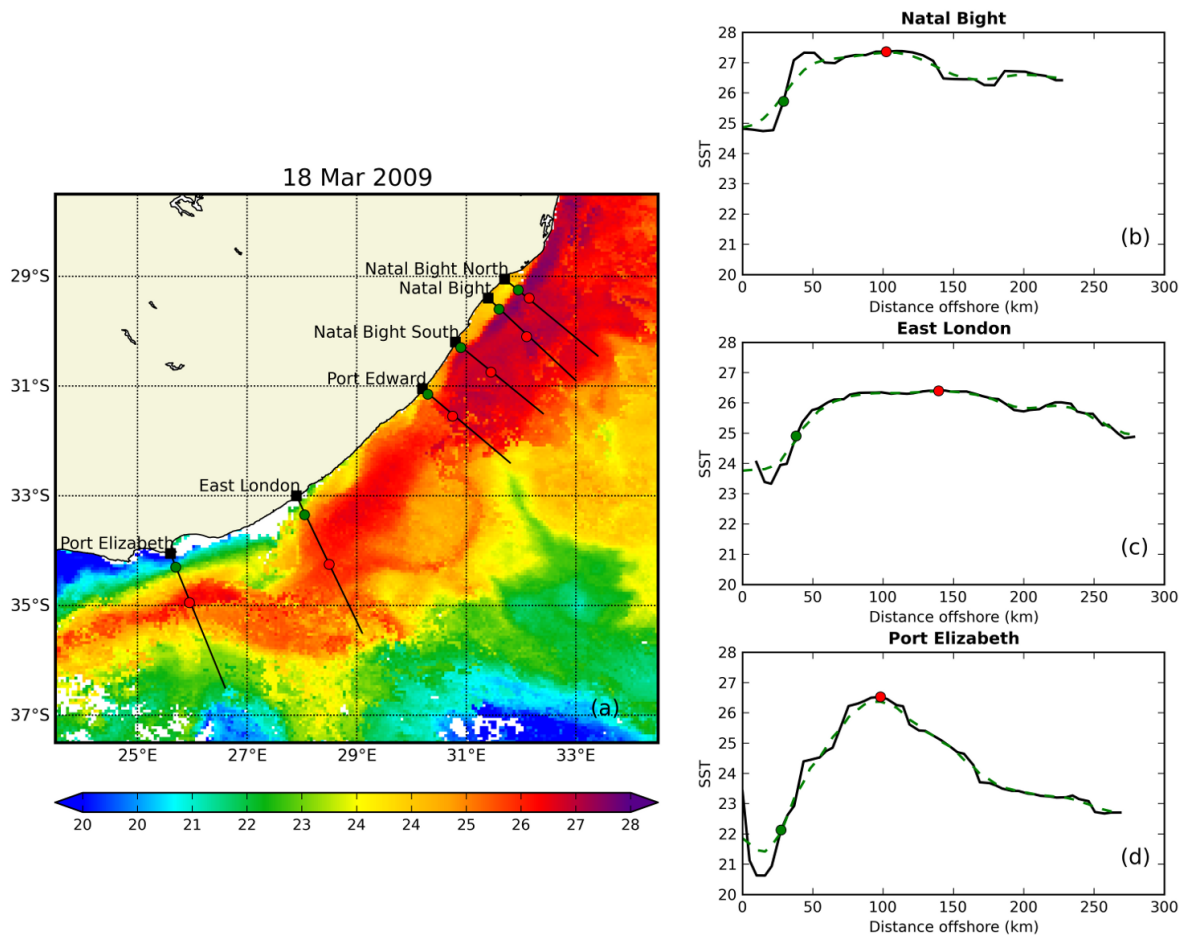
Figure 5.1: *Example of output from the Agulhas front-detection algorithm applied on a 3-day average map of SST centred around the 18th of March 2009. (a) Shows a colour contour map of SST over the region of study. The position of the Agulhas Current was tracked along 6 transects plotted as thin black lines and referenced to as Natal Bight North, Natal Bight, Natal Bight South, Port Edward, East London and Port Elizabeth. The position of the Agulhas Current core detected using the algorithm is plotted with a red dot while a green dot shows the position of the detected Agulhas Current inshore front. SST as well as the identified Agulhas Current core and inshore front positions are plotted for 3 selected transects at the Natal Bight (b), East London (c) and Port Elizabeth (d). The solid black lines in (b), (c) and (d) correspond to the SST along the transect while the stippled green line shows the smoothed SST profiles used for the estimation of the Agulhas Current core's position.*

method for the inshore front-detection algorithm involves deriving an approximate position for the Agulhas Current core and then searching for the current's inshore boundary between the estimated core position and the coastline. SST values are extracted from the 3-day average maps in a band of 15 km around the transect lines. The median over the width of the SST band is then computed prior to searching for the positions of the Agulhas Current core and inshore front. Before searching for the Agulhas Current core, SST transects are smoothed with a Gaussian filter of sigma value 2 to remove large spikes. All local SST maxima encountered over a 50 km moving window are identified and the local maximum associated with the largest SST is then selected as the point where the Agulhas Current core lies. For the position of the Agulhas Current inshore front, all local maxima in the SST gradient and over 75 km moving windows are identified. The local peak associated with the largest SST gradient and located closest to the Agulhas Current core is then selected as the position of the inshore front. When no local maxima are found within the transect, absolute maxima are selected. In the search for the Agulhas Current's inshore front position, minimal smoothing with a Gaussian filter of sigma value 1 is undertaken to avoid removing the gradients all together. Window lengths for the algorithm are selected to capture SST features associated with the Agulhas Current, such as the doming of the SST at the center of the Agulhas Current or the sharp increase in SST at the Agulhas Current front followed by its slow decrease to beyond the current core. Both the window size and smoothing criterion are set with the aim to minimize the selection of spikes, small patches of warm or cold water or large homogeneous water bodies. The size of the moving window does not impact on the scale of the Natal Pulses which can be identified by the algorithm. An example of algorithm output for the 3-day composite map of the 18th of March 2009 is provided in Figure 5.1.

In our analysis of the Agulhas Current's front movements, Natal Pulses are defined as excursions in the path of the Agulhas's inshore front exceeding 30 km from the mean in the 10-day low-passed time-series. The Natal Pulses detected in the time-series are therefore selected using only two simple criteria: 1) that the Agulhas Current inshore front meander more than 30 km from its mean position and 2) that the Natal Pulse lasts for a period of 10 days or

more. The region of origin, the direction of propagation of the perturbations or the existence of an inshore cyclonic circulation, are not taken into account when identifying Natal Pulses. Any offshore meander observed at the inshore front and which does not qualify as a Natal Pulse according to our criteria is simply referred to as an offshore meander. The threshold of 30 km selected for the detection of Natal Pulses is chosen based on a previous study which reported that Natal Pulses grow from about 30 km in the Natal Bight to 200 km or more (van Leeuwen et al. [2000]). In their analysis of in-situ measurements off Port Edward, Bryden et al. [2005] found that the average time-scale associated with alongshore fluctuations in the Agulhas Current was 10.2 days, with Natal Pulses lasting between 50 and 70 days. Currently, observations combining several altimeters are able to observe mesoscale features of the ocean circulation at a sampling period of about 10 days (LeTraon and Dibarboure [2002]). The selection of a 10-day low-pass filter therefore seems appropriate for the detection of Natal Pulses and allows us to better compare our results with previous observations of Natal Pulses from altimetry.

The effects of varying the 30 km size threshold or the 10-day cut-off period of the low-pass filter on the number of Natal Pulses detected along each transect were addressed in a sensitivity study. The number of Natal Pulses detected at each of the transects using size thresholds of 20, 30 and 40 km was determined. The effect of varying the low-pass cut-off period from 7 to 14 days was also addressed. The sensitivity study shows that changing the properties of the low-pass filter or the size threshold for the detection of Natal Pulses impacts on the number of Natal Pulses detected at most transects. The detection of Natal Pulses along each transect is most sensitive to a lowering of the size threshold from 30 km to 20 km. The northern Natal Bight, Natal Bight and Southern Natal Bight transects, all located in the region of origin of the Natal Pulses, show marked increases in the number of Natal Pulses detected when lowering the size threshold from 30 km to 20 km. The tendency of Natal Pulses to grow downstream from their region of origin implies that the Natal Pulse detection algorithm becomes less and less sensitive to a lowering of the size threshold south of the Natal Bight South transect, with little or no change in the number of Natal Pulses estimated at the East London and Port Elizabeth transects.

Absolute geostrophic current velocities are used to support the analysis conducted on the SST data. The absolute geostrophic currents are derived by combining Maps of Sea Level Anomaly (MSLA) produced by AVISO to the CNES-CLS09 Mean Dynamic Topography (MDT) of Rio and Larnicol [2011]. The MSLA consist in a merged dataset of the latest sea surface height measurements available from the OSTM/Jason-2, Jason-1 and Envisat altimeters. It is provided on a rectilinear grid with a $1/3°$ spatial resolution. The derivation of the CNES-CLS09 MDT involves similar methods to those described in Rio et al. [2005], but benefits from the assimilation of extended datasets of drifting buoy velocities (1993-2008) and dynamic heights (1993-2007). The CNES-CLS09 MDT enables a better definition of the velocity gradient across the Agulhas Current and improves the portrayal of the Agulhas Current dynamics from altimetry (Rouault et al. [2010]). The AVISO product suffers from the same limitations as other altimetry dataset and is not be expected to provide accurate measurements near the coast (within 50 km) or to resolve the meso-scale circulation over periods of less than 10 days. In the case studies presented in Sections 5.3.1.1, 5.3.1.2 and 5.3.1.3, the AVISO near real-time product (NRT) is used as an indication of the general oceanic circulation and offshore mesoscale activity. At the Port Elizabeth section, where the current lies furthest to the shore, the delayed time (DT) AVISO product (completed with weekly values extracted from the NRT product from the 31st of March 2010 onwards) is used to support our analysis.

5.3 Results

5.3.1 Instabilities at the Agulhas Current front

The Seviri SST imagery reveals a number of meso and sub-mesocale processes at the inshore front of the Agulhas Current. Some of the instabilities observed include oscillations along the inshore boundary of the current, plumes and frontal eddies. Most of the instabilities observed at the inshore front of the Agulhas Current seem to develop during the downstream propagation of Natal Pulses along the Agulhas Current's edge. While the origin and offshore extent of the Natal Pulses may vary, the triggering of instabilities associated with the downstream

progression of Natal Pulses seem to follow one common pattern. Section 5.3.1.1 provides an example of the initial stages of development of an Agulhas inshore front instability during the passage of a Natal Pulse. In Sections 5.3.1.1, 5.3.1.2 and 5.3.1.3, different scenarios for the evolutions of instabilities at the Agulhas Current's inshore boundary are show-cased. The three case studies selected for this paper are aimed to provide an overview of the different modes of evolution for the instabilities observed at the Agulhas Current inshore front.

5.3.1.1   Meander dissipation

Figure 5.2 shows an example of instabilities observed at the Agulhas Current's inshore front between Port Edward and East London. In mid-May 2007, an anti-cyclonic eddy originating from the East Madagascar Current reaches the waters offshore the Natal Bight and triggers the development of a Natal Pulse around the 15th of May 2007 (not shown) in a manner similar to that previously described by Schouten et al. [2002]. By the 4th of June 2007, the small Natal Pulse has moved southward and can be seen at 29.5°E and 32.5°S in Figure 5.2a. Part of the anti-cyclonic eddy responsible for triggering the Natal Pulse appears in shades of grey in Figure 5.2a, between 31°S and 32°S.

The oscillation associated with this Natal Pulse is clearly visible when looking at the 23°C isotherm, plotted as a red contour line in Figure 5.2. The trailing edge of the Natal Pulse (located at about 29.6°E, 31.8°S), starts interacting with the shelf, generating a small offshore meander upstream. By the 7th of June 2007, the upstream instability resulting from the interaction of the Natal Pulse with the topography has evolved into a secondary offshore meander of similar amplitude to that of the original Natal Pulse (Figure 5.2b). The SST composite map of the 10th of June 2007 (Figure 5.2c) shows that after 3 days, the initial Natal Pulse has significantly shrunk in size and has progressed just south of East London. In the mean time, the secondary offshore meander upstream of the initial Natal Pulse has remained fairly stationary and has grown in amplitude. The SST imagery collected on the 13th June 2007 (Figure 5.2d) shows that the initial Natal Pulse perturbation has dissipated. Its progress downstream to 27.2°E, 33.7°S can only be evaluated thanks to the presence of relatively cooler water on the shelf. By contrast,

the secondary upstream offshore meander has expanded further, now approximating 90 km in diameter. It is this secondary offshore meander, which on the 5th of July 2007, is detected as a Natal Pulse near Port Elizabeth. To be noted is the presence of an anti-cyclonic flow at the offshore boundary of the Agulhas Current from the 4th to the 13th of June 2007. The growth of the secondary offshore meander from the 10th to the 13th of June 2007 occurs during a period of intensification in the offshore anti-cyclonic circulation (Figure 5.2c and Figure 5.2d).

Observations of Seviri SST maps show that on their journey from the Natal Bight to Port Elizabeth, Natal Pulses systematically interact with the coastal topography to generate upstream perturbations. These upstream offshore meanders occur when the trailing edge of the original Natal Pulse comes in close proximity to the shore. During the initial phase of development of the upstream meander, a warm water plume of Agulhas Current water flowing northward along the coastal region is commonly found. Interactions between Natal Pulses and the topography were observed at multiple locations between the Natal Bight and Port Elizabeth, with each Natal Pulse often generating upstream instabilities more than once on their downstream course to Port Elizabeth. Characterising and quantifying the upstream meanders formed during the passage of Natal Pulses is difficult as they vary in size, occur over short time scales and develop sporadically over the northern Agulhas Current region. The fate of these secondary upstream meanders also varies. The meanders might flatten in shape and dissipate while others such as that presented in Figure 5.2, might grow in size and propagate southward as separate perturbations in the Agulhas Current. On other occasions, the secondary upstream offshore meanders progress downstream to later re-merge with the Natal Pulse initially responsible for their inception. Section 5.3.1.2 provides such an example of merging instabilities at the Agulhas Current's inshore front.

5.3.1.2 Meander merging

Interactions between successive offshore meanders can lead to intricate structures at the Agulhas Current's inshore front such as that observed in the SST imagery of Figure 5.3. On the 18th of February 2009, a large Natal Pulse centred at 31°E, 33°S between Port Edward and East
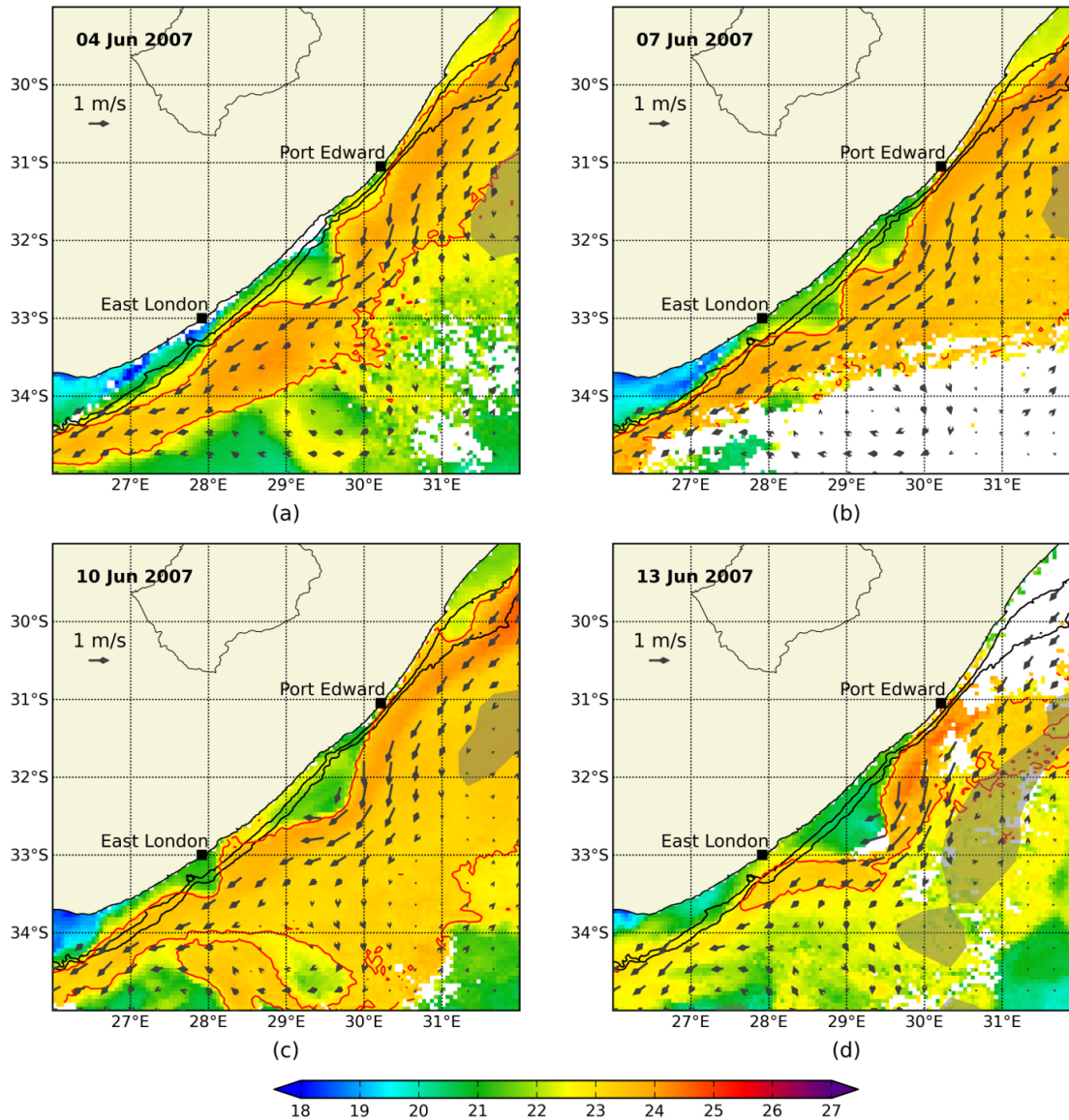
Figure 5.2: *SST daily composite maps showing the development of an upstream perturbation during the passage of a Natal Pulse between Port Edward and East London. The red contour line marks the position of the 23°C isotherm. Overlaid are absolute geostrophic current vectors derived by combining the AVISO MSLA (NRT) product with the CNES-CLS09 MDT. The shaded areas provide an indication of the presence of anticyclonic flow east of the Agulhas Current. The positions of the 200 m and 1000 m isobaths are plotted as black contour lines.*

London is observed (Figure 5.3a). Warm surface waters originating from the Agulhas Current have entrapped cooler coastal waters in a cyclonic circulation. Absolute geostrophic current associated with the Natal Pulse are around 1 m.s^{-1}. On the 26th of February 2009 (Figure 5.3b), the Natal Pulse has become elliptical in shape and is now situated at 30°E, 34°S. The Agulhas front shows oscillatory motions upstream of the Natal Pulse. In particular, one cyclonic offshore meander has progressed downstream to 29.5°E, 32.5°S, directly south of the original Natal Pulse. By the 3rd of March 2009 (Figure 5.3c), both the Natal Pulse and the offshore meander directly upstream of it have merged near East London to form one large Natal Pulse centred at 29°E, 33.5°S. This large Natal Pulse will further continue downstream to reach Port Elizabeth in early April 2009. Between the 18th of February and the 3rd of March 2009, an anticyclonic eddy interacts with the offshore boundary of the Natal Pulse. Figure 5.3 shows that secondary offshore meanders formed during the passage of a Natal Pulse can in turn grow and generate their own upstream instability. What follows is a train of meanders in the path of the initial Natal Pulse perturbation, as shown in Figure 5.3b, where the first of the upstream generated offshore meander centred at 29.5°E, 32.5°S is followed by two small upstream perturbations, with the first one located directly offshore Port Edward and a second perturbation visible in the Natal Bight.

5.3.1.3 Meander occlusion

Occasionally, Natal Pulses become so unstable that they develop an enclosed cyclonic eddy which detaches from the Agulhas Current to move further offshore. Over more than 6 years of observations, the detachment of an offshore meander from the Agulhas Current was observed on only two occasions. The first observation of an eddy occlusion event occurred off the Natal Bight in January 2005 (not shown). The other case of an offshore meander detaching from the Agulhas Current occurred in July 2008, during the development of the largest Natal Pulse identified near Port Elizabeth over the June 2004 to December 2010 period. The evolution and eventual detachment of the July 2008 offshore meander is shown in Figure 5.4. On the 5th of July 2008 (Figure 5.4a), a Natal Pulse is observed at 30°E, 33.5°S. An offshore meander centred
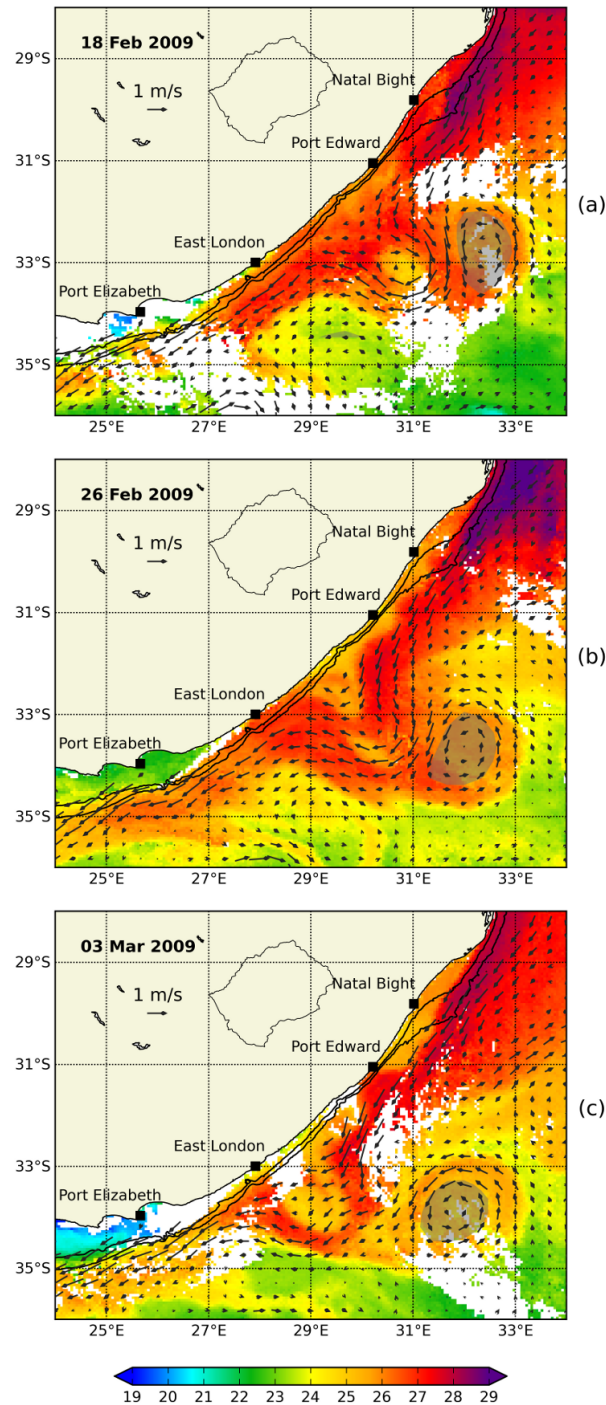
Figure 5.3: *Example of merging meanders revealed from daily SST composite maps in February and March 2009. A large Natal Pulse centred at 31°E, 33°S (a) merges with an upstream instability located at 29.5°E, 32.5°S in (b) and evolves into a single cyclonic meander in (c). Overlaid are absolute geostrophic current vectors derived by combining the AVISO MSLA (NRT) product with the CNES-CLS09 MDT. The shaded areas in (a), (b) and (c) are an indication of the presence of an anticyclonic eddy east of the Agulhas Current. The positions of the 200 m and 1000 m isobaths are plotted as black contour lines.*
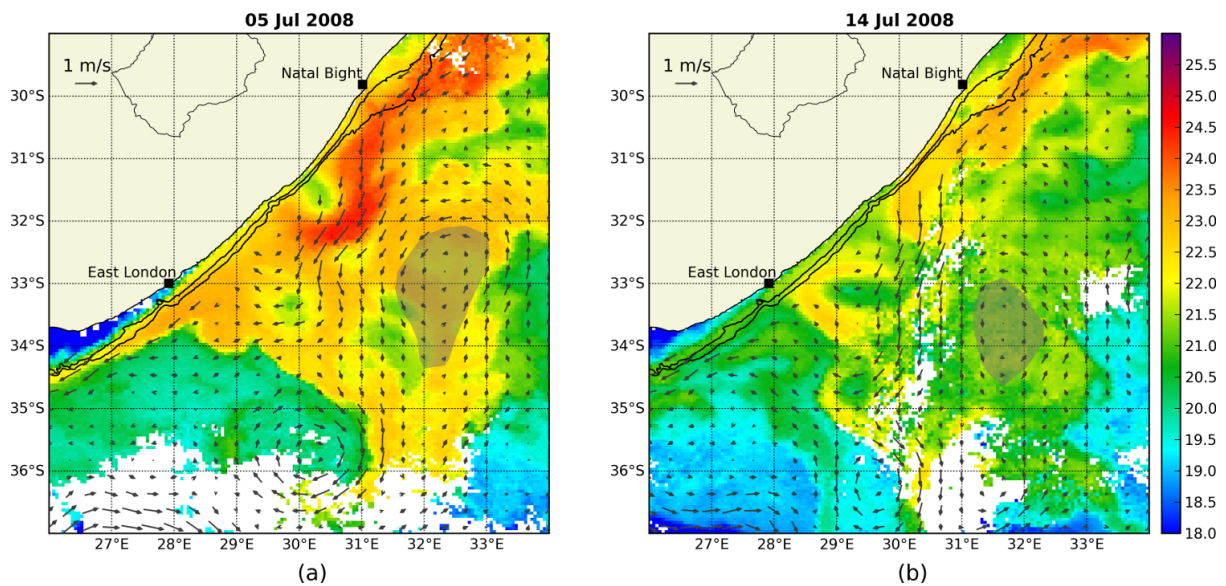
Figure 5.4: *Evidence of Natal Pulse detachment revealed from daily SST composite maps in July 2008. Colour contours of SST are overlaid with absolute geostrophic current vectors derived by combining the AVISO MSLA (NRT) product with the CNES-CLS09 MDT. A Natal pulse initially observed at $30°E$, $33.5°S$ on the 5th of July 2008 becomes an occluded cyclonic eddy and separates from the Agulhas Current. On the 14th of July 2008, the occluded eddy has progressed to $29.3°E$, $34.7°S$. The shaded areas provide an indication of the presence of anticyclonic flow east of the Agulhas Current. The positions of the 200 m and 1000 m isobaths are plotted as black contour lines.*

at $30.2°E$, $31.5°S$ can also be seen upstream of the Natal Pulse. Both the Natal Pulse and the upstream meander are associated with a belt of warm Agulhas water ($> 22°C$) surrounding a core of cooler water ($\simeq 20°C$) of coastal origin. The SST map derived on the 14th of July 2008 shows that the upstream meander has progressed downstream to $29.7°E$, $33°S$. This upstream meander has grown three-fold within 1 week and is now associated with a well-defined cyclonic circulation. Shades of yellow associated with the $22°C$ SST contour show warm Agulhas water looping back in a cyclonic motion just offshore East London. Over the same period, the original Natal Pulse has moved to $29.3°E$, $34.7°S$ and has become an enclosed cyclonic eddy, separated from the Agulhas Current. To be noted is the presence of an anti-cyclonic eddy which moves downstream at the offshore boundary of the Natal Pulse and which can be seen in vector plots of the geostrophic currents in Figure 5.4.

High frequency SST data acquisitions from the MSG-2 geostationary satellite reveal that a range of dynamical processes occur at the inshore front of the Agulhas Current. Case studies

presented in Sections 5.3.1.1, 5.3.1.2 and 5.3.1.3 show that during their downstream progression, Natal Pulses observed at the Agulhas Current's inshore front do not always grow steadily in size. Instead, the southward progression of Natal Pulses is often associated with the triggering of new upstream instabilities which propagate downstream together with the initial pulse. The observed meso and sub-meso scale instabilities at the Agulhas' inshore edge develop over short periods of time (typically less than 1 week). As they progress downstream, instabilities triggered at the inshore front of the Agulhas Current during the passage of Natal Pulses either dissipate, re-merge with the original pulse or detach from current. Over extended period of time, Natal Pulses therefore result from the downstream propagation of either 1 or a group of successive offshore meanders at the inshore boundary of the Agulhas Current. In Section 5.3.2, we attempt to evaluate how the instabilities which develop at the Agulhas Current's inshore front impact on the variability of the whole northern Agulhas Current by monitoring the position of the Agulhas Current's inshore front throughout more than 6 years of SST observations.

5.3.2   Variability at the inshore front of the northern Agulhas Current

The position of the Agulhas Current inshore front derived along 6 transects of the northern Agulhas using the method described in Section 5.2 is plotted in Figure 5.5. The Natal Pulses identified in Figure 5.5 represent extended periods of offshore meandering in the Agulhas Current associated with the passage of either 1 or a group of offshore meanders. About 80% of the detected Natal Pulses could be confirmed using SST and merged altimetry maps. The front-detection algorithm performs best at the Natal Bight and Port Elizabeth transects, where stronger temperature gradients between the Agulhas Current and coastal waters are encountered (Lutjeharms [2006]). Failures in the algorithm to correctly identify the position of the Agulhas Current's inshore front result from various factors, ranging from missing data or poor data quality (due principally to cloud contamination) to very weak SST gradients or a complex SST structure around the Agulhas Current. In the northern part of our study region, weak SST gradients between the Agulhas Current core and offshore regions at times lead to the Agulhas Current core position being estimated too far offshore. Wrong estimates of the Agulhas

Current core position can in turn induce errors when deriving the position of the Agulhas Current's inshore front. In the region between the southern Natal Bight and East London, the proximity of the Agulhas Current to the coast represents an additional challenge for the detection of the inshore front of the Agulhas Current. When the current hugs the coastline, the few number of data points which remain available to perform a search for the inshore gradient can lead to errors when estimating the position of the current's inshore edge. Overall, the front-detection algorithm is able to detect most Natal Pulses successfully. Off the Natal Bight, the inshore front of the Agulhas Current lies on average 36 km from the coast, at a position which roughly corresponds to the location of the 200 m isobath (Figure 5.5a). Standard deviations in the Agulhas Current's inshore front position average to about 19 km. These results are in good agreement with the mean and standard deviation (15 km) estimated by Gründlingh [1983] for the position of the Agulhas Current using hydrographic data collected off the Natal Bight. Along the Port Elizabeth transect, the inshore boundary of the Agulhas Current is found to lie on average 49 km from the coast, with standard deviation in its path of about 22 km. The mean position and standard deviation of the inshore front of the Agulhas Current near Port Elizabeth derived here, agree with those estimated by Goschen and Schumann [1990] (mean of 51 km and standard deviation of 24 km) at the same location (Cape Recife) and over a 3-year period.

One of the interesting results coming out of the analysis is the lack of seasonal variability in the position of the Agulhas Current's inshore edge across all selected transects. From the northern Natal Bight to Port Elizabeth, variability at the Agulhas Current's inshore front is instead dominated by the irregular passage of offshore meanders. The frequency and size of these meanders vary from one transect to the next. At the Natal Bight North transect, the position of the Agulhas Current's inshore front exhibits little variability, with only 1 Natal Pulse identified around the 21st of October 2005. From the northern Natal Bight to Port Edward, the number of Natal Pulses increases from 6 at the Natal Bight transect, to 9 at the Natal Bight South transect and reaches a maximum of 11 at the Port Edward transect. From Port Edward to Port Elizabeth, fewer Natal Pulses are observed at the Agulhas Current's inshore front with
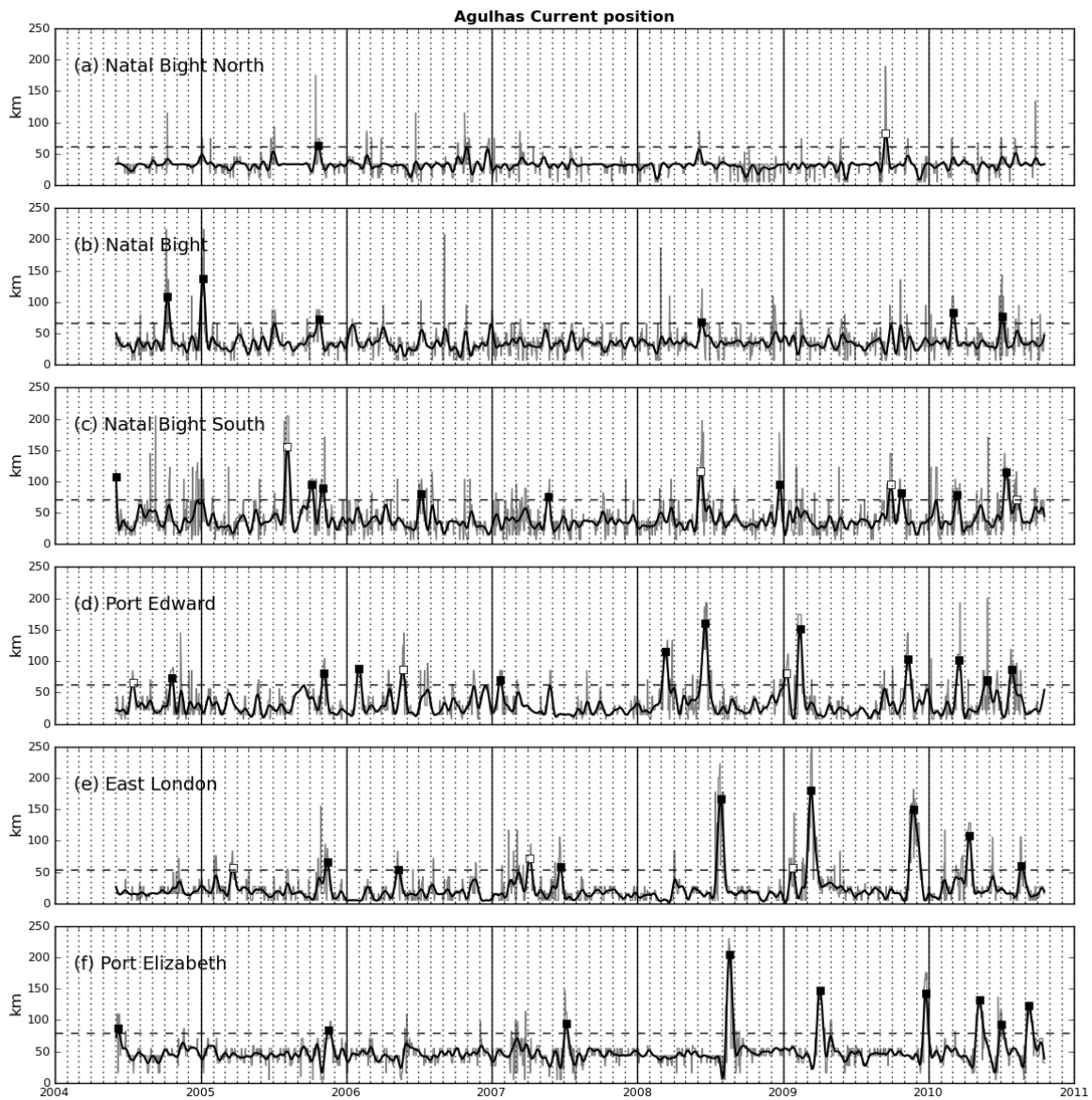
Figure 5.5: *Fluctuations of the mean position of the Agulhas Current inshore front at the Natal Bight North (a), Natal Bight (b), Natal Bight South (c), Port Edward (d), East London (e) and Port Elizabeth (f) transects estimated from 3-day moving averages of Seviri SST. The thick black line represents variations from the mean position of the Agulhas Current inshore front after applying a 10-day, 4th order Butterworth low-pass filter. The dashed line shows the 30 km threshold used for the identification of Natal Pulses. Natal Pulses in the Agulhas Current are identified by black squares. Natal Pulses which could not be confirmed after visual examination of SST maps have been plotted as white squares. Solid vertical lines mark the 1st of January for each year while the vertical and stippled black lines indicate the beginning of each month.*

only 8 Natal Pulses detected off East London and 9 near Port Elizabeth. The largest Natal Pulse was detected near Port Elizabeth in August 2008, when the current meanders about 160 km offshore from its mean position. This particular event was previously identified by Rouault et al. [2010] as a precursor to the anomalous early retroflection of the Agulhas Current in September/October 2008.

The front-detection analysis shows that not all Natal Pulses observed in the Agulhas Current's path grow steadily in size as they progress downstream. The two largest Natal Pulses observed at the Natal Bight transect around October 2004 and January 2005 for example do not propagate downstream to Port Elizabeth. The Natal Pulse of October 2004 decreases in size downstream while that observed in January 2005, which corresponds to the case of eddy occlusion mentioned in Section 5.3.1.3, detaches from the Agulhas Current before it reaches Port Edwards. Similarly two of the Natal Pulses identified at the Port Elizabeth transect around the 18th of November 2005 and the 6th of July 2007 do not exhibit significant growth from their region of origin to Port Elizabeth. In the case of the Natal Pulse observed off Port Elizabeth in July 2007, the reason for the Natal Pulse not expanding was highlighted in Section 5.3.1.1. On the low-passed time-series both the initial pulse detected at the Natal Bight South transect on the 22nd of May 2007 and the one detected near Port Elizabeth on the 7th of July 2007 appear to be due to one single meander propagating downstream when in reality, it was observed in Section 5.3.1.1, that this Natal Pulse constituted of to two separate instabilities at the Agulhas Current's inshore front. The properties of all Natal Pulses that progressed southward to Port Elizabeth and which are identified by black markers in Figure 5.5f are summarized in Figure 5.6. The origin of these Natal Pulses, their propagation speeds and the extent of the offshore meandering associated with their passage are plotted in Figure 5.6a, Figure 5.6b and Figure 5.6c, respectively. From the 9 Natal Pulses detected at the Agulhas Current's inshore front off Port Elizabeth, 6 find their origin in the region of the Natal Bight and 2 are detected first at the Port Edward transect. The first Natal Pulse detected at the Port Elizabeth transect occurs at the beginning of the measurement period and for this reason, its region of origin can not be determined. In Figure 5.6a, the Natal Pulses which reached Port Elizabeth are classified

as merging, dissipating or occluding based on the type of instability that developed during their downstream progress. This classification, undertaken using visual observations of SST maps, appears to indicate that most of the secondary meanders that develop during the passage of Natal Pulses later re-merge with the initial perturbation. However, this result is purely indicative of what could be observed from the SEVIRI dataset. A proper quantification of the number of dissipating, merging or occluding instabilities associated with Natal Pulses could only be undertaken using high frequency in-situ measurements at multiple transects locations. Figure 5.6b shows that Natal Pulses generally have propagation speeds between 10 and 20 km per day, in agreement with previous findings (van der Vaart and de Ruijter [2001]). One exception is found in the Natal Pulse of November 2005, which displays much larger phase velocities. Figure 5.6c confirms that the growth of Natal Pulses downstream is not always monotonic. From June 2004 to the end of 2007, the position of the Agulhas Current's inshore front near Port Elizabeth shows remarkably little variability as only three small Natal Pulses are observed (Figure 5.5f). Deviations from the mean inshore path of the Agulhas Current associated with these 3 Natal Pulses are less than 50 km. From 2008 to 2010, both the size and the number of Natal Pulses observed near Port Elizabeth increase, with 6 Natal Pulses causing fluctuations in the inshore path of the Agulhas Current of 91 km from the mean, on average.

5.3.3 A retrospective on Natal Pulses from altimetry

Cyclonic motions over the continental shelf associated with the passage of Natal Pulses induce flow reversals at the mean position of the Agulhas Current core (located at 25.8°E, 34.7°S according to Rouault et al. [2010]), with the current direction changing from south-westerly to north-easterly. A time-series of the eastward current velocity extracted at 25.8°E, 34.7°S shows that all Natal Pulse events identified using the Seviri SST front-detection algorithm are associated with large fluctuations in the eastward geostrophic flow. In the AVISO time-series, anomalous events are defined as variation in the eastward flow exceeding 1 standard deviation from the mean. From the 10 anomalous events detected using the AVISO eastward current velocity at 25.8°E, 34.7°S, 9 correspond to Natal Pulses identified with the SST front-detection
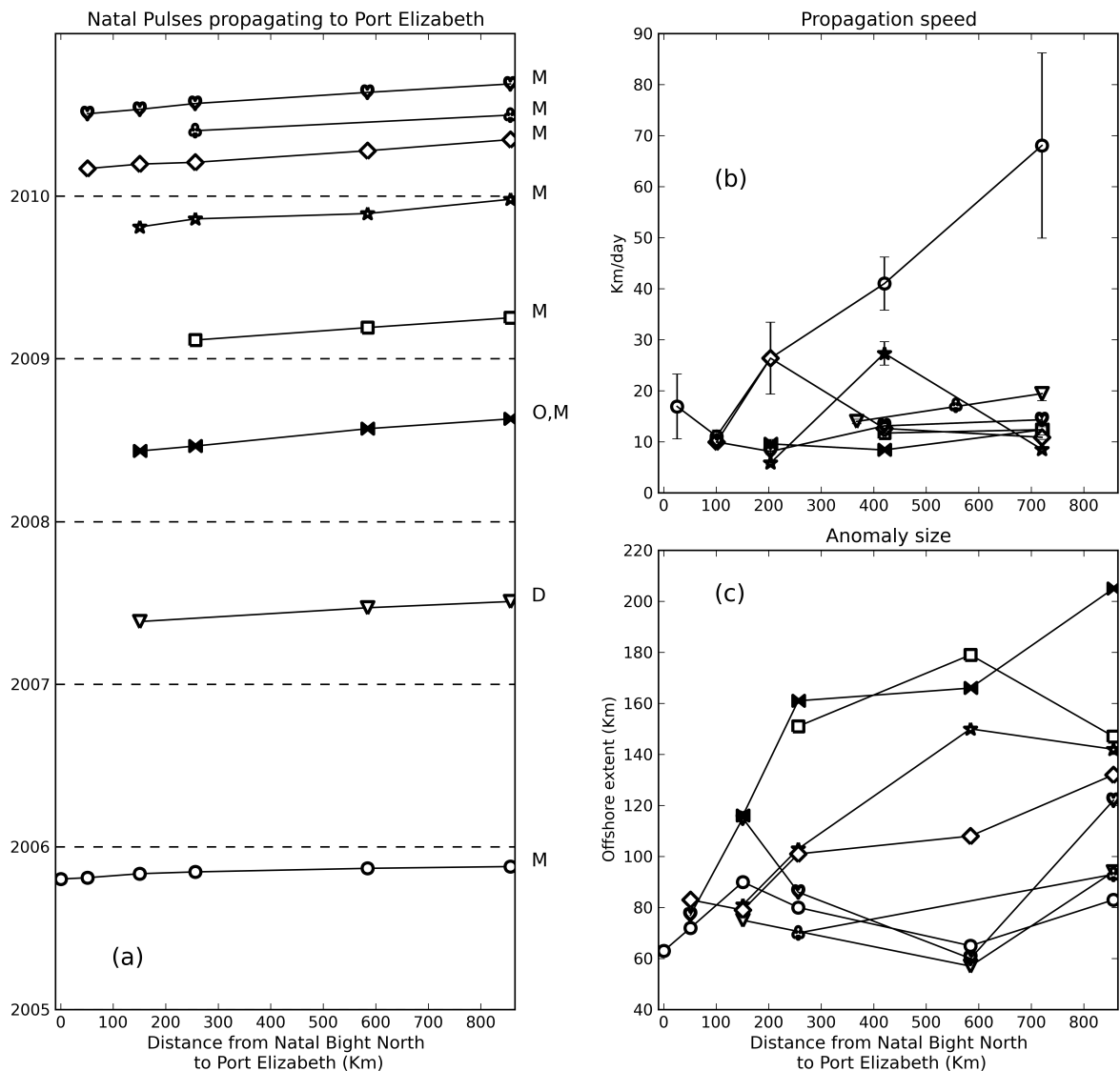
Figure 5.6: *Origin and properties of the Natal Pulses which reached the Port Elizabeth transect. (a) shows the propagation of each Natal Pulse detected near Port Elizabeth from their region of origin. Each Natal Pulse propagating at the inshore boundary of the Agulhas Current can be identified by its marker. The label on the x-axis represents the distance in km from the Northern Natal Bight to the Port Elizabeth transect with markers showing the position of each transect on the line plots. The letters M, O and D on the right hand side of panel (a) indicate instances of Merging (M), Occluding (O) and Dissipating (D) instabilities associated with the Natal Pulses. Propagation speeds derived for all Natal Pulses are plotted in (b) with error bars showing the uncertainty associated with using 3-day SST composites. (c) shows the offshore deviation of the mean position of the Agulhas Current's inshore front associated with the passage of the Natal Pulses.*

Figure 5.7: *Variations in absolute geostrophic current velocities at the Agulhas Current core associated with the passage of Natal Pulses offshore Port Elizabeth. The low-passed position of the Agulhas Curre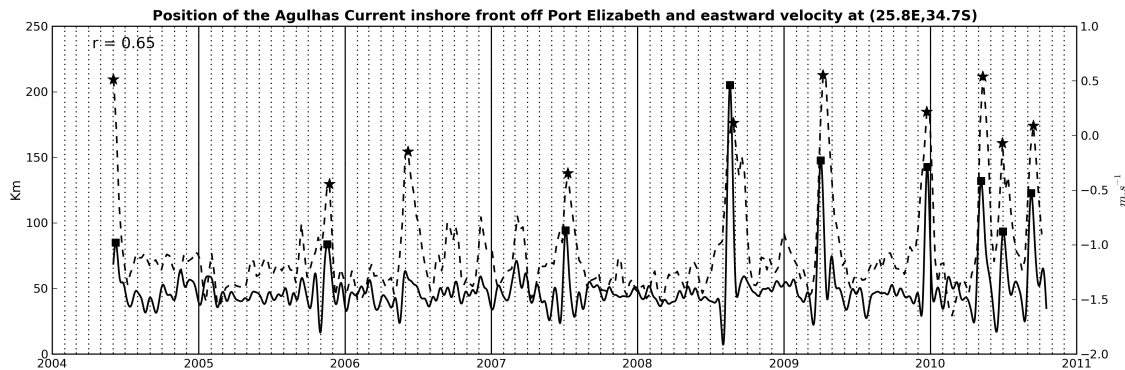nt's inshore front is plotted as a black line with Natal Pulses identified by black square markers. The eastward current velocity extracted at 25.8°E, 34.7°S from the AVISO maps of absolute geostrophic velocities is plotted as a stippled black line with stars showing fluctuations in the eastward current velocity greater than 1 standard deviation. A Pearson's correlation coefficient r of 0.65 is found between the 7-day low-pass time-series of the Agulhas Current inshore front and the absolute eastward geostrophic velocity at the Agulhas Current core. The correlation coefficient r is highly significant at the 99% confidence interval. Solid vertical lines mark the 1st of January for each year while the vertical and stippled black lines indicate the beginning of each month.*

algorithm (Figure 5.7). While the AVISO eastward current anomaly does not necessarily relate well to the scale of the Natal Pulses, the AVISO dataset appears to provide an excellent indicator for the occurrence of Natal Pulses offshore Port Elizabeth.

One surprising result of the SEVIRI SST front-detection analysis is that from June 2004 to the end of 2010, few Natal Pulses were observed at Port Elizabeth. On average the number of Natal Pulses reaching the waters off East London and Port Elizabeth only amounted to about 1.6 per year. Building on the good correlation between the AVISO and the Agulhas Current's inshore front time-series (Figure 5.7), a time-series of the eastward geostrophic current at 25.8°E, 34.7°S is used to estimate the frequency of occurrence of Natal Pulses over a 17-year period. Variations in the eastward current derived from the AVISO dataset between the 14th of October 1992 and the 8th of December 2010 are plotted in Figure 5.8. As in Figure 5.7, fluctuations in the eastward current velocity exceeding 1 standard deviation from the mean are used as indication of Natal Pulse events. The average number of Natal Pulses detected using
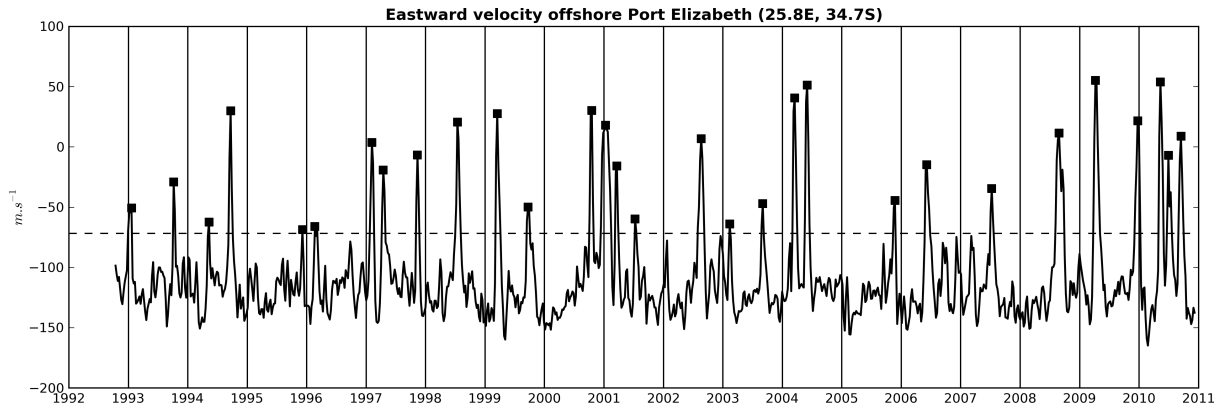
Figure 5.8: *Eastward current at 25.8°E, 34.7°S extracted from the AVISO maps of absolute geostrophic velocities. Eastward current velocity fluctuations exceeding 1 standard deviation from the mean are identified with black squares. Solid vertical lines mark the 1st of January for each year.*

the AVISO dataset over the 17-year AVISO time-series averages to 1.65 per year, an estimates which compares well with that derived from our SST front-detection analysis.

Using AVISO maps of absolute dynamic topography and associated geostrophic currents (not shown), it is possible to relate some of the events detected in Figure 5.8 to previous observations of Natal Pulses. For example, the Natal Pulse observed on the 6th of October 1993 by van Leeuwen et al. [2000] can be seen in Figure 5.8. The Natal Pulses identified by Lutjeharms et al. [2001] and Lutjeharms [2006] (pp. 116) in July 1998 and in May/June 2004, are also apparent in Figure 5.8. Using the AVISO merged maps of absolute dynamic topography, it was possible to identify all 5 Natal Pulses observed by Bryden et al. [2005] off Port Edward in April 1995, September 1995, November 1995, December 1995 and March 1996. From these 5 Natal Pulses, 3 observed in April 1995, September 1995 and March 1996 seem to disappear from the merged altimetry maps before reaching Port Elizabeth.

5.4 Discussion

Previous studies (Bryden et al. [2005]; Lutjeharms [2006]) have consistently pointed to the Natal Pulse as the dominant mode of variability upstream of the Agulhas Retroflection. While our analysis of the Agulhas Current's inshore front supports the hypothesis that downstream propagating offshore meanders are the dominant drivers of variability in the northern Ag-

ulhas, it also shows that large excursions in the Agulhas Current's path are not necessarily associated with the passage of one large solitary offshore meander. Instead, Natal Pulses are often the result of 1, 2 or more cyclonic offshore meanders, which together, progress southward at the inshore border of the Agulhas Current. Undulations at the inshore front of the Agulhas Current upstream of Port Elizabeth have been previously noted by Goschen and Schumann [1990], who suggested that such oscillations might occur prior to the formation of shear-edge eddies. Current measurements undertaken in the northern Agulhas in 1976 and 1977 (Schumann [1983]) have shown the sporadic occurrence of wave-like oscillations between Port Edwards and Richards Bay (north of the Natal Bight). These meandering motions propagated northward along the coast with a speed of 3.9 m.s^{-1} (337 km/day) and were associated with marked current and temperature variations, with upwelling and associated offshore flow in the upper layers. In his analysis, Schumann [1983] could not relate the wave-like motions to atmospheric perturbations and expressed uncertainty as to the generation mechanism for these northward propagating coastal waves. In a study on Natal Pulses, van Leeuwen et al. [2000] used SST imagery collected on the 27th February 1987 (plate1-a) to identify 2 consecutive offshore meanders at the landward edge of the Agulhas Current. From these two large offshore meanders, only one could be detected off the south-east African coastline less than a month later (plate1-b). van Leeuwen et al. [2000] suggested that the two pulses observed on the 27th of February 1987 might form part of a unique Natal Pulse event but provided no explanation as to why a Natal Pulse should consists of two meanders and why the same Natal Pulse would later become a single meander. Takeda [1983] showed that changes in the vorticity structure of the water column over a varying topography can induce the formation of topographically trapped waves, with the properties of the generated waves being dependent on the rate of stretching and shrinking of the vortex tubes. In his studies of the "interactions of a eddy with a continental slope", Xioming [1992] found that cyclonic eddies impinging on a coastal shelf and slope induce wave-like perturbations whose dispersion relation obey that of shelf-trapped mode. Laboratory and numerical experiments conducted by Sanson and van Heijst [2000] showed that interactions between barotropic cyclonic vortices and a steep con-

tinental slope can generate an intense meandering current along the slope from which new cyclonic vortices are formed. Observations of SST imagery and the case studies presented in Section 5.3 show that in a similar fashion, when the trailing edge of a Natal Pulse comes in close proximity to the coast, a secondary offshore meander can be generated upstream of the initial perturbation. Interactions between offshore meanders and the topography can lead to the formation of 1 or more upstream meanders each travelling southward with the initial Natal Pulse. Near the coast, the downstream propagation of Natal Pulses and their associated frontal instabilities induce wave-like oscillations which might resemble those associated with northward propagating coastal trapped waves.

High frequency SST observations collected from the SEVIRI instrument onboard MSG-2 have shown that Natal Pulses are complex and rapidly evolving features of the Agulhas Current associated with a range of non-linear processes. The interaction of Natal Pulses with the continental shelf and the concomitant development of upstream instabilities (as seen in Figures 5.2, 5.3 and 5.4) is a possible indication of a direct cascade of energy towards the smaller scales. A recent paper on the oceanography of the South-African east coast (Roberts [2010]) also suggests that erosion of cyclonic eddies at the inshore boundary of the northern Agulhas Current occurs.

Figure 5.5 shows that the frequency characteristics of the northern Agulhas Current's inshore front vary regionally. From the northern Natal Bight to Port Edward, both the size and frequency of Natal Pulses increase while south of Port Edward, there is a reduction in the number of Natal Pulses observed. The Natal Bight appears to be a key region for the development and growth of instabilities in the northern Agulhas. Vortex stretching due to the sudden steepening of the continental slope from the northern Natal Bight to the southern Natal Bight could provide a mechanism by which negative (cyclonic) vorticity is input into the main flow and which feeds the growth of Natal Pulses southward (Herbert and Bryan [1976]). Oceanic eddies at the boundary of the Agulhas Current might also constitute a source or sink of vorticity for Natal Pulses. Theoretical investigations have shown that both cyclonic and anti-cyclonic eddies reaching a stable jet will generate meanders (Stern and Flierl [1987]; Bell and Pratt [1992]).

Previous studies have pointed to Mozambique anti-cyclonic eddies as being the main trigger for the development of Natal Pulses (de Ruijter et al. [1999]; Schouten et al. [2002]). This was recently confirmed by Tsugawa and Hasumi [2010] who found that upon reaching the coastline, anti-cyclonic eddies extracted water from the shelf and slope and generated cyclonic vorticity through vortex stretching, resulting in the formation of a Natal Pulse. In case studies 5.3.1.1 and 5.3.1.2, the growth of cyclonic meanders was concurrent with the presence of an anti-cyclonic eddy on the seaward border of the current. In both case studies 5.3.1.1 and 5.3.1.3, the cyclonic meander closest to the anti-cyclonic eddy was seen to expand while the original cyclonic perturbation located further downstream decreased in size. The datasets used in this study are limited and further investigations would be required to undertake a vorticity budget and precisely assess the influence of both cyclonic and anti-cyclonic eddies on the expansion of Natal Pulses.

One surprising result of the SST analysis is that very few Natal Pulses are observed between June 2004 and the end of 2010. On average the number of Natal Pulses reaching the waters off Port Elizabeth only amounts to about 1.6 per year. A retrospective analysis of altimetry data seems to confirm that on average only 1.6 Natal Pulse per year reach the latitude of Port Elizabeth. With the exception of Goschen and Schumann [1990] who found that approximately 2 Natal Pulses occur per year, most previous studies on Natal Pulses have estimated their frequency at 4 to 6 per year. Our current knowledge of Natal Pulses relies on scarce in-situ observations, some analyses of altimeter data (de Ruijter et al. [1999]; van Leeuwen et al. [2000]) and a few numerical studies (Biastoch et al. [2008b]; Tsugawa and Hasumi [2010]). Upstream of Port Elizabeth, where the current lies close to the shore, altimetry datasets suffer considerable data loss due to land contamination (Madsen et al. [2007]; Vignudelli et al. [2008b]). The scarcity of altimeter observations between the Natal Bight and East London combined to a previously poorly resolved Mean Dynamic Topography (MDT) in the Agulhas Current region represent serious challenges when attempting to follow rapidly evolving features such as Natal Pulses (Byrne and McClean [2008]; Rouault et al. [2010]). To date the most extensive dataset of the northern Agulhas Current consists in a 9-month record of moored array data collected

off Port Edward in 1995 (Bryden et al. [2005]). Other historic in-situ observations of the northern Agulhas Current include 237 hydrographic sections of mainly vertical temperature profiles collected across 8 transects between the northern Natal Bight and Port Elizabeth (Gründlingh [1983]).

Our analysis suggests that the number of Natal Pulses decreases from Port Edward to Port Elizabeth. One could argue that the threshold selected for the identification of Natal Pulses in their region of origin is too restrictive and limits the number of Natal Pulses detected through our analysis. For example, the Natal Pulse observed by Schouten et al. [2002] in May/June 2000 would probably have been too small in size to qualify as a Natal Pulse under our selection criteria. However, changing the size threshold for the identification of Natal Pulses would not modify the result that very few Natal Pulses reach the Port Elizabeth transect. Natal Pulses have been defined as large intermittent and solitary meanders (Lutjeharms and Roberts [1988]) that "invariably" originates in the Natal Bight and which "always grows in seaward extent on translating downstream" (Lutjeharms [2006], pp. 114). Due to limitations in previous satellite remote sensing datasets, it was not possible in the past to accurately follow perturbations from the Natal Bight all the way south to Port Elizabeth. Based on the assumption that Natal Pulses would always grow downstream and could only originate from the Natal Bight region, most southward propagating offshore meanders observed in the northern Agulhas Current and with spatial scales ranging from 30 to 250 km have been labelled Natal Pulses. As our knowledge on the variability of the northern Agulhas progresses, it becomes necessary to re-examine what constitutes a Natal Pulse.

5.5 Conclusion

A front-detection algorithm applied to more than 6 years of SST imagery was used to track fluctuations in the path of the northern Agulhas Current. Time-series of the Agulhas inshore front derived between the Natal Bight and Port Elizabeth showed no seasonality in the position of the Agulhas Current and confirmed that variability at the northern Agulhas Current's

inshore front is dominated by the intermittent passage of Natal Pulses. Different patterns of variability were observed within the northern Agulhas Current, with an increasing number of Natal Pulses detected between the northern Natal Bight and Port Edward, followed by a drop in the number of Natal Pulses south of Port Edward (Figure 5.5). High frequency observations from the SEVIRI sensor showed that as they propagate southward, Natal Pulses grow and start to interact with the topography to generate a secondary meander which either splits, re-merges or detaches from the original perturbation. The generation of smaller eddies during the passage of Natal Pulses (as seen in Figures 5.2, 5.3, and 5.4) provides a possible indication of a cascade of energy towards the smaller scales and could explain the downstream decrease in the number of Natal Pulses south of Port Edward. Over more than 6 years of SST observations, only 1.6 Natal Pulses per year was found to reach the latitude of Port Elizabeth. A retrospective analysis using altimetry data offshore Port Elizabeth appears to confirm that on average, approximately 1.6 Natal Pulses per year reach the southern Agulhas Current. The high spatial and temporal resolution of the SST dataset used in this study allow for a better imaging of the northern Agulhas Current dynamics compared to previously used remote sensing techniques. Some of the features revealed in the SST imagery expose crucial knowledge gaps in our current understanding of the northern Agulhas Current and the need for new theoretical and observational studies.

<div style="text-align: right; font-size: 4em;">6</div>

Variability in the southern Agulhas Current

6.1 Introduction

In Section 5.3.3 of Chapter 5, an inshore front detection algorithm applied to the SEVIRI SST dataset was used to identify and track Natal Pulses on their journey south, from the Natal Bight to Port Elizabeth. Offshore Port Elizabeth, where the inshore edge of the Agulhas Current lies on average about 50 km from the shore, large meanders in the path of the Agulhas Current inshore front were coincident with anomalies in the absolute geostrophic current velocities, suggesting that in the southern Agulhas region, the AVISO merged altimetry product is suited to the identification of large meanders. In this chapter, a method similar to that proposed in Chapter 5 is applied to the AVISO merged maps of absolute geostrophic currents to track variations in the path of the southern Agulhas Current over an 18-year period. The position of the Agulhas Current is derived across multiple transects with the aim to 1) better characterise the periodicity and the scales of large offshore meanders which progress to the southern Agulhas Current region, 2) follow the evolution of these perturbations downstream of Port Elizabeth and 3) highlight potential regional differences in the southern Agulhas Current's variability. The availability of current velocity information in the altimetry dataset provides an opportunity to better quantify the impact of large offshore meanders on the circulation of the eastern Agulhas Bank. By following the Agulhas Current it becomes possible to separate the intrinsic

variability of the Agulhas Current from that of its surrounding waters. Our results suggest that the variability of the Agulhas Current differs from that of the surrounding coastal and shelf waters and provides interesting insights on the mechanisms which drives the variability of the Agulhas Current at sub-annual and annual time-scales. The data and methodology used to study the variability of the southern Agulhas Current are described in Section 6.2. In Section 6.3.1, variations in the path of the southern Agulhas Current are used to identify large perturbations in the Agulhas Current and assess their impact on the coastal and shelf water regions. Modulations at the Agulhas Current core and their relation to large scale forcing are presented in Sections 6.3.2 and 6.3.3. The results of this chapter are discussed in Section 6.4, with conclusions presented in Section 6.5.

6.2 Data and method

To characterise the variability of the southern Agulhas Current, an approach similar to that described in Chapter 5 is followed. The position of the Agulhas Current core is derived from the merged altimetry dataset along three transects, located offshore Port Elizabeth, Knysna and Mossel Bay and plotted in Figure 6.1. Near the Agulhas Retroflection, temporary occlusions of the Agulhas Current associated with the formation of Agulhas Rings make it difficult to accurately track the current. The transects chosen for our analysis are thus limited to the eastern Agulhas Bank region, where the dynamics of the Agulhas Current are not influenced by the shedding of Agulhas Rings. To derive the position of the Agulhas Current along each transect, the predominant current direction is first established. This predominant current direction, which we refer to as the along-shore direction, is then used to separate the absolute geostrophic current fields into along-shore and across-shore components. All local maxima in the along-shore geostrophic current speeds encountered over a 50 km moving window are identified and the local maximum associated with the strongest flow is then selected as the point where the Agulhas Current core lies. The path of the Agulhas Current core is then compared to that estimated from the SEVIRI SST, using the method described in Section 5.2. In
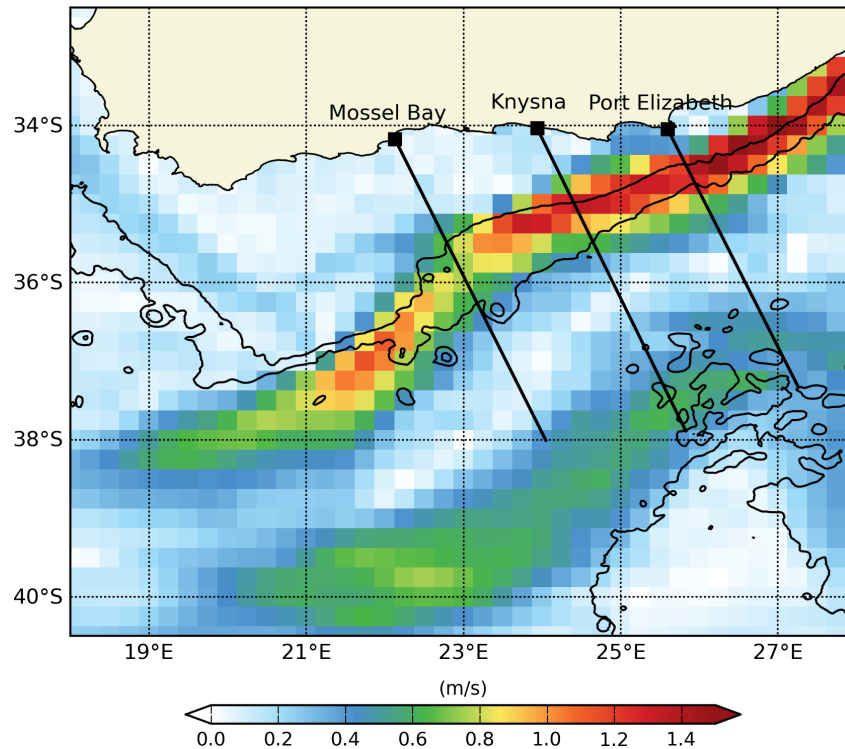
Figure 6.1: *Colour contour map of absolute geostrophic current speed produced with the CNES-CLS09 MDT of Rio and Larnicol [2011] over the southern Agulhas region. The position of the southern Agulhas Current's core was tracked along 3 transects plotted as black lines and referenced to as Port Elizabeth, Knysna and Mossel Bay. The positions of the 1000 m and 3000 m isobaths are plotted as black contour lines.*

our analysis of the southern Agulhas Current's core movements, excursions in the path of the Agulhas's current core exceeding 1 standard deviation from the mean are referred to as "Anomalous Pulses", rather than as Natal Pulses, since we do not associate these large meanders with a specific region of origin. The duration of an Anomalous Pulse is defined as the time interval separating the two zero-crossing points which surround the detected Anomalous Pulse, with the threshold for zero-crossing equal to the mean position of the Agulhas Current core.

Tracking the position of the Agulhas Current using altimetry rather than SST presents the advantage of providing current velocity information and enables us to analyse perturbations in the current velocity field induced by the passage of large offshore meanders. To characterise the circulation associated with Anomalous Pulses, composite maps of absolute

geostrophic current velocities are generated over the duration of Anomalous Pulse events. Anomalies in the circulation associated with Anomalous Pulses represent differences between the composite-averaged velocity field and the annual climatological mean.

Fourier and wavelet transform methods are used to characterise the periodicity associated with the meandering of the Agulhas Current's path. Spectral and wavelet analyses are also conducted on the time-series of the Agulhas Current core velocity to provide greater insight on what physical drivers may modulate the strength of the Agulhas Current. The significance of the wavelet and power spectrum analyses were tested using red-noise Fourier power spectrum calculated according to the method of Gilman et al. [1963].

In the final part of this chapter, we attempt to relate variations in the strength of the Agulhas Current to wind forcing over the South Indian Ocean through the Sverdrup relation. In the South Indian Ocean, winds drive a predominantly northward flow over most of the oceanic basin which must be balanced at the western boundary by the southward flowing Agulhas Current. In an homogeneous ocean in geostrophic equilibrium, the transport at the western boundary can thus be estimated by integrating the wind driven transport across meridional lines from the eastern to the western boundary. Along a selected latitude, the Sverdrup transport stream function ψ is expressed by:

$$\psi = \frac{1}{\beta\rho} \int_{x_E}^{x} \nabla \times \tau \, dx \tag{6.1}$$

where β is the meridional derivative of the Coriolis parameter, ρ is the mean density of the ocean and τ is the wind stress. x_E and x represents the eastern and western boundary defining the domain of integration with $\psi = 0$ at x_E.

In this chapter, the Sverdrup transport is integrated along the 34°S latitude from the west coast of the Australia to the African continent. The Sverdrup transport at 34°S is then compared to fluctuations in the Agulhas Current core speeds near Port Elizabeth (Port Elizabeth is positioned at 25°40′E, 33°58′S). The Sverdrup transport is calculated using monthly mean fields of the wind stress curl over the period August 1999 to December 2010. The monthly

wind fields are based on synoptic observations from the NASA SeaWinds scatterometer on-board QuikSCAT and are provided by the CERSAT on a $0.5°$ rectilinear grid.

Estimates of the Sverdrup transport derived through equation 6.1 do not account for the contribution of the Indonesian Throughflow, which has been evaluated to ± 15 Sv (Ganachaud et al. [2000]). Here we focus on the impact of wind forcing over the South Indian ocean. Although changes in the Indonesian Throughflow might influence the overall Agulhas Current transport, investigating the links between the Indonesian Throughflow and the Agulhas Current variability falls outside the scope of the research presented in this chapter.

6.3 Results

6.3.1 Variations in the path of the southern Agulhas Current

Figure 6.2 shows the estimated position of the Agulhas Current core at the Port Elizabeth (a), Knysna (b) and Mossel Bay (c) transects. The position of the Agulhas Current core derived from the SEVIRI SST and the merged altimetry dataset are in good agreement, providing further confirmation that the AVISO merged altimetry product is suited to tracking the position of the Agulhas Current south of Port Elizabeth. The Agulhas Current follows the eastern Agulhas Bank continental shelf, with its center moving progressingly offshore from 82 km at Port Elizabeth to 200 km off Mossel Bay, on average (Table 6.1). South of Port Elizabeth the Agulhas Current becomes less steady, with standard deviations in its path increasing from 28 km at Port Elizabeth to 33 km and 42 km offshore Knysna and Mossel Bay, respectively.

The two largest excursions in the path of the southern Agulhas Current are observed in January-February 2001 and August-September 2008, at times of anomalous upstream retroflection of the Agulhas Current (also referred to as Early Retroflections). It is necessary to note that during Early Retroflections, the position of the Agulhas Current estimated with our algorithm along the Knysna and Mossel Bay transects might not correspond to the position of the Agulhas Current core, but instead represent the location at which the strongest south-westerly
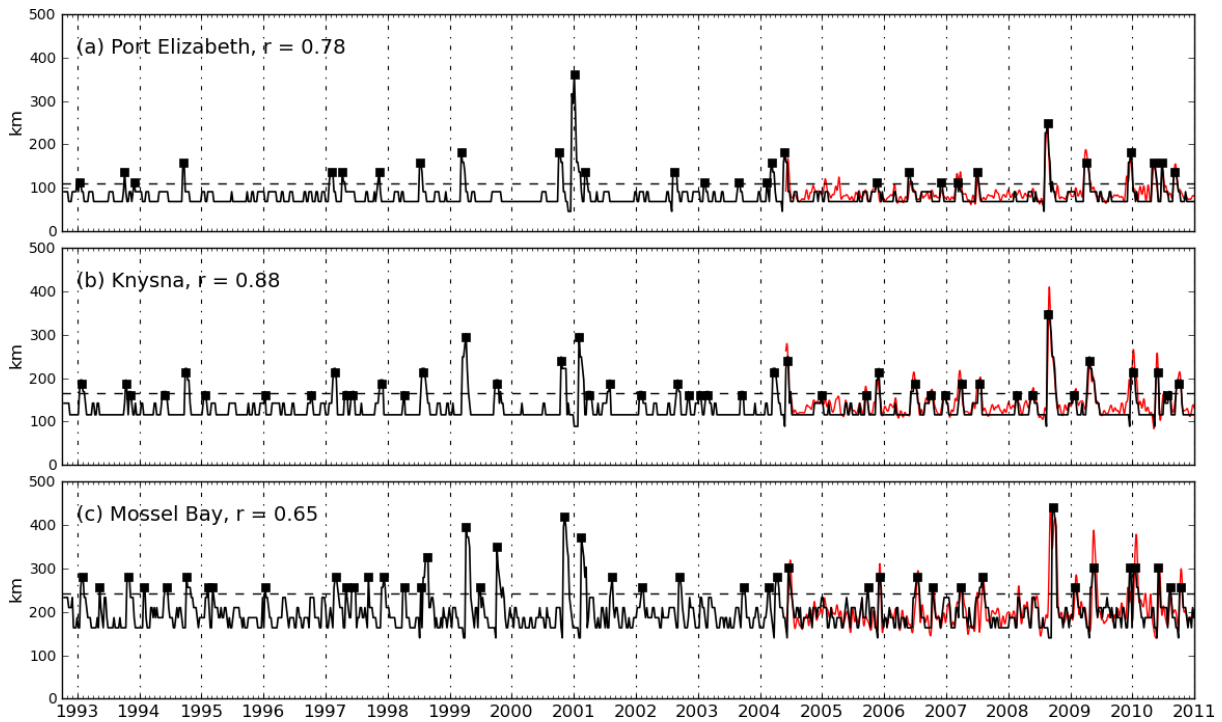
Figure 6.2: *Position of the Agulhas Current core at the Port Elizabeth (a), Knysna (b) and Mossel Bay (c) transects. The position of the Agulhas Current's core estimated from the AVISO maps of absolute geostrophic velocities is plotted as a black line with squares showing fluctuations in the Agulhas Current position greater than 1 standard deviation. The red line represents the position of the Agulhas Current's core derived from the 3-day moving averages of Seviri SST after applying a 10-day, 4th order Butterworth low-pass filter (similarly to results presented in Figure 5.5). Pearson's correlation coefficients between the altimetry and SST time-series of the Agulhas Current's core position are equal to $r = 0.78$, $r = 0.88$ and $r = 0.65$ for the Port Elizabeth, Knysna and Mossel Bay transects, respectively. The correlation coefficients r are all highly significant at the 95% confidence interval. Stippled black vertical lines mark the 1st of January for each year.*

Table 6.1: *Mean statistics for Anomalous Pulses detected off Port Elizabeth, Knysna and Mossel Bay*

	Pulse frequency (per year)	Mean current core position	Standard deviation (km)	Number of pulses	Pulse mean offshore extent (km)	Pulse mean duration (days)
Port Elizabeth						
Altimetry	1.6	82	28	29	152	50
SST	2	89	23	11	153	44
Knysna						
Altimetry	2.5	133	33	45	190	46
SST	1.8	144	35	10	240	43
Mossel Bay						
Altimetry	2.4	200	42	43	286	43
SST	2.5	204	44	14	308	35

flow is observed along the transect. This is particularly relevant for the largest and longest of the two Early Retroflections which occurred in January-March 2001, and during which the Agulhas Current retroflected upstream and eastward of the Knysna and Mossel Bay transects (Rouault and Lutjeharms [2003]). In January-March 2001, the absence of the Agulhas Current along both the Knysna and Mossel Bay transects results in an under-estimation of the scale of the Anomalous Event detected by the algorithm, as seen in Figure 6.2, (b) and (c). Results based on the altimetry data show that between the Port Elizabeth and Knysna transects, the number of Anomalous Pulses increases sharply. The larger value of the standard deviation in the Agulhas Current path derived off Mossel Bay implies that the threshold for anomalous pulse detection increases downstream. This explains why despite the increasing meandering nature of the Agulhas Current downstream of Port Elizabeth, the number of Anomalous Pulses remains relatively unchanged between Knysna and Mossel Bay. The size of Anomalous Pulses increases from the Port Elizabeth to the Mossel Bay transects. The properties of 22 Anomalous Pulses tracked along all three transects and which excluded the 2 events associated with Early

Retroflections showed that on average, the offshore extent of Anomalous Pulses relative to the mean position of the Agulhas Current grows from 64 km off Port Elizabeth to 92 km near Mossel Bay. The persistence of these large offshore meanders does not change markedly from Port Elizabeth to Mossel Bay, with Anomalous Pulses lasting approximately 1.5 months. Using the time at which Anomalous Pulses are first detected along the Mossel and Port Elizabeth transects, we estimate the average propagation speed for Anomalous Pulses in the southern Agulhas Current to about 8 km/day. The AVISO absolute geostrophic current velocities are provided at weekly time-intervals. An uncertainty of 7 days in the time of the Anomalous Pulse arrival would result in an error in the estimation of the southward propagation speed of about 2 km/day.

Anomalous Pulses are associated with distinct velocity anomalies at the mean position of the Agulhas Current core. Figure 6.3 shows that at all three transects, the passage of Anomalous Pulses causes similar perturbations in the current velocity field. In the initial phase of an Anomalous Pulse, the current direction changes from south-westerly to southerly. As the Agulhas Current is further displaced offshore, a marked decrease in the current speed is observed, followed by a reversal of the currents towards the north-west when the Anomalous Pulse reaches is maximum offshore extent. Near Mossel Bay, where the meandering nature of the Agulhas Current increases, the arrival of Anomalous Pulses is often preceded by an onshore intrusion of the Agulhas Current and a strengthening in the westerly component of the flow (Figure 6.3 c). This strengthened onshore circulation is indicative of the leading edge of the Anomalous Pulse reaching the transect. The evolution of the current velocity field induced by Anomalous pulses in the southern Agulhas Current is similar to that observed by Bryden et al. [2005] during the passage of Natal Pulses off Port Edwards.

The spatial extent of the velocity perturbations typically associated with Anomalous Pulse events is revealed in composites maps generated from the 22 Anomalous Pulses events previously mentioned. These composites maps are plotted in Figure 6.4. Panels on the left hand side show the mean current velocities averaged over the duration of all Anomalous Pulse events. Right hand side panels in Figure 6.4 show plots of the geostrophic current anomalies associ-
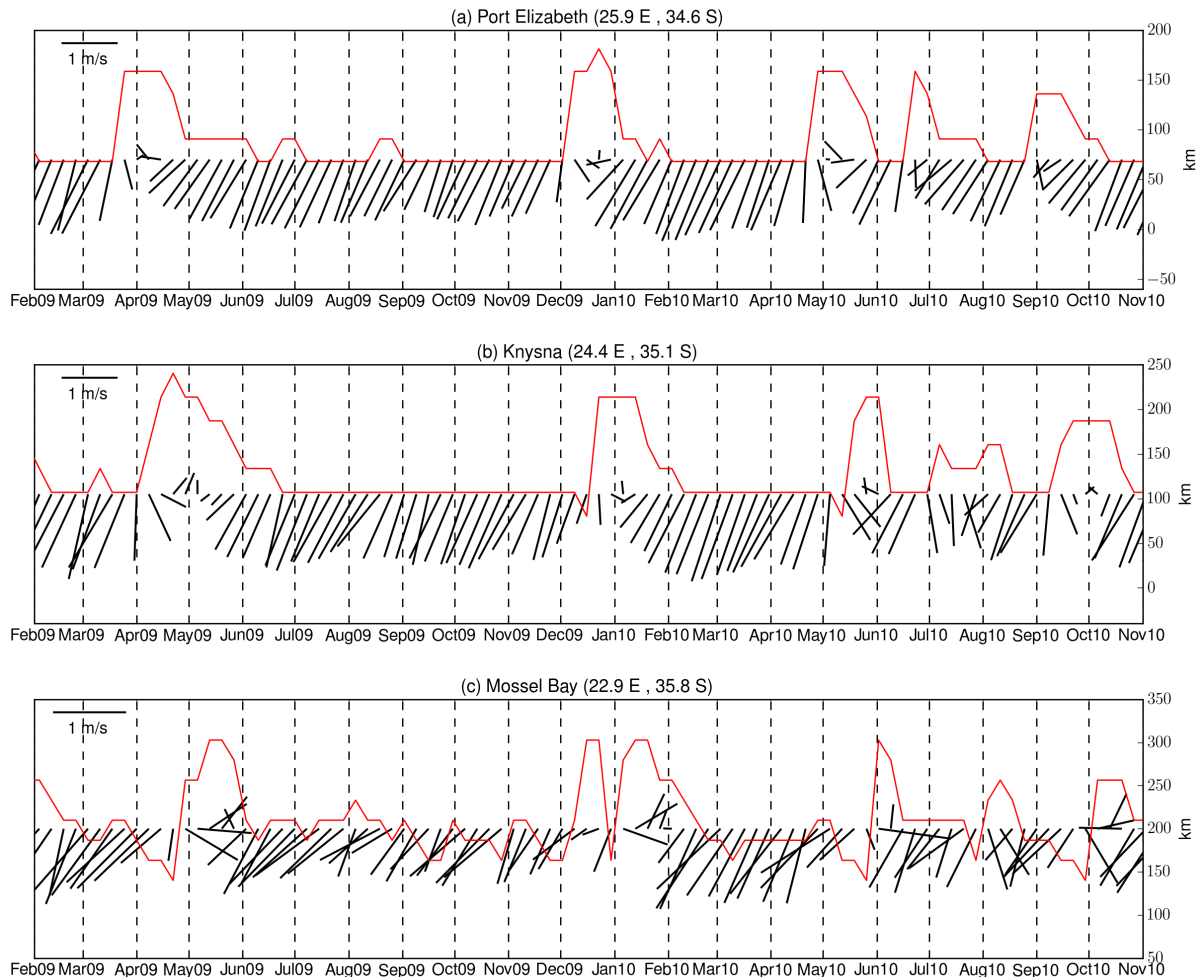
Figure 6.3: *Variations in the geostrophic current velocities associated with the passage of 5 Anomalous Pulses between February 2009 and December 2010 at the mean location of the Agulhas Current core. The red line represents the distance between the Agulhas Current core and the coast while the black lines are stick plots of the current vectors at the mean position of the Agulhas Current core along the Port Elizabeth (a), Knysna (b) and Mossel Bay (c)transects. The length of the sticks are proportional to the geostrophic current speed with south-westerly currents pointing towards the lower left. Note changes in the current stick scales between panes (a), (b) and (c)*

ated with the 22 Anomalous Pulses. Over the duration ΔT of an Anomalous Pulse, the time-averaged flow retains a predominantly south-westerly direction (as seen in panels a, b and c of Figure 6.4). Anomalous Pulse events induce strong cyclonic anomalies in the circulation, with velocities anomalies reaching about 0.5 m.s^{-1}. These cyclonic anomalies cause weaker than average currents at the usual location of the Agulhas Current. Where the offshore edge of the Agulhas Current usually resides, a stronger than normal south-westerly flow occurs. The cyclonic anomaly cell associated with Anomalous Pulses has the shape of an ellipse with a approximate length and width of 350 km and 180 km, respectively. The center of this cyclonic cell anomaly is roughly aligned with the 3000 m isobath, with its inshore edge typically bounded by the 200 m isobath. On average, Anomalous Pulses reach the Knysna transect approximately 12 days after having first been detected off Port Elizabeth. The averaged time-delay separating the initial detection of Anomalous Pulses between the Knysna and Mossel bay transects is about 15 days. Off Port Elizabeth, the cell of anomalous flow plotted in Figure 6.4 (d) is located slightly west of the transect line. This indicates that when an Anomalous Pulse is detected offshore Port Elizabeth, over the duration of the Anomalous Pulse the offshore meander is encountered for a greater portion of the time to the west of the Port Elizabeth's transect line. By contrast near Mossel Bay (Figure 6.4 f), the cell of anomalous flow is encountered east of the Mossel Bay transect line throughout the greater part of the Anomalous Pulse's duration. Figure 6.4 (d), (e) and (f) shows that the propagation speeds of Anomalous Pulses decreases southward of Port Elizabeth. Upon reaching the Agulhas Bank, Anomalous Pulses tend to get trapped at the Agulhas Bank's bight with their center confined to within the 24°E and 25°E longitudes. On average, Anomalous Pulses reside along the Agulhas Bank's bight for approximately 80 days. By the time Anomalous Pulses reach the southernmost transect off Mossel Bay, the cell of anomalous cyclonic flow has weakened with maximum velocities anomalies decreasing from about 0.5 m.s^{-1} to 0.3 m.s^{-1} (Figure 6.4 f).

Results from the wavelet and spectral analyses conducted on the time-series of the Agulhas Current core position presented in Figure 6.5, show that the path of the southern Agulhas Current varies predominantly at intra-annual frequencies of 1 to 3 months. As in the northern
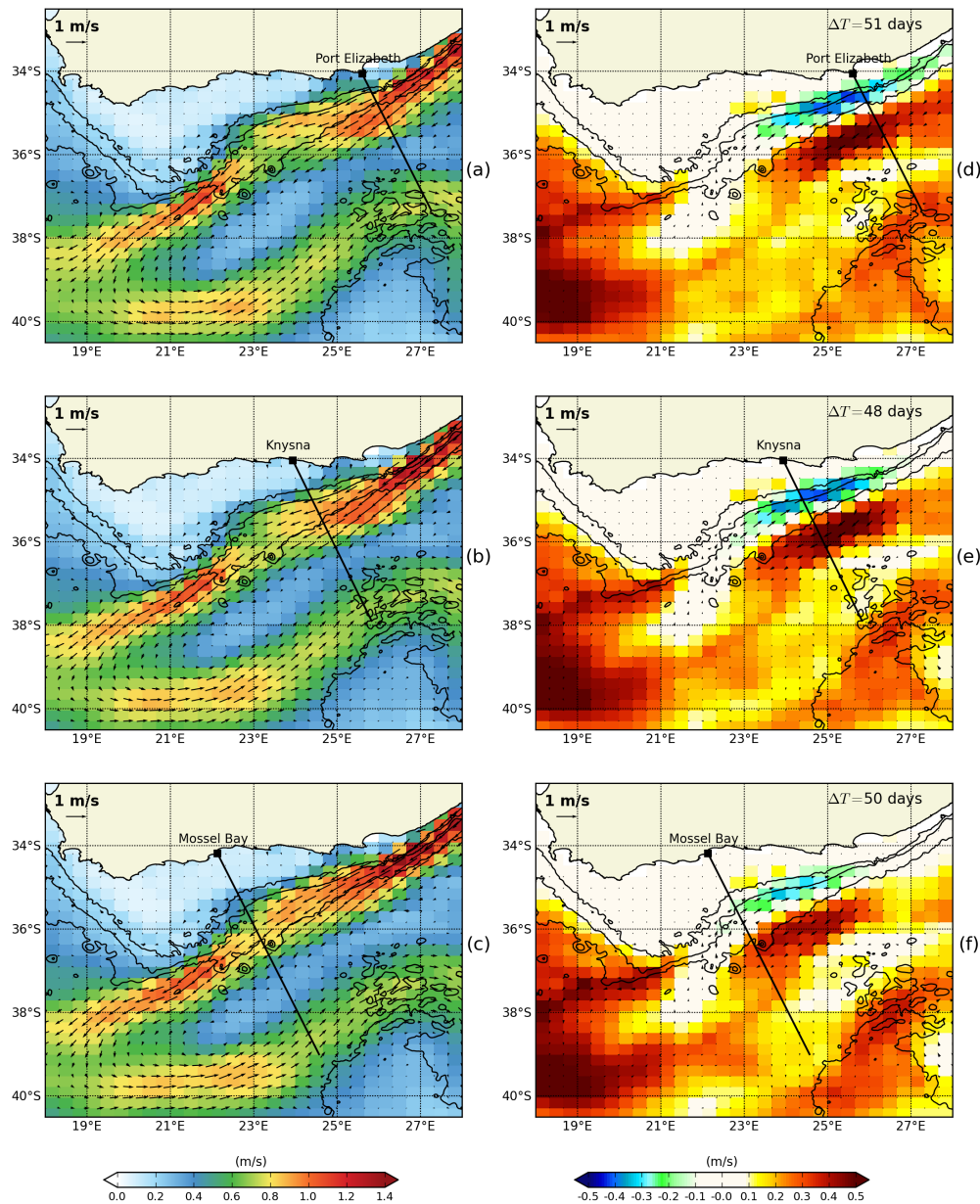
Figure 6.4: *Left panels show the mean current velocity fields computed over the duration of 22 Anomalous Pulse events at the Port Elizabeth (a), Knysna (b) and Mossel Bay (c) transects and derived using the AVISO merged maps of absolute geostrophic currents. Right panels show anomalies in the current velocity field computed over the duration of Anomalous Pulse events at the Port Elizabeth (d), Knysna (e) and Mossel Bay (f) transects. In panels (a), (b) and (c), stronger currents appear in shades of yellow and red, with current vectors providing an indication on the strength and direction of the flow. In panels (d), (e), and (f), colour contours represent anomalies in the absolute geostrophic current speeds, with shades of blue / red associated with regions of a weaker / stronger flow. Overlaid are the associated current vectors anomalies. The ΔT values in (d), (e) and (f) are the average duration of Anomalous Pulse events in days. The positions of the 200 m, 1000 m and 3000 m isobaths are plotted as black contour lines.*
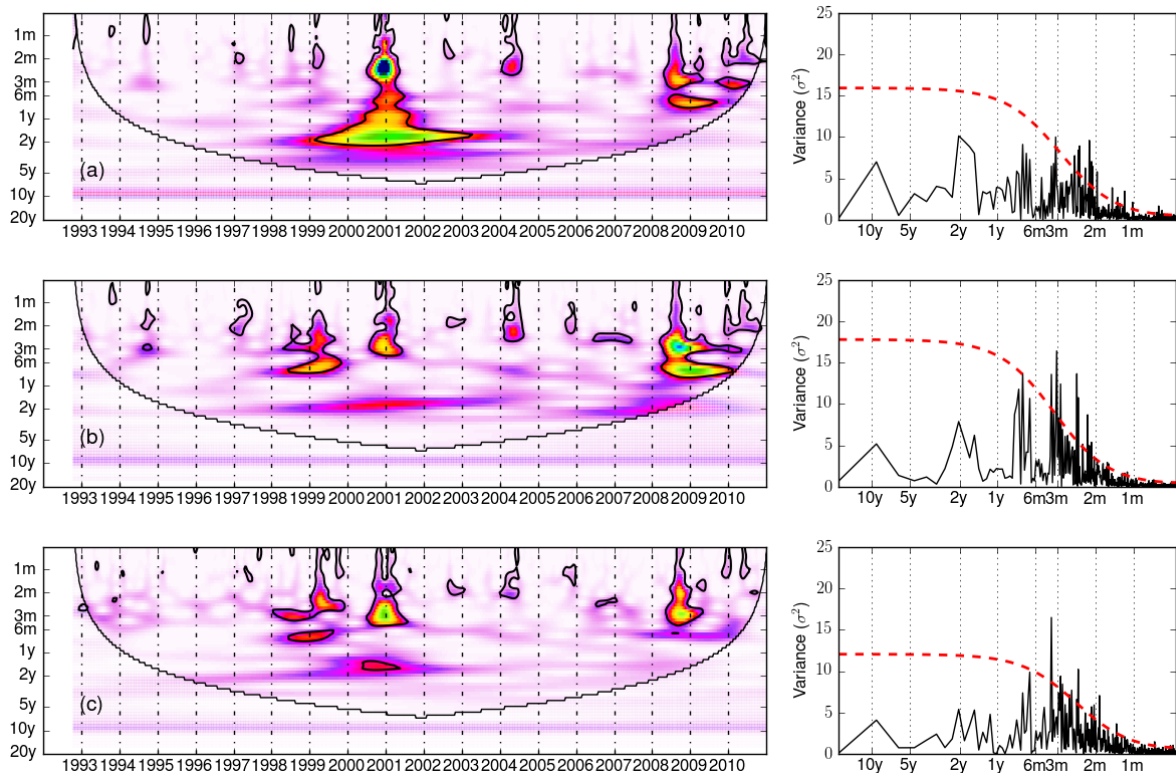
Figure 6.5: *Continuous Wavelet Transform (left panels) and Fourier energy spectra (right panels) derived from time-series of the Agulhas Current's core position at the Port Elizabeth (a), Knysna (b) and Mossel Bay (c) transects. The x-axis in the wavelet colour contour plots represents the years over which the time-series analysis was conducted. Black contour lines show the 95% confidence interval. In the Power spectrum plots, the stippled red line shows the limit for the 95% confidence level.*

Agulhas Current region (ref. Chapter 5), fluctuations in the path of the southern Agulhas Current generally occur as a result of southward propagating Natal Pulses or other large offshore meanders. The Early Retroflection of 2001 is coincident with a two-year frequency modulation of the Agulhas Current's path between the years 1999 and 2003. The Early Retroflection of 2008 also occurs at time when frequencies with periods of about 6 months and lower influence the position of the Agulhas Current. The energy peak coincident with the 2001 Early Retroflection and associated with a two-year period could be an artefact of the wavelet transform method resulting from energy spills over adjacent harmonics.

6.3.2 Modulations at the Agulhas Current core

In Section 6.3.1, it was shown that the downstream progression of Anomalous Pulses is associated with a sharp decrease in the flow strength at the location where the Agulhas Current usually lies. Within the Agulhas Current proper however, the occurrence of Anomalous Pulses merely modifies the direction of the flow from south-west to southerly or slightly south-easterly, with limited impact on the current speed. For example at 29.9°E, 34.6°S (a position which corresponds to the mean location of the Agulhas Current offshore Port Elizabeth), the standard deviation for the current speed is equal to 0.27 m.s^{-1} while at the location of the Agulhas Current core, the standard deviation for the current speed equals 0.16 m.s^{-1}. The relatively weaker impact of Anomalous Pulses on the Agulhas Current core velocities also becomes evident when plotting current speeds at the Agulhas Current core alongside those at 29.9°E, 34.6°S (as shown in Figure 6.6). A frequency analysis conducted on the current velocity of the moving Agulhas Current core offshore Port Elizabeth, reveals that although intra-annual frequencies associated with Natal Pulses or other offshore meanders do modulate the strength of the Agulhas Current flow, the main spectral peak occurs at a period of 1 year. Both the wavelet and the spectral analyses show that the geostrophic current speed at the Agulhas Current core exhibits a strong annual cycle (Figure 6.7). Seasonal variations in the Agulhas Current's velocity were confirmed in a separate analysis (not shown) based on the JASON-1 along-track data near Port Elizabeth (Track 20). Frequency analyses conducted on the timeseries of the Agulhas Current core velocity along the Knysna and Mossel Bay transects (not shown) also revealed the predominance of the annual cycle. South of Port Elizabeth however, the annual cycle had a less distinct spectral signature due to the relatively larger influence of high frequency fluctuations (linked to a downstream increase in the number of meanders, as seen in Section 6.3.1).

A monthly climatology of the Agulhas Current core velocity off Port Elizabeth was computed by averaging all monthly means of absolute geostrophic current speed over an 18 year period extending from January 1993 to December 2010. The monthly climatology was then
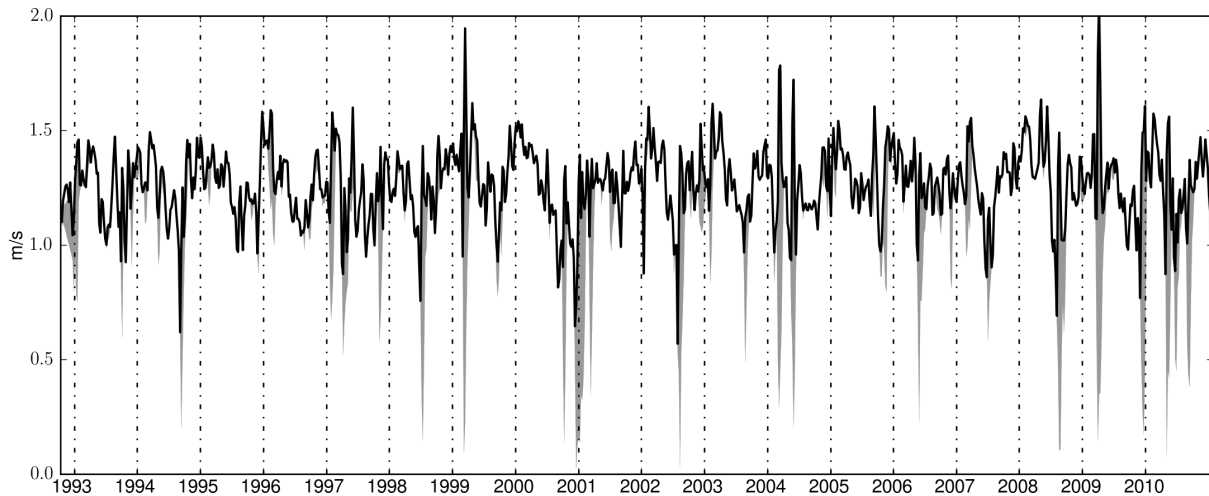
Figure 6.6: *Variations in the absolute geostrophic current velocity at the position of the Agulhas Current core, offshore Port Elizabeth are plotted in a solid black line. Shades of grey show differences in the current velocities between the varying position of Agulhas Current core and the time-averaged position of the Agulhas core (at 29.9°E, 34.6°S). Large differences in current velocities between the time-averaged and the varying location of Agulhas Current Core are observed during Anomalous Pulses events.*

slightly smoothed with a Gaussian filter of sigma value 1. The climatology of the Agulhas Current core velocity is plotted as a red solid line in Figure 6.7 c. Seasonal variations in the current speed at the Agulhas Current core show a stronger flow during the austral summer (January to March) and weaker velocities experienced over the austral winter (July and August). Seasonal geostrophic current speeds varied from 1.35 m.s^{-1} in February to 1.18 m.s^{-1} in August, with an annual average of 1.27 m.s^{-1}. Seasonal variations in the Agulhas Current core velocities account for 29.2% of the signal's variance.

6.3.3 The Sverdrup connection

The Agulhas Current forms the western boundary of the wind-driven south-Indian sub-gyre. As noted in Chapter 2, wind forcing over the south Indian ocean changes substantially between the winter and summer months, with wind stress curl intensifying and moving southward during the summer months, between December and February (Ffield et al. [1997]). Using numerical model and altimetry data, Matano et al. [2008] showed that the circulation of the south Indian ocean is primarily driven by the winds and that the seasonal adjustment of the ocean to wind stress forcing is essentially barotropic. Here we test the relationship between
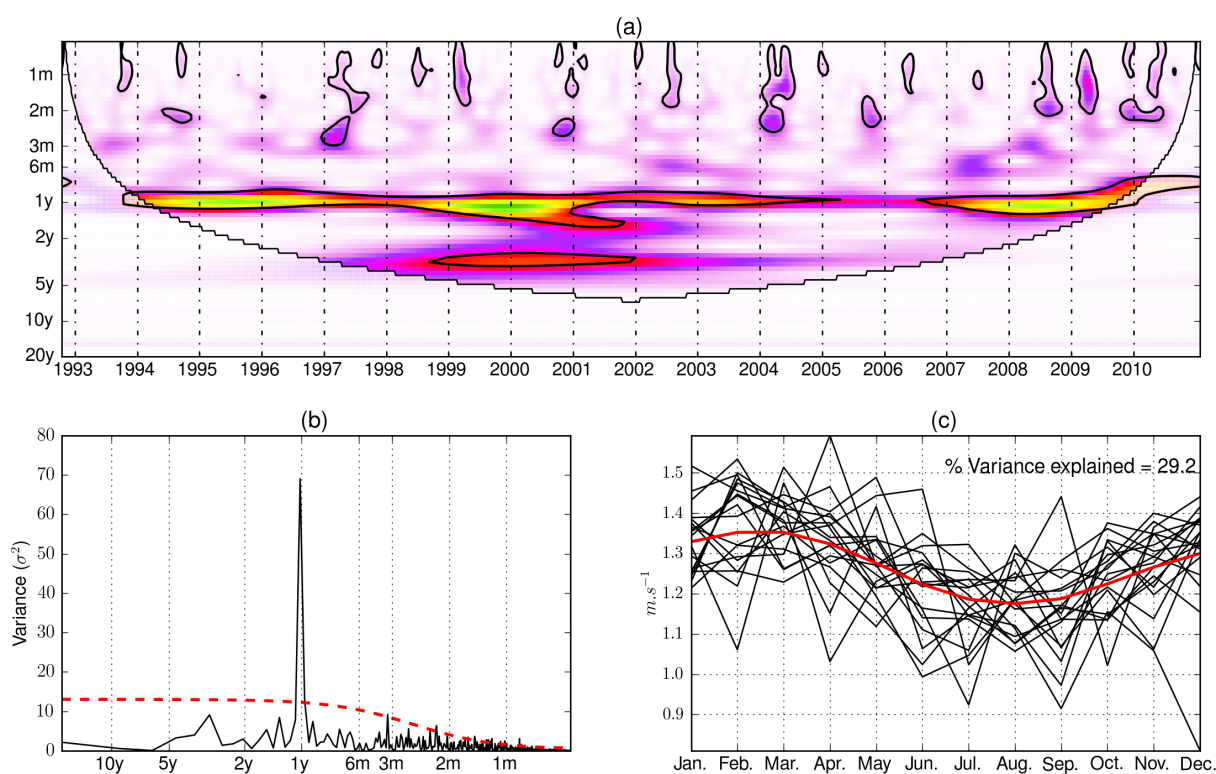
Figure 6.7: *(a) shows the wavelet transform associated with current speed fluctuations when following the Agulhas Current core offshore Port Elizabeth. The x-axis in the wavelet colour contour plots represents the years over which the time-series analysis was conducted. Black contour lines show the 95% confidence interval. (b) shows the period spectra of the current speed when following the Agulhas Current core with the stippled red line showing the limit for the 95% confidence level. (c) shows monthly seasonal variations in the Agulhas Current core velocities (in $m.s^{-1}$) with the mean climatology plotted as a thick red line. The annual cycle explains 29.2% of the Agulhas Current core velocity variance.*

the observed seasonal variability at the Agulhas Current core and wind stress forcing over the south Indian ocean through the Sverdrup approximation.

Estimates of the Agulhas Current transport at 32.5°E, 34°S (off Port Elizabeth) were computed by integrating the QuikSCAT wind stress curl data along the 34°S latitude, using the method described in Section 6.2. Variations in the Agulhas Current Sverdrup transport at 32.5°E, 34°S between August 1999 and December 2010 are plotted in Figure 6.8a. The 9 months low-passed data plotted as a red line in Figure 6.8a shows clear annual oscillations in the wind-driven Agulhas Current transport. Most of the variability for the estimated Sverdrup transport near Port Elizabeth occurs at periods of 1 year and 0.5 year, with a third significant peak encountered at a period of about 8 months (Figure 6.8 b). The mean southward transport near Port Elizabeth is estimated to 72.5 Sv. The Agulhas Current transport estimated through the Sverdup relationship does not include for contribution from the Indonesian Throughflow and should therefore provide a lower bound estimate of the total Agulhas Current transport. Still, the averaged southward transport estimated from the wind-stress curl data falls within the range of those previously reported in the literature (Bryden et al. [2005]; Casal et al. [2009]). The amplitude of the wind-driven seasonal transport is equal to about 20 Sv, with a maximum southward transport occurring in August and a minimum southward transport in February (Figure 6.8 c). The percentage of variance explained by the seasonal cycle in the Agulhas Current's Sverdup transport is 23.6%. A Lanczos band-pass filter with cut-off periods of 9 and 15 months was applied to both time-series of the Agulhas Current core velocity and the wind-driven Sverdrup transport near Port Elizabeth to compare variations associated with the annual cycle (Figure 6.9). The Sverdrup transport estimated from the wind stress curl and the geostrophic current speed within the Agulhas Current are generally inversely related, with the Agulhas Current transport lagging that estimated through the Sverdrup relation by 6 months. Between the years 2000 and 2003 however, the phase lag between seasonal variations in the Agulhas Current core velocities and the wind-derived Sverdrup transport increases, with a maximum lag of about 9 months occurring in 2001.
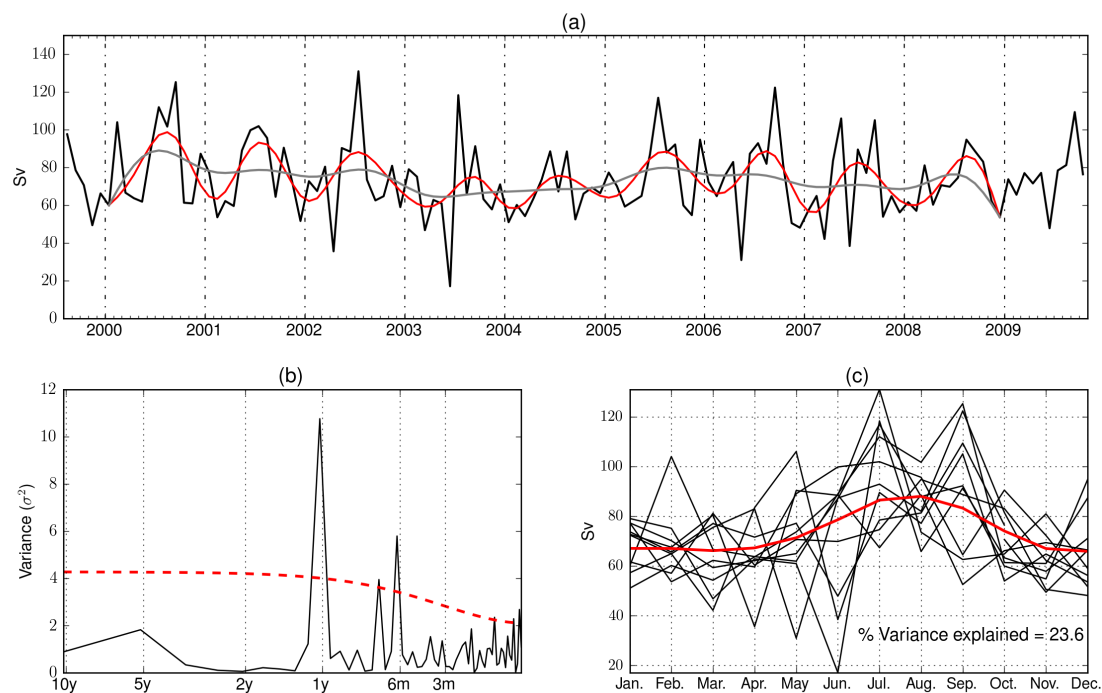
Figure 6.8: *(a) Transport in the Agulhas Current estimated at 32.5°E, 34°S (in Sv) by integrating the CERSAT QuickSCAT monthly mean wind fields of the wind stress curl along the 34°S latitude. The thick black lines in (a) show the monthly values of the Sverdrup transport off Port Elizabeth. The Sverdrup transport time-series was low-passed with cut-off of 9 months (red line) and 15 months (grey line) to highlight variability at annual and inter-annual time-scales. (b) represents the period spectra of the Sverdrup transport estimated at 32.5E, 34S with the stippled red line showing the limit for the 95% confidence level. (c) shows seasonal fluctuations in the monthly Sverdup transport (in Sv) at 32.5°E, 34°S with the climatological mean plotted as a thick red line.*

Figure 6.9: *Fluctuations in the Agulhas Current Sverdrup transport (in Sv) near Port Elizabeth occurring within the 9 to 15 months period range are plotted in black. The velocity variations at the Agulhas Current core (in $m.s^{-1}$) near Port Elizabeth and within the 9 to 15 months period range are plotted in red.*

6.4 Discussion

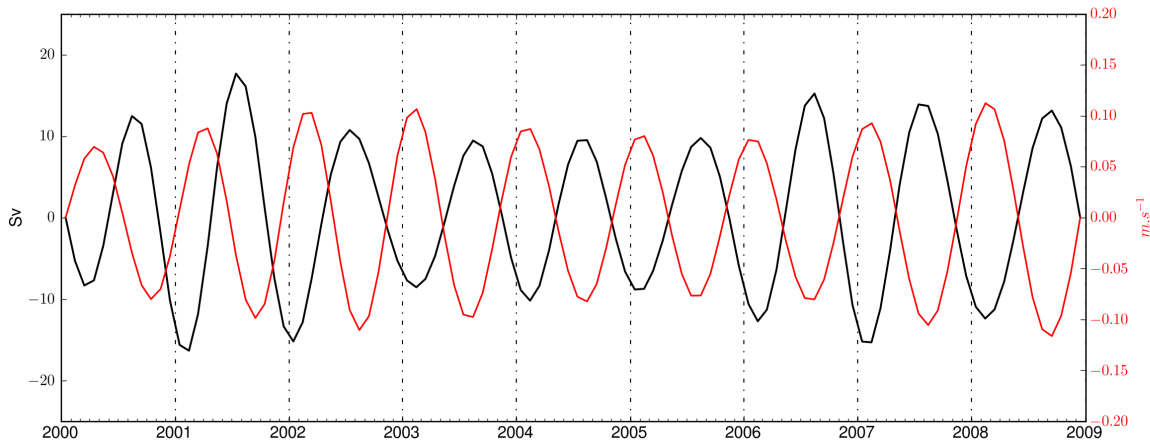As in the northern Agulhas Current region, changes in the path of the southern Agulhas Current occur as a result of large offshore meanders propagating southwards. Time-series of the Agulhas Current's path derived from altimetry confirm the increasingly meandering nature of the Agulhas Current southward of Port Elizabeth previously mentioned by Lutjeharms [2006], in his review of the Agulhas Current. The analysis undertaken using the merged altimetry data and summarised in table 6.1, shows that a significant portion (about 35%) of the Anomalous Pulses observed along the Knysna transect are features which originate in the southern Agulhas region. Previous studies have pointed to the eastern Agulhas Bank as a region of shear-edge eddy generation (Lutjeharms et al. [2003a]; Lutjeharms et al. [2003b]). Goschen and Schumann [1990] found that small meanders originating in the region of Port Elizabeth could develop into much larger frontal eddies further south. Lutjeharms and van Ballegooyen [1984] attributed the formation of these shear-edge eddies to a decrease in topographic steering at the widening Agulhas Bank, south of Port Elizabeth. SST satellite imagery and in-situ observations indicate that these shear-edge features range from 50 to 100 km in size and are

associated with raised isotherms in their center (Lutjeharms et al. [1989]). Numerical model results suggest that cyclonic vorticity from these shear-edge eddies may result in the formation of a cyclonic lee eddy at the southern tip of the Agulhas Bank, with the lee eddy eventually being shed into the Atlantic ocean (Penven et al. [2001]; Lutjeharms et al. [2003b]).

Our observations (Figure 6.4 d, e and f) show that once they reach the southern Agulhas, large offshore meanders at the landward border of the Agulhas Current stagnate at the eastern edge of the Agulhas Bank for periods of approximately 80 days, on average. This result is consistent with early modelling studies (Lutjeharms et al. [2003b]) which have shown that shear-edge eddies which develop in the southern Agulhas region tend to remain trapped along the eastern Agulhas Bank. Based on the merged altimetry dataset, the influence of large offshore meanders on the circulation of the southern Agulhas region is confined to the shelf regions, with no evidence of anomalous flow found inshore of the 200 m isobath. Considering that the large offshore meanders observed in our altimetry data reside along the eastern Agulhas Bank for long period of times and are associated with large cyclonic anomalies, their influence is likely to extend beyond the regions of cyclonic anomalies observed in Figure 6.4 d, e and f. In addition, near Mossel Bay, the intensity of the cyclonic anomaly associated with Anomalous Pulses was seen to decrease (Figure 6.4 f). This suggests that significant amounts of energy could be transferred from Anomalous Pulses to the shelf waters of the eastern Agulhas Bank. As mentioned in Chapter 4.2, altimetry observations are compromised in the coastal and shelf regions due to inadequate spatial and temporal sampling, land contamination and inaccurate atmospheric or geophysical corrections (Vignudelli et al. [2011]). As anomalous Pulses interact with the surrounding flow, energy might be dissipated from the meso to the sub-mesoscales, through a-geostrophic interactions which can not be resolved with altimetry. Understanding the mechanisms through which energy is dissipated away from Anomalous Pulses goes beyond the objectives of this thesis and would require the use of new data sources such as in-situ observations and numerical simulations, which help resolve the circulation in the vertical dimension. There is certainly good evidence that border eddies at the inshore edge of the Agulhas Current influence the structure of the water column on eastern Agulhas Bank

waters. Early SST imagery (Harris et al. [1978]; Lutjeharms [1981]) has shown that warm water plumes of entrained surface Agulhas Current water generally develop at the leading edge of offshore meanders. The shoreward advection of warm surface water from these plumes is thought to promotes the formation of an intense thermocline over the eastern Agulhas Bank (Swart and Largier [1987]). Upwelling through the core of cyclonic border eddies might also contribute to the stratification and nutrient enrichment of the water column on the eastern Agulhas Bank (Lutjeharms [2006]).

Results presented in this chapter suggest that large offshore meanders which progress into the southern Agulhas Current region strongly influence the circulation along the continental shelf of the eastern Agulhas Bank. However, within the Agulhas Current proper, the variability driven by these large offshore meanders on the Agulhas Current velocity and hence, on its southward transport, is significantly less than that resulting from seasonal wind-forcing over the south Indian Ocean. By following the Agulhas Current core, it was possible to isolate the variability of the Agulhas Current from that of the surrounding flow. This new approach enabled us to show that seasonal wind forcing over the south Indian ocean constitutes the main driver of variability for surface current speeds at the core of the southern Agulhas Current. Annual variations in wind-driven Sverdrup transport derived near Port Elizabeth generally preceded those observed in the Agulhas Current core by about 6 months (Figure 6.9). Frequency analyses of the absolute geostrophic current velocity at the Agulhas Current core showed that the annual cycle explained 29.2% of the signal's variance near Port Elizabeth. If we were to assume that the geostrophic velocity at the core of the Agulhas Current is directly proportional to the Agulhas Current's transport, this would imply a seasonal cycle with an amplitude of 21.5 Sv, a value very close to the 20 Sv estimated through the Sverdrup relation. Note that both these estimates are based on a mean Agulhas Current transport of 72.5 Sv. Evidence of an annual cycle in the Agulhas Current have been reported in a number of modelling studies (Biastoch et al. [1999]; Matano et al. [2002]; Hermes et al. [2007]; Chang [2009]). In agreement with the results presented in this chapter, numerical models of the Agulhas Current show a maximum poleward transport in austral winter (August) and a minimum in austral summer

(February). In a high resolution (8 km) model of the southern Agulhas Current, Chang [2009] finds that offshore Port Elizabeth, seasonal variations in the maximum current speed of the Agulhas Current are of the order of 0.1 to 0.2 m.s^{-1}. Our analysis of the AVISO merged altimetry data similarly indicates seasonal fluctuations in the Agulhas Current maximum geostrophic current speed of 0.17 m.s^{-1}.

6.5 Conclusion

An algorithm applied to the AVISO merged altimetry data provided a simple, yet effective way of monitoring modulations in the southern Agulhas Current. By tracking the position of the southern Agulhas Current, it was possible to better characterise the periodicity and influence of large offshore meanders on southern Agulhas Current region. Composite analyses based on a large number of Anomalous Pulses (22) allowed us to quantitatively estimate the typical residence times and size of large offshore perturbations which propagate from northern to southern Agulhas Current. The results presented in this chapter confirmed the increasingly meandering nature of the Agulhas Current south of Port Elizabeth, as mentioned in Lutjeharms [2006]. The increase in the number of offshore perturbations observed between Port Elizabeth and Mossel Bay was attributed to the generation of border-eddies at the inshore edge of the Agulhas Current. Despite the net increase in the number of large offshore meanders south of Port Elizabeth, the frequency of Anomalous Pulse events observed off Knysna and Mossel Bay still remains low, with only 2.5 large offshore pulses occurring each year, on average. The algorithm presented in this study provided the means to separate the variability of the Agulhas Current from that of its surrounding waters and enabled us to reveal the strong dominance of the annual cycle on the variability of the southern Agulhas Current.

7
Summary and conclusions

The Agulhas Current is a key component of the global climate (Beal et al. [2011]). At a regional scale, the Agulhas Current has a profound impact on coastal and shelf ecosystems and a thorough understanding of its strength and variability is necessary to monitor environmental change, maintain safety at sea and support shipping, fishing and offshore prospecting activities. Despite its importance at both the global and regional scales, relatively few in-situ observations of the Agulhas Current are available. Over the last 2 decades, satellite remote sensing observations have provided a cost-effective alternative to in-situ measurements for many regions of the world's ocean. The sampling capabilities of the Agulhas Current from space have significantly improved in recent years due to an increase in satellites' spatial and temporal coverage, the emergence of new remote sensing methods and the use of more robust algorithms for the derivation of ocean properties. One of the first objectives of this thesis was to evaluate the suitability of satellite-based observations to study the dynamics and the variability of the Agulhas Current. For this purpose we analysed data from multiple satellite-based sensors, including two datasets not previously used in the Agulhas Current region: the MSG-2 high frequency acquisitions of SST from SEVIRI and the newly available surface current velocities from ASAR. Our analyses of satellite imagery sheds new lights into the variability of the Agulhas Current at the intra-annual and annual time scales.

7.1   Observing the Agulhas Current from space

The Agulhas Current is a strong and powerful current associated with a warm and narrow core and affected by a wide range of meso and sub-mesoscale processes such as rings, eddies, filaments or plumes (Lutjeharms [2006]). The highly variable and complex circulation associated with the Agulhas Current provides an ideal natural laboratory for testing the potential and limitations of satellite-based observations. One could argue that the main indicators of variability for western boundary currents which are available from space, are current speeds and current position. Current speeds provide an indication of the varying strength of the flow, while perturbations in the current's path are revealing of meso-scale activity.

For many years, altimetry, through the use of the geostrophic approximation, was the only mode of observations for surface current velocities. Altimetry has been used with great success over the last 18 years to estimate the upper transport and magnitude of the world's major ocean currents, track eddies or even discover new currents (Siedler et al. [2006]). Since July 2007, maps of surface current velocities in the Agulhas Current region have been systematically recovered from the Envisat's ASAR, under the European Space Agency (ESA) funded SAR ocean wind-wave-current project (Collard et al. [2008]; Johannessen et al. [2008]). The ASAR surface current velocities present us with a new opportunity to study the dynamics of the Agulhas Current region from space. An assessment of the ASAR surface current velocities in the Agulhas Current region was undertaken in Chapter 4. The accuracy of ASAR surface current velocities velocities was estimated through comparisons with surface drifter data. SST imagery and merged maps of altimetry were used to establish ASAR's capacity to represent the surface circulation in the Agulhas Current region.

The derivation of surface current information from ASAR relies on the careful analysis of the Doppler centroid anomaly; the anomaly accounting for the motion of surface roughness elements on the ocean surface corrected for the rotation of the earth, and enables one to derive estimates of the surface current velocity in the line of sight of the radar. ASAR observations thus provide a direct measurement of surface current velocities while altimeters rely on the

validity of the geostrophic approximation. The ASAR range-directed velocities proved a powerful new mode of imaging the surface circulation, particularly in the coastal zone region, where altimetry suffers from serious limitations due to factors such as land contamination, atmospheric errors, inaccurate tidal correction or inaccuracies in the estimation of the Mean Dynamic Topography (MDT) (Vignudelli et al. [2011]; Vignudelli et al. [2008b]; Madsen et al. [2007]). Mapping the surface circulation from altimetry involves spatial and temporal merging of SSH observations, with the net effect of aliasing high-frequency signals in the surface variability and reducing the spatial resolution (as mentioned in Section 4.2 of Chapter 4). In contrast, quasi-instantaneous maps of range-directed surface currents can be derived from ASAR imagery over large regions of the Agulhas Current. The synoptic nature of ASAR acquisitions combined with the relatively high resolution of the ASAR surface current velocities allowed synoptic maps of the Agulhas Current core to be produced for the first time. The patterns of the circulation revealed in the ASAR imagery were highly coherent with those depicted from synoptic maps of SEVIRI SST. But our analysis showed that the systematic use of ASAR maps of range-directed surface current velocities is compromised by our inability to consistently separate the contributions of wind and ocean currents to the Doppler shift signal measured by ASAR. At times, the predicted contribution of the wind-induced Doppler shift is wrongly estimated due to inaccurate wind field products. These inaccurate wind fields induce strong outliers in the ASAR range-directed velocity dataset, particularly at radar incidence angles of less than 30°. Despite the occasional wind-induced bias, the ability of the ASAR range-directed velocities to systematically highlight regions of strong current and shear combined to the synoptic nature of ASAR acquisitions, make ASAR an attractive sensor for the study of meso to sub-mesoscale processes and western boundary current dynamics. After adequate filtering at low radar incidence angle, we were able to produce an improved map of the time-averaged flow in the Agulhas Current from the ASAR range-directed velocities.

Comparisons between altimetry, ASAR and SST observations showed that merged-altimetry can not accurately image sub-mesoscale features of the circulation (less than 30 km) and is unable to resolve variability occurring within time-scales typically less than 10 days. The prox-

imity of the Agulhas Current to the shore, also makes altimetry inadequate for the study of the northern Agulhas Current variability. However, altimetry remains very valuable for tracking deep-sea eddies and investigating their evolution at the seaward edge of the Agulhas Current. Wind-induced bias in ASAR imagery prevent the systematic use of ASAR range-directed velocities to monitor variations in the strength of the Agulhas Current's flow. The ability of the ASAR instrument to highlight regions of strong shear could be used to track the position of the Agulhas Current in both the northern and southern Agulhas region. At present however, ASAR is the only SAR instrument to be used systematically in the Agulhas Current region. This implies that unlike altimetry, where range-directed current velocities can be merged to derive a complete two-dimensional picture of the circulation, surface current velocities available from SAR sensors remain 1-dimentional and unable to resolve the cross-shelf component of the circulation in the Agulhas Current region. The volume of ASAR imagery available in the Agulhas Current region is still too low for meaningful time-series analyses to be conducted, particularly in the northern Agulhas Current region (see Figure 3.7). Synoptic patterns of the Agulhas Current 's circulation observed using the SEVIRI SST dataset were coherent with those revealed in ASAR images. The high frequency acquisitions from the MSG-2 satellite over the Agulhas Current region made the SEVIRI SST dataset well suited to tracking meso to sub-mesoscale features of the Agulhas Current's circulation.

7.2 Agulhas Current Variability

Previous studies have consistently pointed to Natal Pulses as the dominant mode of variability north of the Agulhas Retroflection (Lutjeharms [2006]). Natal Pulses have been described as large solitary meanders originating in the Natal Bight region and associated with a cold water-core and a cyclonic circulation inshore of the Agulhas Current (Lutjeharms and van Ballegooyen [1988]; Bryden et al. [2005]). As mentioned in Chapter 2 and Chapter 5, these large offshore meanders are important to the coastal and shelf regions, where they drive strong localized upwelling (Bryden et al. [2005]). Natal Pulses also affect the circulation downstream and

have been related to Agulhas Ring formation (van Leeuwen et al. [2000]) and Early retroflection events (Lutjeharms and van Ballegooyen [1988]; Rouault et al. [2010]).

In Chapter 5, a simple front-detection algorithm applied to more than 6 years of high-frequency SEVIRI SST imagery was used to follow perturbations at the inshore front of the Agulhas Current, between the northern Natal Bight and Port Elizabeth. The mean position and standard deviations in the path of the Agulhas Current derived using the front-detection algorithm were in close agreement with those previously reported in the literature. Results from the front-detection analysis showed that variability at the inshore edge of the Agulhas Current was driven by the passage of large offshore meanders, or Natal Pulses, in agreement with observations conducted by Bryden et al. [2005] off Port Edward. No seasonal variation in the position of the Agulhas Current's inshore front was observed. The proposed front-detection algorithm was able to correctly identify about 80% of all Natal Pulses, with better algorithm performance offshore the Natal Bight and Port Elizabeth regions, where temperature gradients between the Agulhas Current and the coastal and shelf waters are strongest (Rouault et al. [1995]; Lutjeharms [2006]). The Natal Pulse downstream propagation speeds estimated through our analysis (generally between 10 and 20 km/day) were consistent with those previously reported (van der Vaart and de Ruijter [2001]). What the front-detection algorithm revealed, together with selected SST imagery, was the often complex interactions between Natal Pulses and the continental slope. Natal Pulses were found to interact with the topography to form secondary offshore meanders which propagated in the lee of the original perturbation. Over time, these secondary meanders dissipated, re-merged with the original Natal Pulse, or detached from the Agulhas Current. Another surprising result of the front-detection analysis was the net decrease in the number of large offshore meanders from the southern Natal Bight / Port Edward regions to Port Elizabeth. Our analysis showed that regional differences in the variability of the northern Agulhas Current region existed, with a large number of perturbations occurring in the southern Natal Bight and Port Edward areas and a decrease in variability both south and north of these regions. It was proposed in Section 5.4 of Chapter 5 that interactions between Natal Pulses and the topography could provide a mechanism through which

energy is eroded away from Natal Pulses, and which could account for the southward decrease in variability observed from Port Edward to Port Elizabeth.

Another result of the front-detection algorithm which again seriously challenges our pre-conceptions of the Agulhas Current's dynamics and variability is that on average only 1.6 Natal Pulse per year reach the southern Agulhas Current region, in sharp contrast with the 4 to 6 previously estimated from in-situ observations (Bryden et al. [2005]), remote sensing analyses (de Ruijter et al. [1999]; Schouten et al. [2002]) and numerical modelling studies (Tsugawa and Hasumi [2010]). This periodicity of Natal Pulses, as determined in the SST front-detection analysis offshore Port Elizabeth, was confirmed in separate analyses of merged altimetry data (see Section 5.3.3 of Chapter 5 and Section 6.3.1 of Chapter 6).

From Port Elizabeth southward, a good correlation between the position of the Agulhas Current derived from the merged altimetry and SEVIRI SST dataset existed, allowing us to use the 18-year altimetry record to study the variability of the southern Agulhas Current. The analysis undertaken in Chapter 6 on the altimetry data was similar to that described in Chapter 5 and involved tracking the core of the Agulhas Current along 3 transects to better characterise the variability of the Agulhas Current along the eastern Agulhas bank. As mentioned in Chapter 4 (Section 4.3.4.1), the Agulhas Bank is both a spawning and nursing area (Hutchings et al. [2002]) and understanding the mechanisms which regulate cross-shelf exchange along the eastern Agulhas Bank is important for adequate fishery management. The analysis undertaken in Chapter 6 provided quantitative information on the typical residence time and impact of of large offshore meanders on the eastern Agulhas Bank. Results presented in Chapter 6 also allowed us to identify the main drivers of variability in the southern Agulhas Current region.

Variations in the position of the southern Agulhas Current confirmed the increasing meandering nature of the Agulhas Current south of Port Elizabeth (previously noted by Lutjeharms [2006]). As in the northern Agulhas Current, the position of the Agulhas Current did not display any seasonal modulations. Perturbations in the path of the southern Agulhas Current occurred due to cyclonic offshore meanders propagating southward at the inshore edge of the current. Between port Elizabeth and Mossel Bay, the number of large offshore meanders in-

creased by approximately 30%. The increase in the number of offshore meanders south of Port Elizabeth was attributed to the generation of shear-edge eddies in the bight of the Agulhas Bank. Large offshore meanders with an origin in the northern Agulhas Current region had long residence time, persisting for periods of approximately 1.5 months, on average at each of the 3 transects. Upon reaching the southern Agulhas, these large offshore meanders appeared to remain trapped in the bight of the Agulhas Bank for extended period of time (between 2 and 3 months). Similarly to the Natal Pulses observed by Bryden et al. [2005] in the northern Agulhas Current, the large offshore meanders which propagated from the northern to the southern regions of the Agulhas Current were associated with large cyclonic velocity anomalies, with weaker flow at the usual location of the Agulhas Current and stronger flow where the offshore edge of the Agulhas Current usually resided. Perturbations in the velocity field associated with these large offshore meanders had a typical spatial scale of 350 km by 180 km and velocity anomalies averaging 0.5 $m.s^{-1}$, when computed over the duration of the offshore pulse. The regions of anomalous flow mapped from the altimetry dataset were confined to the continental shelf, with the inshore edge of the cyclonic anomaly generally aligned with the 200 m isobath.

Results presented in Chapters 5 and 6 showed that the region of Port Elizabeth is well suited to tracking the Agulhas Current. The path of the Agulhas Current offshore Port Elizabeth is rarely perturbed and the size and time-scale associated with the large offshore meanders which reach Port Elizabeth make them easily detectable using either altimetry or SST. By following the Agulhas Current at Port Elizabeth we were able to separate the intrinsic variability of the Agulhas Current from that of the surrounding waters. This allowed us to show that seasonal modulations in the strength of the southern Agulhas Current are related to seasonal wind-forcing over the south Indian Ocean. Annual variations in current speed within the Agulhas Current and offshore Port Elizabeth accounted for close to 30% of the variability. Geostrophic current speeds at the Agulhas Current core were inversely related to fluctuations in the wind-driven transport estimated at 34°S through the Sverdrup relation. Based on our Sverdrup calculation, the amplitude of the seasonal cycle near Port Elizabeth was estimated to

be ~20 Sv, with a maximum southward transport in austral summer (February) and a minimum southward transport in austral winter (August).

7.3 Research outlook

Results presented in this thesis have exposed crucial gaps in our current understanding of the northern Agulhas Current's dynamics. In the northern Agulhas, the complex evolution of Natal Pulses, the proximity of the current to the coast and the strong evaporation rates above the current are all factors which seriously challenge satellite-based observations. A new generation of SST dataset have emerged under the Group for High resolution Sea Surface Temperature (GHRSST) initiative. The currently available GHRSST dataset merge IR and microwave SST observations to improve the resolution and coverage of SST observations. Future research to validate and utilise these high resolution merged SST products could help improve our understanding of the Agulhas Current. Projects such as the ESA funded COASTALT which aims at the "Development of Radar Altimetry Data Processing in the Coastal Zone", are likely to improve the quality of altimeter-based observations near the coast with anticipated benefits in the northern Agulhas and the coastal and shelf regions of the southern Agulhas. High resolution surface current information derived from SARs could also contribute significantly to improving our knowledge of the northern Agulhas Current in the future. Research is being undertaken to derive wind direction information directly from the SAR measured Doppler shift. Accurate wind direction estimates from SARs would improve the reliability of SAR derived surface current velocities and would increase our ability to monitor the northern Agulhas Current from space.

At present, numerical ocean models of the Agulhas Current region are not able to adequately represent the behaviour and evolution of Natal Pulses. Further research is needed to understand how Natal Pulses interact with the topography or how energy is transferred from Natal Pulses to the surrounding flow. Such theoretical investigations are required to improve our oceanographic models of the northern Agulhas Current and to understand the impact of

Natal Pulses on the eastern African shores. In Chapter 5, we also noted the recurring presence of anti-cyclonic eddies offshore Natal Pulses. While the role of offshore anti-cyclonic eddies in triggering a Natal Pulse has been addressed in previous theoretical studies (de Ruijter et al. [1999]; Tsugawa and Hasumi [2010]), the influence of either cyclonic or anti-cyclonic eddies propagating downstream together with Natal Pulses is unknown. At present the extent to which offshore eddies drive the growth or decay of Natal Pulses downstream remains uncertain.

Satellite remote sensing observations are inherently limited to the surface expression of the ocean. With no information on the vertical structure of the water column, geophysical parameters of interest to oceanographers such as volume and heat fluxes, cross-shelf exchange or upwelling can not be quantified. Integrating and assimilating remote sensing measurements into numerical ocean models together with in-situ vertical observations would add significant value to the results presented in this thesis. The Agulhas Current Transport (ACT) 3-year measurement program (currently under way near East London) will provide much needed in-situ observations to answer some of the research questions raised in this thesis and to further our understanding of the dynamics and variability of the Agulhas Current.

Bibliography

Alpers, W. and Melsheimer, C. (2004). *Synthetic Aperture Radar Marine User's Manual*, chapter Principles of Synthetic Aperture Radar, pages 355–371. National Oceanic and Atmospheric Administration. 41

Atlas, D. (1994). Footprints of storms on the sea: A view from spaceborne Synthetic Aperture Radar. *J. Geophys. Res.*, 99(C4):7961–7969. 42

Baquero-Bernal, A. and Latif, M. (2005). Wind-Driven Oceanic Rossby Waves in the Tropical South Indian Ocean with and without an active ENSO. *J. Phys. Oceanogr.*, 35(5):729–746. 13

Bard, E. and Rickaby, R. E. M. (2009). Migration of the subtropical front as a modulator of glacial climate. *Nature*, 460(7253):380–383. 1

Barton, I. J. (1995). Satellite-derived sea surface temperatures: current status. *J. Geophys. Res.*, 100:8777–8790. 22

Barton, I. J. and Checet, R. P. (1989). Comparison and optimization of AVHRR sea surface temperature algorithms. *J. Atmos. Oceanic Technol.*, 6:1083–1089. 21

Beal, L. M. and Bryden, H. L. (1999). The velocity and vorticity structure of the Agulhas Current at 32S. *J. Geophys. Res.*, 104(C3):5151–5176. 8, 18, 61

Beal, L. M., Chereskin, T. K., Lenn, Y. D., and Elipot, S. (2006). The sources and mixing characteristics of the Agulhas Current. *J. Phys. Oceanogr.*, 36(11):2060–2074. 10

Beal, L. M., de Ruijter, W. P. M., Biastoch, A., and Zahn, R. (2011). On the role of the Agulhas system in ocean circulation and climate. *Nature*, 472(7344):429–436. 1, 109

Bell, G. I. and Pratt, L. J. (1992). The interaction of an eddy with an unstable jet. *J. Phys. Oceanogr.*, 22(11):1229–1244. 83

Biastoch, A., Böning, C. W., and Lutjeharms, J. R. E. (2008a). Agulhas leakage dynamics affects decadal variability in Atlantic overturning circulation. *Nature*, 456(7221):489–492. 1

Biastoch, A., Lutjeharms, J. R. E., Boning, C. W., and Scheinert, M. (2008b). Mesoscale pertur-
bations control inter-ocean exchange south of Africa. *Geophys. Res. Lett.*, 35(20):L20602–. 1,
18, 62, 84

Biastoch, A., Reason, C. J. C., Lutjeharms, J. R. E., and Boebel, O. (1999). The importance of flow
in the Mozambique channel to seasonality in the greater Agulhas Current system. *Geophys.
Res. Lett.*, 26(21):3321–3324. 15, 17, 106

Boebel, O., Rossby, T., Lutjeharms, J. R. E., Zenk, W., and Charlie, C. (2003). Path and variability
of the Agulhas Return Current. *Deep-Sea Res. II: Topical Studies in Oceanography*, 50(1):35–56.
16

Brown, G. (1977). The average impulse response of a rough surface and its applications. *IEEE
J. Oceanic Eng.*, 2(1):67–74. 23

Bryden, H. L., Beal, L. M., and Duncan, L. M. (2005). Structure and transport of the Agulhas
Current and its temporal variability. *J. Oceanogr.*, 61:479–492. 1, 4, 7, 8, 10, 12, 17, 18, 19, 48,
57, 61, 63, 66, 81, 85, 94, 102, 112, 113, 114, 115

Byrne, D. A. and McClean, J. L. (2008). Sea level anomaly signals in the Agulhas Current
region. *Geophys. Res. Lett.*, 35(13):L13601–. 48, 84

C., F., Flechtner, F., Schmidt, R., U. Meyer, Stubenvoll R.and Barthelmes F.and, K. R. N. K.-H.,
and Rothacher M.andReigber Ch. andBiancale R.and Bruinsma S.and, L. J.-M. R. J. C. (2005).
A new high resolution global gravity field model derived from combination of grace and
champ mission and altimetry/gravimetry surface gravity data. In *Presented at EGU General
Assembly 2005, Vienna, Austria*. 30

Casal, T. G. D., Beal, L. M., Lumpkin, R., and Johns, W. E. (2009). Structure and down-
stream evolution of the Agulhas Current system during a quasi-synoptic survey in February
- March 2003. *J. Geophys. Res.*, 114:C03001–. 7, 10, 16, 63, 102

Chang, C. and Curlander, J. (1992). Application of the multiple PRF technique to resolve Doppler centroid estimation ambiguity for spaceborne SAR. *IEEE Trans. on Geosci. Remote Sens.*, GE-30(5):941–949. 33

Chang, N. (2009). *Numerical ocean model study of the Agulhas Bank and the Cool Ridge*. PhD thesis, University of Cape Town, Cape Town, South Africa,. 17, 106, 107

Chapron, B., Collard, F., and Kerbaol, V. (2004). Satellite Synthetic Aperture Radar sea surface Doppler measurements. *Proc. of the 2nd Workshop on Coastal and Marine Applications of SAR, ESA SP-565*, pages 133–140. 33

Chelton, D. B., Ries, J. C., Haines, B. J., Fu, L. L., and Callahan, P. S. (2001). *Satellite altimetry and Earth sciences*, chapter Satellite Altimetry, pages 1–131. Academic Press. 30

Cheney, R. A., Marsh, J. G., and Deckley, B. D. (1983). Global mesoscale variability from collinear tracks of SEASAT altimeter data. *J. Geophys. Res.*, 88(C7):4343–4354. 17, 54

Collard, F., Mouche, A., Chapron, B., Danilo, C., and Johannessen, J. A. (2008). Routine high resolution observation of selected major surface currents from space. *Proc. of Workshop SEASAR 2008, ESA SP-656*. 34, 42, 44, 110

Danilo, C. (2009). *Evaluation des courants de surface oceanique au moyen d'un radar a ouverture synthetique*. PhD thesis, Universite de Brest, Brest, France. 31

de Ruijter, W. P. M., Ridderinkhof, H., Lutjeharms, J. R. E., Schouten, M. W., and Veth, C. (2002). Observations of the flow in the Mozambique Channel. *Geophys. Res. Lett.*, 29:1401–1403. 16

de Ruijter, W. P. M., Ridderinkhof, H., and Schouten, M. W. (2005). Variability of the southwest Indian Ocean. *Phil. Trans. R. Soc. London Ser. A*, 363:63–76. 12, 13

de Ruijter, W. P. M., van Aken, H. M., Beier, E. J., Lutjeharms, J. R. E., Matano, R. P., and Schouten, M. W. (2004). Eddies and dipoles around South Madagascar: formation, pathways and large-scale impact. *Deep-Sea Res. I*, 51(3):383–400. 15

de Ruijter, W. P. M., van Leeuwen, P. J., and Lutjeharms, J. R. E. (1999). Generation and evolution of Natal Pulses: Solitary meanders in the agulhas current. *J. Phys. Oceanogr.*, 29(12):3043–3055. 18, 19, 57, 61, 84, 114, 117

Donlon, C. J. (2010). *Oceanography from space*, chapter Sea Surface Temperature Measurements from Thermoal Infrared Satellite Instruments: Status and Outlook, pages 211 – 227. Springer. 22

Donohue, K. A., Firing, E., M., L., and Beal (2000). Comparison of three velocity sections of the Agulhas Current and Agulhas Undercurrent. *J. Geophys. Res.*, 105(C12):28,585–28,593. 10

Donohue, K. A. and Toole, J. M. (2003). A near-synoptic survey of the Southwest Indian Ocean. *Deep Sea Res. II: Topical Studies in Oceanography*, 50(12-13):1893–1931. 15, 16

Ffield, A., Toole, J. M., and Wilson, W. D. (1997). Seasonal circulation in the South Indian Ocean. *Geophys. Res. Lett.*, 24(22):2773–2776. 12, 100

Ganachaud, A. S., Wunsch, C., Marotzke, J., and Toole, J. (2000). Meridional overturning and large-scale circulation of the indian ocean. *J. Geophys. Res.*, 105(C11):26,117âĂŞ26,134. 91

Gilman, D. L., Fuglister, F. J., and Mitchell, J. M. (1963). On the power spectrum of "red noise". *J. Atmos. Sci.*, 20(2):182–184. 90

Goldstein, R. M. and Zebker, H. A. (1987). Interferometric radar measurement of ocean surface currents. *Nature*, 328(6132):707–709. 33

Gordon, A. L. (1985). Indian-Atlantic transfer of thermocline water at the Agulhas Retroflection. *Science*, 227:1030–1033. 1

Gordon, A. L., Lutjeharms, J. R. E., and Grundlingh, M. (1987). Stratification and circulation at the Agulhas Retroflection. *Deep-Sea Res.*, 34A:565–599. 10, 16

Gordon, A. L., Ma, S., Olson, D. B., Hacker, P., Field, A., Talley, L. D., Wilson, D., and Baringer, M. (1997). Advection and diffusion of Indonesian Throughflow water within the Indian Ocean South Equatorial Current. *Geophys. Res. Lett*, 24(21):2573–2576. 13

Goschen, W. S. and Schumann, E. H. (1990). Agulhas Current variability and inshore structures off the Cape Province, South Africa. *J. Geophys. Res.*, 95:667–678. 7, 63, 75, 82, 84, 104

Gründlingh, M. L. (1983). On the course of the Agulhas Current. *S. Afr. Geogr. J.*, 65(1):49–57. 8, 17, 18, 48, 75, 85

Harris, T. F. W., Legeckis, R., and van Foreest, D. (1978). Satellite infra-red images in the Agulhas Current system. *Deep-Sea Res.*, 25:543–548. 18, 53, 106

Herbert, E. H. and Bryan, K. (1976). Topographically generated eddies. *Deep-Sea Res.*, 23(8):655–679. 83

Hermes, J. C., Reason, C. J. C., and Lutjeharms, J. R. E. (2007). Modeling the variability of the greater Agulhas Current system. *J. Clim.*, 20(13):3131–3146. 15, 17, 106

Holt, B. (2004). *Synthetic Aperture Radar Marine User's Manual*, chapter SAR imaging of the ocean surface, pages 25–80. National Oceanic and Atmospheric Administration. 33

Horstmann, J., Koch, W., and Lehner, S. (2004). Ocean wind fields retrieved from the advanced Synthetic Aperture Radar aboard ENVISAT. *Ocean Dynam.*, 54(6):570–576. 46

Hutchings, L., Beckley, L. E., Griffiths, M. H., Roberts, M. J., Sundby, S., and van der Lingen, C. (2002). Spawning on the edge: spawning grounds and nursery areas around the southern African coastline. *Mar. Freshw. Res.*, 53:307–318. 114

Johannessen, J. A., Chapron, B., Collard, F., Kudryavtsev, V., Mouche, A., Akimov, D., and Dagestad, K.-F. (2008). Direct ocean surface velocity measurements from space: Improved quantitative interpretation of envisat asar observations. *Geophys. Res. Lett.*, 35(22):L22608–. 34, 110

Johannessen, J. A., Kudryavtsev, V., Akimov, D., Eldevik, T., Winther, N., and Chapron, B. (2005). On radar imaging of current features: 2. mesoscale eddy and current front detection. *J. Geophys. Res.*, 110(C7):C07017–. 34

Jury, M. R., Valentine, H. R., and Lutjeharms, J. R. E. (1993). Influence of the Agulhas Current on summer rainfall on the southeast coast of South Africa. *J. Appl. Meteorol.*, 32(7):1282–1287. 2

Kilpatrick, K. A., Podesta, G. P., and Evans, R. (2001). Overview of the NOAA/NASA Advanced Very High Resolution Radiometer Pathfinder algorithm for sea surface temperature and associated matchup database. *J. Geophys. Res.*, 106(C5):9179–9197. 21

Koshlyakov, M. N. (1986). *Synoptic eddies in the ocean*, chapter Eddies of western boundary currents, pages 208–264. D. Reidel Publishing Company. 53

Largier, J. L., Chapman, P., Peterson, W. T., and Swart, V. P. (1992). The western Agulhas Bank: circulation, stratification and ecology. *S. Afr. J. Mar. Sci*, 12:319–339. 53

Le Provost, C. (2000). *Satellite Altimetry and Earth Sciences*, chapter Ocean Tides. Academic Press. 30

Lee, T., Atkinson, L., and Legeckis, R. (1981). Observations of a Gulf Stream frontal eddy on the Georgia continental shelf. *Deep-Sea Res.*, 28:347–378. 53

LeTraon, P. Y. and Dibarboure, G. (2002). Velocity mapping capabilities of present and future altimeter missions: The role of high-frequency signals. *J. Atmos. Ocean. Tech.*, 19(12):2077–2087. 66

Lutjeharms, J. R. E. (1981). Features of the southern Agulhas Current circulation from satellite remote sensing. *S. Afr. J. Sci.*, 77:231–236. 106

Lutjeharms, J. R. E. (2006). *The Agulhas Current*. Springer. 1, 2, 3, 4, 5, 7, 8, 12, 13, 16, 17, 18, 19, 22, 48, 52, 53, 57, 61, 63, 74, 81, 85, 104, 106, 107, 110, 112, 113, 114

Lutjeharms, J. R. E., Boebel, O., and Rossby, H. T. (2003a). Agulhas cyclones. *Deep-Sea Res. II*, 50(1):13–34. 104

Lutjeharms, J. R. E., Boebel, O., van der Vaart, P. C. F., de Ruijter, W. P. M., Rossby, T., and Bryden, H. L. (2001). Evidence that the Natal Pulse involves the Agulhas Current to its full depth. *Geophys. Res. Lett.*, 28(18):3449–3452. 19, 81

Lutjeharms, J. R. E., Catzel, R., and Valentine, H. R. (1989). Eddies and other boundary phenomena of the Agulhas Current. *Cont. Shelf Res.*, 9(7):597–616. 53, 105

Lutjeharms, J. R. E., Cooper, J., and Roberts, M. J. (2000). Upwelling at the inshore edge of the Agulhas Current. *Cont. Shelf Res.*, 20(7):737–761. 2

Lutjeharms, J. R. E., Penven, P., and Roy, C. (2003b). Modelling the shear edge eddies of the southern Agulhas Current. *Cont. Shelf Res.*, 23:1099–1115. 18, 53, 61, 104, 105

Lutjeharms, J. R. E. and Roberts, H. R. (1988). The Natal Pulse: An extreme transient on the Agulhas Current. *J. Geophys. Res.*, 93:631–645. 4, 18, 61, 85

Lutjeharms, J. R. E. and van Ballegooyen, R. C. (1984). Topographic control in the Agulhas Current system. *Deep-Sea Res.*, 31(11):1321–1337. 18, 104

Lutjeharms, J. R. E. and van Ballegooyen, R. C. (1988). Anomalous upstream retroflection in the Agulhas Current. *Science*, 240(4860):1770–1772. 19, 57, 112, 113

Madsen, K. S., Hoyer, J. L., and Tscherning, C. C. (2007). Near-coastal satellite altimetry: Sea Surface Height variability in the North Sea-Baltic Sea area. *Geophys. Res. Lett.*, 34:L14601–. 62, 84, 111

Madsen, S. N. (1989). Estimation the doppler centroid of SAR data. *IEEE Trans. Aerospace Electron. Syst.*, AES-25(2):134–140. 33

Mason, S. J. (1995). Sea-surface temperature - South African rainfall associations, 1910-1989. *Int. J. Clim.*, 15(2):119–135. 2

Matano, R. P., Beier, E. J., and Strub, P. T. (2008). The seasonal variability of the circulation in the South Indian Ocean: Model and observations. *J. Mar. Syst.*, 74(1-2):315–328. 18, 100

Matano, R. P., Beier, E. J., Strub, P. T., and Tokmakian, R. (2002). Large-scale forcing of the Agulhas variability: The seasonal cycle. *J. Phys. Oceanogr.*, 32(4):1228–1241. 12, 15, 17, 106

Matano, R. P., Simionato, C. G., de Ruijter, W. P., van Leeuween, P. J., Strub, P. T., Chelton, D. B., and Schlax, M. G. (1998). Seasonal variability in the Agulhas Retroflection region. *Geophys. Res. Lett.*, 25(23):4361–4364. 17

Monaldo, F. M. and Beal, R. (2004). *Synthetic Aperture Radar Marine User's Manual*, chapter Wind speed and direction, pages 305–320. National Oceanic and Atmospheric Administration. 46

Morrow, R. and Birol, F. (1998). Variability in the southeast Indian Ocean from altimetry: Forcing mechanisms for the Leeuwin Current. *J. Geophys. Res.*, 103(C9):18,529–18,544. 13

Mouche, A., Chapron, B., Reul, N., and Collard, F. (2008). Predicted Doppler shifts induced by ocean surface displacements using asymptotic electromagnetic wave scattering theories. *Waves Random Complex Medium*, 18(1):185–196. 34

Nauw, J. J., van Aken, H. M., Webb, A., Lutjeharms, J. R. E., and de Ruijter, W. P. M. (2008). Observations of the southern East Madagascar Current and undercurrent and countercurrent system. *J. Geophys. Res.*, 113(C8):C08006–. 15

Niiler, P. P., Maximenko, N. A., and McWilliams, J. C. (2003). Dynamically balanced absolute sea level of the global ocean derived from near-surface velocity observations. *Geophys. Res. Lett.*, 30(22):2164–. 27

Palastanga, V., van Leeuwen, P. J., Schouten, M. W., and de Ruijter, W. P. M. (2007). Flow structure and variability in the subtropical Indian Ocean: Instability of the South Indian Ocean Countercurrent. *J. Geophys. Res.*, 112(C1):C01001–. 13

Pearce, A. F. and Grundlingh, M. L. (1982). Is there a seasonal variation in the Agulhas Current ? *J. Mar. Res.*, 40(1):177–184. 18, 48

Penven, P., Lutjeharms, J. R. E., Marchesiello, P., Roy, C., and Weeks, S. J. (2001). Generation of

cyclonic eddies by the Agulhas Current in the lee of the Agulhas Bank. *Geophys. Res. Lett.*, 27:1055–1058. 52, 53, 105

Perigaud, C. and Delecluse, P. (1992). Annual sea level variations in the southern tropical Indian Ocean from Geosat and shallow-water simulations. *J. Geophys. Res.*, 97(C12):20,169–20,178. 13

Portabella, M., Stoffelen, A., and Johannessen, J. (2002). Toward on optimal inversion method for Synthetic Aperture Radar wind retrieval. *J. Geophys. Res.*, 107(C8):3086–. 44

Probyn, T. A., Mitchell-Innes, B., and Searson, S. (1995). Primary productivity and nitrogen uptake in the subsurface chlorophyll maximum on the Eastern Agulhas Bank. *Cont. Shelf Res.*, 15:1903–1920. 53

Quartly, G., Buck, J., Srokosz, M., and Coward, A. (2006). Eddies around Madagascar – the retroflection re-considered. *J. Mar. Syst.*, 63(3-4):115–129. 15

Quartly, G. D. and Srokosz, M. A. (2002). SST observations of the Agulhas and East Madagascar Retroflections by the TRMM Microwave Imager. *J. Phys. Oceanogr.*, 32(5):1585–1592. 15

Ridderinkhof, H., van der Werf, P. M., Ullgren, J. E., van Aken, H. M., van Leeuwen, P. J., and de Ruijter, W. P. M. (2010). Seasonal and interannual variability in the Mozambique Channel from moored current observations. *J. Geophys. Res.*, 115:C06010–. 13, 16, 18

Rio, M.-H. and Hernandez, F. (2004). A Mean Dynamic Topography computed over the world ocean from altimetry, in situ measurements, and a geoid model. *J. Geophys. Res.*, 109:C12032–. 27, 28, 29, 30

Rio, M.-H., Schaeffer, P., Lemoine, J.-M., and Hernandez, F. (2005). Estimation of the ocean Mean Dynamic Topography through the combination of altimetric data, in-situ measurements and GRACE geoid: From global to regional studies. In *Proceedings of the GOCINA international workshop, Luxembourg*. 48, 67

Rio, M. H., S. G. and Larnicol, G. (2011). The new CNES-CLS09 global Mean Dynamic Topography computed from the combination of GRACE data, altimetry and in-situ measurements. *J. Geophys. Res.*, in press. 9, 15, 28, 29, 38, 48, 67, 89

Risien, C. M. and Chelton, D. B. (2008). A global climatology of surface wind and wind stress fields from eight years of QuikSCAT scatterometer data. *J. Phys. Oceanogr.*, 38(11):2379–2413. 12, 14

Roberts, M. J. (2010). Coastal currents and temperatures along the eastern region of Algoa Bay, South Africa, with implications for transport and shelf-bay water exchange. *Afr. J. Mar. Sci.*, 32(1):145–161. 83

Robinson, I. S. (2004). *Measuring the oceans from space: The principles and methods of satellite oceanography*. Springer-Praxis books in geophysical science. 21, 22, 25, 28, 32

Romeiser, R., Breit, H., Eineder, M., Runge, H., Flament, P., de Jong, K., and Vogelzang, J. (2005). Current measurements by SAR along-track interferometry from a space shuttle. *IEEE Trans. Geosci. Remote Sens.*, 43(10):2315–2324. 33

Rouault, M., Lee-Thorp, A. M., Ansorge, I., and Lutjeharms, J. R. E. (1995). Agulhas Current Air-Sea Exchange Experiment. *S. Afr. J. Sci.*, 91:493–496. 22, 63, 113

Rouault, M., Lee-Thorp, A. M., and Lutjeharms, J. R. E. (2000). Observations of the atmospheric boundary layer above the Agulhas Current during along-current winds. *J. Phys. Oceanogr.*, 30:70–85. 2, 22, 24

Rouault, M. and Lutjeharms, J. (2003). Microwave satellite remote sensing of sea surface temperature around Southern Africa. *S. Afr. J. Sci.*, 99:489–494. 93

Rouault, M., Penven, P., and Pohl, B. (2009). Warming in the Agulhas Current system since the 1980's. *Geophys. Res. Lett.*, 36(12):L12602–. 1

Rouault, M. J., Mouche, A., Collard, F., Johannessen, J. A., and Chapron, B. (2010). Mapping the

Agulhas Current from space: an assessment of ASAR surface current velocities. *J. Geophys. Res.*, 115:C10026–. 67, 77, 78, 84, 113

Samuel, W., Jr., M., and Jackson, C. R. (2004). *Synthetic Aperture Radar Marine User's Manual*, chapter Principles of Synthetic Aperture Radar, pages 1–24. National Oceanic and Atmospheric Administration. 32

Sanson, L. Z. and van Heijst, G. J. F. (2000). Interaction of barotropic vortices with coastal topography: Laboratory experiments and numerical simulations. *J. Phys. Oceanogr.*, 30(9):2141–2162. 82

Schott, F., Fieux, M., Kindle, J., Swallow, J., and Rainer, Z. (1988). The boundary currents east and north of Madagascar 2. direct measurements and model comparisons. *J. Geophys. Res.*, 93(C5):4963–4974. 15

Schouten, M. W., de Ruijter, W. P. M., van Leeuwen, P. J., and Dijkstra, H. A. (2002). An oceanic teleconnection between the equatorial and southern Indian Ocean. *Geophys. Res. Lett.*, 29(16):1812–. 13, 68, 84, 85, 114

Schouten, M. W., de Ruijter, W. P. M., van Leeuwen, P. J., and Ridderinkhof, H. (2003). Eddies and variability in the Mozambique Channel. *Deep-Sea Res. II: Topical Studies in Oceanography*, 50(12-13):1987–2003. 15

Schumann, E. H. (1983). Long-period coastal trapped waves off the southeast coast of Southern Africa. *Cont. Shelf Res.*, 2(2-3):97–107. 82

Shemer, L., Marom, M., and Markman, D. (1993). Estimates of currents in the nearshore ocean region using interferometric Synthetic Aperture Radar. *J. Geophys. Res.*, 98(C4):7001–7010. 33

Siedler, G., Rouault, M., Biastoch, A., Backeberg, B., Reason, C. J. C., and Lutjeharms, J. R. E. (2009). Modes of the southern extension of the East Madagascar Current. *J. Geophys. Res.*, 114:C01005–. 15

Siedler, G., Rouault, M., and Lutjeharms, J. R. E. (2006). Structure and origin of the subtropical South Indian Ocean Countercurrent. *Geophys. Res. Lett.*, 33:L24609–. 110

Stern, M. E. and Flierl, G. R. (1987). On the interaction of a vortex with a shear flow. *J. Geophys. Res.*, 92:10,733–10,744. 83

Stoffelen, A. and Anderson, D. (1997). Scatterometer data interpretation: Estimation and validation of the transfer function CMOD4. *J. Geophys. Res.*, 102:5767–5780. 44, 46

Stramma, L. and Lutjeharms, J. R. E. (1997). The flow field of the subtropical gyre of the South Indian Ocean. *J. Geophys. Res.*, 102(C3):5513–5530. 16

Swallow, J., Michele, F., and Friedrich, S. (1988). The boundary currents east and north of Madagascar 1. geostrophic currents and transports. *J. Geophys. Res.*, 93(C5):4951–4962. 15

Swart, V. P. and Largier, J. L. (1987). Thermal structure of Agulhas Bank water. *S. Afr. J. Mar. Sci.*, 5(1):243–252. 106

Takeda, H. (1983). Topographically trapped waves over the continental shelf and slope. *J. Oceanogr. Soc. Japan*, 40(5):349–366. 82

Tsugawa, M. and Hasumi, H. (2010). Generation and growth mechanism of the Natal Pulse. *J. Phys. Oceanogr.*, 40(7)(2010):1597–1612. 18, 62, 84, 114, 117

Vachon, P. and Dobson, F. (1996). Validation of wind vector retrieval from ERS-1 SAR images over the ocean. *Global Atmos. Ocean Syst.*, 5:177–187. 46

van der Vaart, P. C. F. and de Ruijter, W. P. M. (2001). Stability of western boundary currents with an application to pulselike behavior of the Agulhas Current. *J. Phys. Oceanogr.*, 31(9):2625–2644. 8, 18, 78, 113

van der Werf, P. M., van Leeuwen, P. J., Ridderinkhof, H., and de Ruijter, W. P. M. (2010). Comparison between observations and models of the Mozambique Channel transport: Seasonal cycle and eddy frequencies. *J. Geophys. Res.*, 115:C02002–. 16

van Leeuwen, P. J., de Ruijter, W. P. M., and Lutjeharms, J. R. E. (2000). Natal Pulses and the formation of Agulhas Rings. *J. Geophys. Res.*, 105(C3):6425–6436. 18, 19, 57, 61, 66, 81, 82, 84, 113

Vianna, M. L. and Menezes, V. V. (2010). Mean mesoscale global ocean currents from geodetic pre-GOCE MDTs with a synthesis of the North Pacific circulation. *J. Geophys. Res.*, 115(C2):C02016–. 28, 29

Vianna, M. L., Menezes, V. V., and Chambers, D. P. (2007). A high resolution satellite-only GRACE-based Mean Dynamic Topography of the South Atlantic Ocean. *Geophys. Res. Lett.*, 34(24):L24604–. 27

Vignudelli, S., Berry, P., and Roblou, L. (2008a). *15 Years of Progress in Radar Altimetry*. ESA. 31

Vignudelli, S., Berry, P., and Roblou, L. (2008b). *15 Years of Progress in Radar Altimetry*, chapter Satellite altimetry near coasts - current practices and a look at the future. ESA. 62, 84, 111

Vignudelli, S., Kostianoy, A., Cipollini, P., and Benveniste, J. (2011). *Coastal Altimetry*. Springer. 3, 31, 62, 105, 111

Walker, N. D. (1986). Satellite observations of the Agulhas Current and episodic upwelling south of Africa. *Deep-Sea Res.*, 33(8):1083–1106. 2

Walker, N. D. (1990). Links between South African summer rainfall and temperature variability of the Agulhas and Benguela Current systems. *J. Geophys. Res.*, 95(C3):3297–3319. 2

Weeks, S. J., Shillington, F. A., and Brundrit, G. B. (1998). Seasonal and spatial SST variability in the Agulhas Retroflection and Agulhas Return Current. *Deep-Sea Res. I*, 45(10):1611–1625. 17

Weijer, W., de Ruijter, W. P. M., and Dijkstra, H. A. (2001). Stability of the Atlantic overturning circulation: Competition between Bering Strait freshwater flux and Agulhas heat and salt sources. *J. Phys. Oceanogr.*, 31(8):2385–2402. 1

Xie, S., Annamalai, H., Schott, F. A., and McCreary, J. P. (2002). Structure and mechanisms of south Indian Ocean climate variability. *J. Clim.*, 15:864–878. 13

Xioming, W. (1992). *Interaction of an eddy with a continental slope*. PhD thesis, Woods Hole Oceanographic Institution. 82

Yang, J., Yu, L., Koblinsky, C. J., and Adamec, D. (1998). Dynamics of the seasonal variations in the Indian Ocean from TOPEX/POSEIDON Sea Surface Height and an ocean model. *Geophys. Res. Lett.*, 25(11):1915–1918. 13